Universidade de Aveiro Departamento de Electrónica, Telecomunicações e Informática,
2018

Rúben Pereira Marques

Transmitter for 5G Systems

Transmissor para Sistemas 5G

Rúben
Pereira Marques

Transmitter for 5G Systems

Transmissor para Sistemas 5G

Dissertação apresentada à Universidade de Aveiro para cumprimento dos requesitos necessários à obtenção do grau de Mestre em Engenharia Eletrónica e Telecomunicações, realizada sob a orientação científica do Professor Doutor Pedro Miguel da Silva Cabral (orientador), Professor Auxiliar do Departamento de Eletrónica, Telecomunicações e Informática da Universidade de Aveiro e do Professor Doutor Adão Paulo Soares da Silva (co-orientador), Professor Auxiliar do Departamento de Eletrónica, Telecomunicações e Informática da Universidade de Aveiro.

o júri / the jury

presidente / president

Professora Doutora Susana Isabel Barreto de Miranda Sargento
Professora Associada com Agregação, Universidade de Aveiro

vogais / examiners committee

Professor Doutor Rui Miguel Henriques Dias Morgado Dinis
Professor Associado com Agregação, Universidade Nova de Lisboa

Professor Doutor Pedro Miguel da Silva Cabral
Professor Auxiliar, Universidade de Aveiro

agradecimentos / acknowledgements

Agradeço à minha namorada o companheirismo prestado que me deu força e motivação para concluir o meu ciclo académico.

Aos meus pais por todo o esforço que fizeram para que esta etapa fosse concluída.

Aos meus irmãos por estarem lá sempre quando é preciso.

Ao meu orientador, Prof. Pedro Cabral, e co-orientador, Prof. Adão Silva, por todo o conhecimento transmitido, disponibilidade e, fundamentalmente, a autonomia que me foi incumbida que tanto me fez crescer ao longo destes meses.

A todos os meus colegas e amigos que me acompanharam durante estes anos, sem os quais isto não seria possível.

À Universidade de Aveiro, ao Departamento de Eletrónica, Telecomunicações e Informática e ao Instituto de Telecomunicações por fornecerem as condições necessárias de trabalho e aprendizagem.

Por fim, mas não menos importante, a todos os que, de uma maneira ou de outra, contribuíram para que este percurso fosse possível.

palavras-chave

5G, Modulação OFDM, Amplificador de Potência, Plataforma de Simulação, SISO, Alamouti 2x1, BER.

resumo

Os atuais sistemas 4G são baseados na modulação Orthogonal Frequency Division Multiplexing (OFDM) que apesar de garantir uma grande flexibilidade e robustez à propagação multi-percurso inerente aos sistemas sem fios, possui grandes variações nas respetivas envolventes temporais o que causa um elevado Peak-to-Average Power Ratio (PAPR) e, consequentemente, limitações no desempenho dos amplificadores de potência (do inglês, Power Amplifiers (PAs)). Neste sentido, o aparecimento dos sistemas 5G têm suscitado grandes esperanças na redução dos problemas mencionados anteriormente, permitindo uma transmissão de dados mais eficiente.

Na simulação de um sistema de comunicações sem fios há dois domínios de simulação principais que se devem ter em consideração: a análise de sistema que permite o estudo de diferentes modulações e a análise de circuito que, por sua vez, permite o estudo de circuitos não-lineares, como é o caso dos PAs presentes nestes sistemas. Desta forma, torna-se importante unir estes dois domínios possibilitando a existência de uma ferramenta de simulação unificadora, à qual se atribuiu a designação de plataforma de simulação. Com a plataforma de simulação consegue-se, além de unir dois domínios até agora analisados separadamente, não só estudar o comportamento de um sistema 5G mas também de qualquer outro devido à sua adaptabilidade.

Assim, a análise de sistema é efetuada com o auxílio do software MATLAB, onde são estudados três tipos de modulação digital (modulação Quadrature Phase Shift Keying (QPSK), 16-Quadrature Amplitude Modulation (QAM) e 64-QAM) juntamente com a modulação OFDM. Para a análise de circuito recorreu-se ao software de simulação de circuitos Advanced Design System (ADS), onde se analisou o comportamento de dois tipos de PAs (um Classe B e um Doherty).

Como forma de teste do funcionamento da plataforma, foi efetuada a simulação para três configurações diferentes: Single-Input Single-Output (SISO), SISO em que se substituiu o modelo do Power Amplifier (PA) por uma aproximação polinomial e Alamouti 2x1 (caso particular da configuração Multiple-Input Single-Output (MISO)). Por último, os testes do funcionamento da plataforma de simulação são finalizados com a comparação das simulações recorrendo ao Bit Error Rate (BER).

keywords 5G, OFDM Modulation, Power Amplifier, Simulation Platform, SISO, Alamouti 2x1, BER.

abstract The current 4G systems are based on the OFDM modulation which, while providing great flexibility and intricacy to the multipath propagation inherent in wireless systems, it has great variations in their temporal envelope which causes high PAPR and, consequently, obstacles in the PAs performance. In this sense, the emergence of 5G systems has given rise high hopes of reducing the above mentioned problems of 4G systems, allowing more efficient data transmission.

In the simulation of wireless communication system there are two simulation domains that must be taken into account: the system analysis that allows the study of different modulations and the circuit analysis that, in turn, allows the study of nonlinear circuits, as is the case of PAs present in these systems. In this way, it becomes important to unite these two domains allowing the existence of a unifying simulation tool, which has been called the simulation platform. With this platform it is possible, besides joining two domains hitherto analyzed separately, not only to study the behaviour of a 5G system but also any other system due to its adaptability.

Thus, the system analysis is performed with the help of MATLAB software, in which three types of digital modulation (QPSK, 16-QAM and 64-QAM modulation) will be studied along with OFDM modulation. For the circuit analysis it was used the ADS circuit simulation software, which will analyze the behavior of two types of PAs (a Class B and a Doherty).

As a way of testing its functioning, the platform simulations were performed for three different configurations: SISO, SISO in which the PA model was replaced by a polynomial approximation, and Alamouti 2x1 (particular case of the MISO configuration). Finally, the tests of functioning of the simulation platform are finalized with the comparison of the simulations using the BER.

Contents

List of Figures

List of Tables

List of Acronyms

1G First Generation

2G Second Generation

3G Third Generation

3GPP 3rd Generation Partnership Project

4G Fourth Generation

5G Fifth Generation

ACPR Adjacent Channel Power Ratio

ADS Advanced Design System

AMPS Advanced Mobile Phone Systems

AWGN Additive White Gaussian Noise

BER Bit Error Rate

CDMA Code Division Multiple Access

CDMA2000 Code Division Multiple Access 2000

CP Cyclic Prefix

D-AMPS Digital Advanced Mobile Phone System

DC Direct Current

DFT Discrete Fourier Transform

DSPs Digital Signal Processors

EDGE Enhanced Data Rates for GSM Evolution

FCC Federal Communications Commision

FDD Frequency Division Duplex

FDM Frequency Division Multiplexing

FDMA Frequency Division Multiplexing Access

FFT Fast Fourier Transform

GPRS General Packet Radio Service

GSM Global System for Mobile Communications

HSPA High Speed Packet Access

ICI InterCarrier Interference

IDFT Inverse Discrete Fourier Transform

IEEE Institute of Electrical and Electronics Engineers

IFFT Inverse Fast Fourier Transform

ISI Inter-Symbol Interference

JTACS Japanese Total Access Communications Systems

LTE Long Term Evolution

MA Multiple Access

MCM Multi-Carrier Modulation

MIMO Multiple-Input Multiple-Output

MISO Multiple-Input Single-Output

MMS Multimedia Messages Service

NAMPS Narrowband AMPS

NMSE Normalised Mean Square Error

NMT Nordic Mobile Telephone

NTACS Narrowband Total Access Communications Systems

NTT Nippon Telegraph and Telephone

OFDM Orthogonal Frequency Division Multiplexing

OFDMA Orthogonal Frequency Division Multiplexing Access

PA Power Amplifier

PAE Power Added Efficiency

PAs Power Amplifiers

PAPR Peak-to-Average Power Ratio

PDC Pacific Digital Cellular

PDP Power Delay Profile

PSD Power Spectral Density

QAM Quadrature Amplitude Modulation

QoS Quality of Service

QPSK Quadrature Phase Shift Keying

RF Radio Frequency

SCM Single-Carrier Modulation

SC-FDMA Single Carrier Frequency Division Multiple Access

SIMO Single-Input Multiple-Output

SISO Single-Input Single-Output

SMS Short Message Service

SNR Signal-to-Noise Ratio

STBC Space-Time Block Code

S/P Serial-to-Parallel

TDD Time Division Duplex

TDMA Time Division Multiple Access

TD-SCDMA Time Division Synchronous CDMA

UMTS Universal Mobile Telecommunications System

WLAN Wireless Local Area Network

W-CDMA Wideband CDMA

ZFC Zero-Force Combining

ZP Zero Padding

Chapter 1

Introduction

This Chapter starts by presenting the background and evolution of cellular communications systems, followed by an introduction to the future deployments. This result in a better understanding of the technologies used for the implemented work. Then the motivations and objectives are identified. Finally, an outline of the document structure is made.

1.1 Background and Evolution of Cellular Communications Systems

At present, it is possible to enjoy a variety of mobile services with high mobility and/or transmission rate. In the following figure 1.1 the relationship between the mobile communication systems of different generations is exemplified.

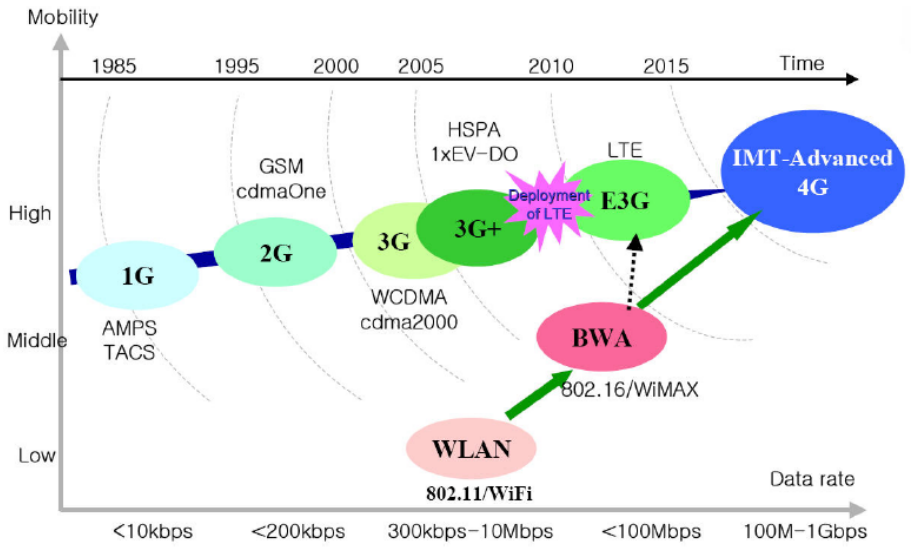

Figure 1.1: Progressive evolution of mobile communication systems, mobility and rate of transmission over the last decades [1].

The first commercial generation of cellular systems born in the 1980s and was characterized by the use of analog signals and the only service provided was voice with poor quality. The First Generation (1G) has been introduced in Japan by Nippon Telegraph and Telephone (NTT), in U.S.A. by the Advanced Mobile Phone Systems (AMPS) and in Europe for the Nordic Mobile Telephone (NMT). In finals of the 1980s, to improve capacity, appear in North America the Narrowband AMPS (NAMPS) and appear in Japan the Japanese Total Access Communications Systems (JTACS) and the Narrowband Total Access Communications Systems (NTACS) systems. All of these presented systems are incompatible with each other due to the way that they are developed in each country [2][3].

Second Generation (2G) systems emerged in 1990s and brought the digital area with more coverage and capacity than the last one. Comparatively to 1G, in 2G it was possible to send Short Message Service (SMS), Multimedia Messages Service (MMS) and this 2G brought the first data services. In this generation, the following techniques are deployed: Global System for Mobile Communications (GSM) in Europe, Digital Advanced Mobile Phone System (D-AMPS) IS-54 in the U.S.A., Code Division Multiple Access (CDMA) IS-95 by Qualcomm in U.S.A. and Pacific Digital Cellular (PDC) in Japan [3][4].

The GSM system is the most dominant system used and nowadays is implanted in more than 200 countries in worldwide. This system support transfer data rates up to 22.8 kb/s [5] and operates in the 900 MHz / 1800 MHz and 850 MHz / 1900 MHz band, depending on the part of the world considered as seen in figure 1.2. This system uses two Multiple Access (MA) technologies to accommodate multiple users on the same frequency: Frequency Division Multiplexing Access (FDMA) and Time Division Multiple Access (TDMA) where FDMA divides the spectrum in sub bands and TDMA divides the partition time in disjoints time slots.

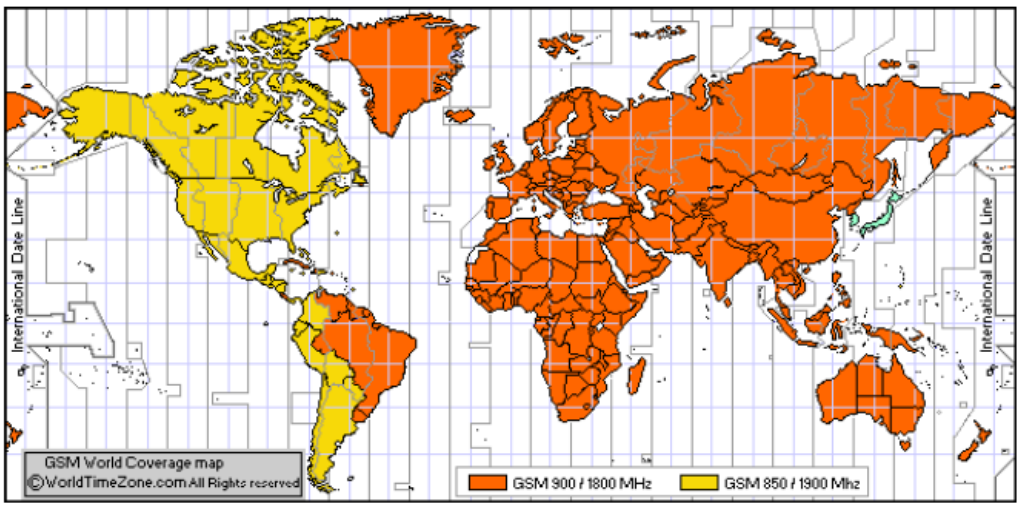

Figure 1.2: GSM Bands Information by Country Currently [6].

Toward Third Generation (3G), General Packet Radio Service (GPRS) has been created, in 2001, to upgrade GSM with the main objective to allow a higher data rate via packet switching. With this improvement, theoretically the data rates increase until 171.2 kb/s when is used a perfect channel. Nevertheless, in practice the data rates vary between 10 to 115 kb/s with an average of 40 kb/s. Another improvement system of the GSM is the Enhanced Data

Rates for GSM Evolution (EDGE) with data rates between 8 and 60 kb/s. With the increase of the mobile data services demand, emerged the necessity to develop another generation of mobile communications [3].

As a result, in 2000 was introduced the 3G with the following main objectives: achieve high data rates until 2 Mb/s, low latency, better Quality of Service (QoS), simplicity and scalability [7]. Nonetheless, 3G do not repeat the success of the previous generation 2G. Initially, two services have been created that accomplish that requirements: Universal Mobile Telecommunications System (UMTS) in Europe and Japan and Code Division Multiple Access 2000 (CDMA2000) in U.S.A.. UMTS support both Time Division Duplex (TDD) and Frequency Division Duplex (FDD) and include two standards: Wideband CDMA (W-CDMA) and High Speed Packet Access (HSPA). Another approach is Time Division Synchronous CDMA (TD-SCDMA) developed also in Europe [8]. The 3rd Generation Partnership Project (3GPP) is a corporation of 6 regions standards groups with the aim of control the evolution and migration of GSM systems, 3G systems and Long Term Evolution (LTE) systems presented below. Moreover, parallel developments such as the introduction of Wireless Local Area Network (WLAN) and selective use of wide area data networks offer potential alternative solutions for in-door applications [9].

The successor of 3G is the Fourth Generation (4G) that appeared in 2009 being marketed as LTE with the aim of give more data capacity with data rates more than 100 Mb/s and a low latency. This generation did not bring as principal objective the increase of the bit rate but the increase of the system capacity. The speed of the peak rate increase over the years where in 2009 was 50 Mb/s, in 2010 was 150 Mb/s and in 2015 was 1000 Mb/s. Nowadays, 4G LTE represents a generation in expansion that has 2.8 Billion of connections, more 0.1 Billion of connection than GSM that is the second system most used [10].

There are two different types of air interfaces used by LTE: one for downlink (from the base station to the terminal), and one for the uplink (from the terminal to the base station). For downlink LTE uses Orthogonal Frequency Division Multiplexing Access (OFDMA), contrary to CDMA and TDMA that have been used for the past mobile generations. The OFDMA scheme is also used in standards as Institute of Electrical and Electronics Engineers (IEEE) 802.11a/b/g, 802.16, HIPERLAN-2, DVB and DAB [11]. On the other hand, for uplink it uses Single Carrier Frequency Division Multiple Access (SC-FDMA), which in this case is better than OFDMA because it has a lower PAPR.

The continuous development of LTE led to the appearance of the LTE-Advanced, which started to be specified in release 10 of the 3rd Generation Partnership Project. On this development the aimed peak data rates were up to 3 Gbps in the downlink and up to 1.5 Gbps in the uplink. This can be achieved with some enhancements, like carrier aggregation, that increases the bandwidth to 100 MHz, and a higher number of antennas in the base station and mobile terminal [12]. The actual global statistics show that LTE was a big weight (38.5%) in the worldwide connection market, as shown in figure 1.3 and the perspective is to increase their influence, like in the last few years, up to approximately 2020, when the Fifth Generation (5G) will start expanding [10].

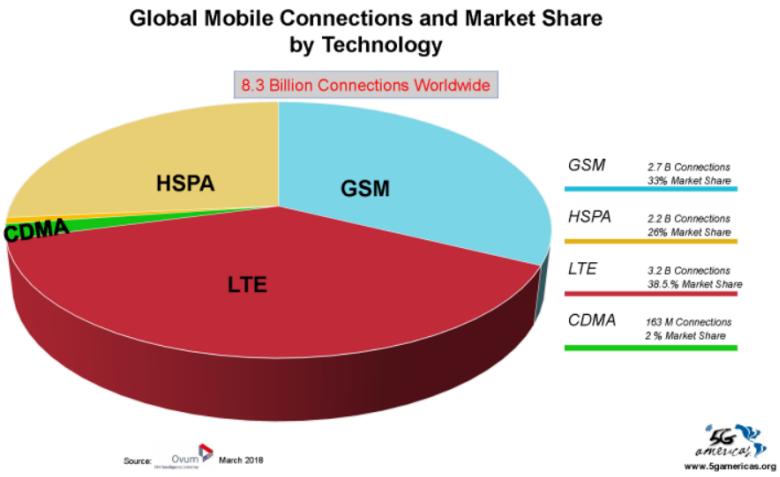

Figure 1.3: Global Statistics of Mobile Systems [10].

1.2 5G Systems

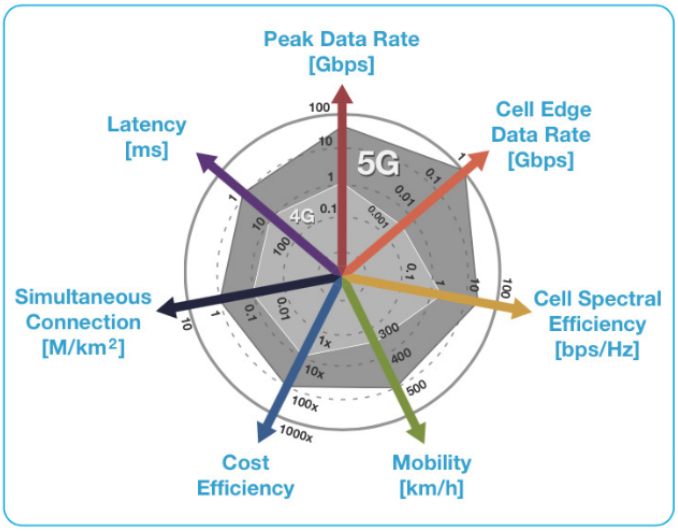

Figure 1.4: Key Parameters for 5G Mobile Communications [13].

The number of wireless network users are increasing day by day due to the services such as video, social networking, music and other interactive applications. As a result, the mobile data traffic has increased over the years and is required a new mobile system. 5G is the fifth generation mobile networks following 4G and it is designed to interconnect billions of objects, to provide extremely high data rates for multimedia applications and to handle the consequent surging mobile network traffic. An example of this demand for data rates and capacity is sport events with many people that share their experience instantly with video or images. It is expected that 5G should be available by 2020 and will achieve a minimum data rate of 1 Gb/s, 5 Gb/s for high mobility users and 50 Gb/s for pedestrian users [14][15]. These rise of number connections devices like smartphones, notebooks, tablets, smart TV's,

etc., make a high consumption on energy that has a great impact in the planet. The figure 1.4 shows the key parameters for 5G.

In figure 1.5 we can see the possible evolution of the systems since 2G until 5G for the next years. 2G and 3G will lose their influence and, as seen before, the 4G-LTE will have a big weight in the next years in the market of mobile telecommunications. Meanwhile, the 5G will have a fast adhesion after its release in 2020 [16].

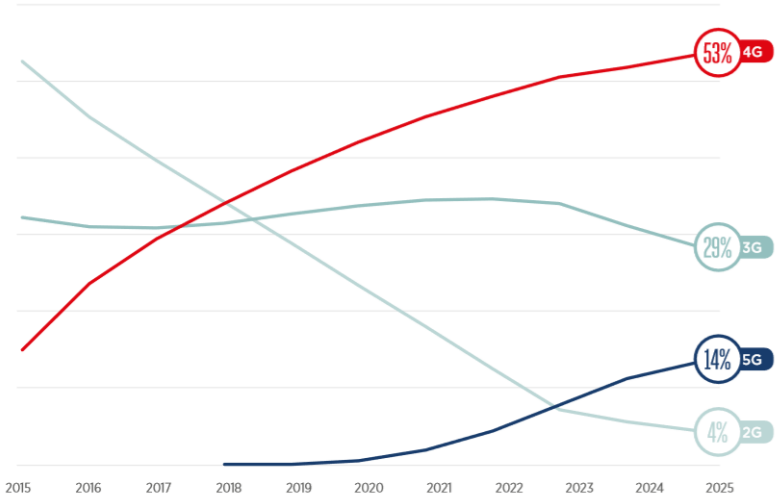

Figure 1.5: Global Mobile Adoption by Technology [16].

Concluding, the 2G is design for voice, 3G for data, 4G for large data stream applications such as music and video and 5G needs to be more efficient to handle not necessarily with a huge amount of data but with a huge number of connected devices.

1.3 Thesis Motivation

Over the years, engineering has been contributed substantially to the development of the various sector of society. As, for example, the robotization of assembly lines in the industry has saved resources and, mainly time that is translated into money, also the construction of increasingly stable and reliable bridges have allowed the advance in the construction area. Because the engineering is as comprehensive as the examples mentioned above, it is subdivided into branches, each one of them destined to the study, creation and improvement of its concepts.

In the electronics and telecommunications area, it is very common to find work groups where each one of them is focuses on a specific area (networks, fiber optics, signal processing, Radio Frequency (RF), etc). When it is necessary for two or more groups to come together in a given project, it becomes clear that the concepts of one group are foreign to the remaining ones, creating some embarrassment and loss of time in their understanding. Due to this, in certain situations it is important that there is a link between the various groups often through the creation of platforms that unify the project in question, giving the idea of a higher level of abstraction.

Nowadays, the urge of 5G systems (transmission in the order of Gigabit per second) has made it possible to satisfy the multiples requests of both users and operators. Current

4G systems are based on OFDM modulation that allows great flexibility and robustness to multipath propagation inherent to wireless systems. However, the major problem in using signals with OFDM modulation is that their temporal envelope is not constant, generating signals in which their mean power is significantly lower than their peak, which causes a high PAPR and consequently barriers in PAs performance.

As the demand for the RF spectrum increases, high-speed data transmission would benefit from bandwidth-efficient modulation schemes. In addition, in wireless applications, portability demands a highly power-efficient system to increase the battery lifetime or the available talk-time in cellular systems, which is heavily degraded due to the power consumption of PAs.

If one looks at the study typically made to a wireless communications system, it is verified that the system analysis is carried out in which it is possible to study the impact of the type of modulation in the data transmission. We are living in an era of communication wherein we can easily transfer any information (video, audio and other data) in the form of electrical signals to any other device or destined area. Although it is common in my perceptual experience that sending or receiving signals or data is simple, but it involves quite complex procedures, possibilities and scenarios within the communication systems. Modulation plays a key role in communication system to encode information digitally in analog world. It is very important to modulate the signals before sending them to the receiver section for larger distance transfer, accurate data transfer and low-noise data reception. Over the years, better modulations have appeared being more and more robust able to eliminate the influence of the noise in the receiver [17][18][19].

However, this system analysis does not contain the influence that a PA, nonlinear circuit, has on the overall performance of the system. With the aim of creating PAs that simultaneously possess great linearity and efficiency, the stimulus on their investigation has led to the appearance of more profitable configurations [20][21][22].

Due to this, it is necessary to introduce the concepts of circuit analysis (another domain) in the system to be simulated, in order to obtain an overall performance of the system more in accordance with what happens in reality. For this, it is necessary to join these two domains (system analysis and circuit analysis) that are normally analyzed separately. To this end, the creation of a platform that allows to study both previously described cases would be pertinent.

1.4 Thesis Objectives

First and foremost, the objective of this thesis is to create a simulation platform that allow us to simulate the behavior of 5G systems.

In order to test different transmission alternatives in wireless communication systems, the platform will enable us to simulate, in addition to the SISO configuration, a particular case of the MISO configuration, more properly the Alamouti 2x1. Then, in order to introduce the concept of polynomial approximation into the behavior of the PA model, a new configuration will be tested in which this model is replaced by a polynomial that approaches its behavior, thus creating an alternative to the SISO configuration.

In addition, the platform will provide us the chance to choose the type of modulation used (QPSK, 16-QAM or 64-QAM), the type of PA used in the transmitter as well as the bandwidth of the signal to be simulated.

Finally, with the aim of understanding the effect that the different alternatives have on the

performance of the system, calculated through the BER, the simulations will be performed based on two PAs with different configurations.

1.5 Thesis Structure

The primary objectives are achieved through five Chapters in the following order:

To understand the role of the communications system blocks used in the simulation, we start providing necessary background on the system theory in Chapter 2. The modulation types and channel models used are also entered here. Besides that, it is introduced the concept of multiple antenna system addressing the spatial diversity in the transmitter, more properly Alamouti 2x1.

Chapter 3 describes the creation of the platform used. In order to understand the effect that the characteristics of the different PAs have on the performance of the system, this Chapter presents the main characteristics of PAs used in simulation.

Chapter 4 introduces various simulations performed using the ADS circuit simulation software and MATLAB software. In this Chapter, it is explained the entire simulation procedure and the results are below the explanation.

Finally, Chapter 5 concludes with a summary of results and suggestions for future work.

Chapter 2

Wireless Communications System

2.1 Introduction

The simple scheme of a digital communications system consists of a transmitter, a channel and a receiver [23], each of which is illustrated by the respective blocks as depicted in figure 2.1.

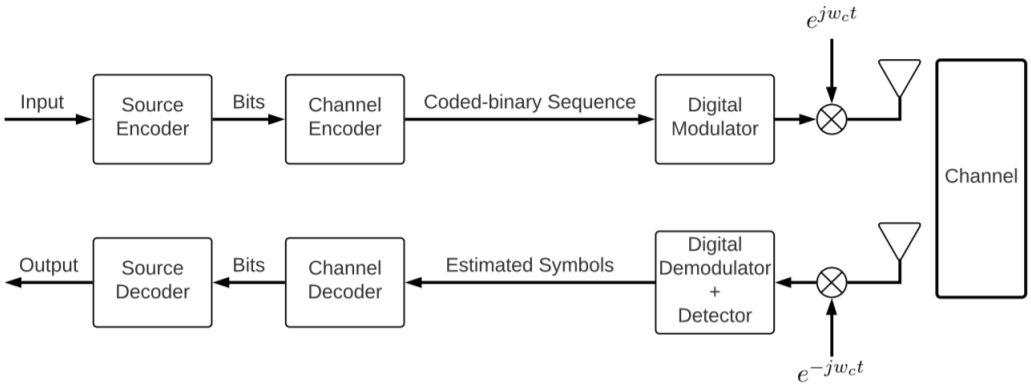

Figure 2.1: Basic building blocks of a wireless communications system.

Normally, the source encoder converts the input information, which can be in form of voice, video or digital data to a stream of bits. This conversion should be as efficient as possible by using as few bits as possible. Then the resulting sequence of binary digits are coded by the channel encoder which introduces redundancy in sequence that can be used at the receiver to combat the noise and interference introduced by the channel. After that, the binary code sequence is transformed into signal waveforms by the digital modulator. In wireless systems, depending on the application, the signals must be transmitted over a particular frequency band. Now, the modulated signal waveforms are up-converted to the desired frequency before being sent over the antenna. The communication channel is the physical medium through which the signal passes from the transmitter to the receiver. Therefore, the channel distorts the transmitted signal due to various factors. At the receiver, the corrupted signals received by the antenna pass through a set of blocks that undo the processing performed on the signals at the transmitter in other to recover the source information. Thus, the received signal waveforms are down-converted back to baseband and thereon pass through the demodulator

and detector that convert the analog signals into a sequence of estimated symbols. Finally, the channel decoder rebuilds the source message as faithfully as possible [24].

This Chapter starts by introducing the fundamental three metrics that quantify the performance of wireless systems (BER, spectral and power efficiency). Thereafter, three kinds of digital modulator (QPSK, 16-QAM and 64-QAM) and the (OFDM) modulation are presented. In addition, two channel models (Additive White Gaussian Noise (AWGN) channel and Rayleigh fading wireless channel) are also presented that will be used in simulation of the wireless communications system. Finally, a particular case of multiple antenna system, more specifically a MISO system, is implemented in order to introduce the concept of diversity.

2.2 Performance Measurement Metrics

After up-conversion, modulated signal waveforms that will be sent over the antenna normally have a high frequency, designated RF. So, in RF design, there are three parameters that are useful in assessing the performance of a digital modulation and demodulation technique: BER, spectral and power efficiency.

2.2.1 Bit Error Rate (BER)

When data is transmitted over a data link, there is a possibility of external effects causing errors that might be introduced into the system. If errors are introduced into the data, the integrity of the system may be compromised. For this reason, it is necessary to access the performance of the system, and BER provides an ideal way in which this can be achieved. This is measured by the system performance metric, BER defined as the average number of erroneous bits observed at the output of the detector divided by the total number of bits received in a unit of time. In digital modulation, BER is expressed in terms of the Signal-to-Noise Ratio (SNR).

Signal-to-Noise Ratio (SNR) SNR is a measure that compares the level of a desired signal to the level of background noise. SNR is defined as the ratio of signal power to the noise power, often expressed in decibels.

2.2.2 Spectral efficiency

Another important characteristic of a modulation scheme is the bandwidth which is occupied by the modulated signal for a certain bandwidth of the baseband signal. The parameter that quantifies such a characterization is bandwidth efficiency (bps/Hz), defined as the data rate (bits per second) over the bandwidth of the modulated signal (Hertz). In band-limited channel applications, such as wireless networks, bandwidth efficiency plays a key criterion [24].

2.2.3 Power efficiency

The error probability of a channel is a function of the Q-function whose argument is $D_{min}/2\sigma$, where $\sigma^2 = N_0/2$ is the noise variance. More specifically, the higher the minimum-distance, D_{min}, between the symbols in the constellation is, the better performance. However, higher D_{min} is achieved at the cost of requiring more signal energy, which is a limited source

and should be as low as possible. This presents the conflicting tradeoff between D_{min} and the signal energy, E_s. Asymptotic power efficiency γ is defined to express "how efficiently a modulation scheme makes use of the available signal energy to generate a given minimum distance" [25] by

$$\gamma = \frac{D_{min}^2}{4E_s} \tag{2.1}$$

Thus, a modulation scheme with a higher power efficiency results in lower error probability with optimum tradeoff between D_{min} and E_s.

2.3 Digital Modulator

In this section, different types of signal modulations are compared in terms of performance, taking into account the parameters already described, considering a rectangular constellation.

2.3.1 QPSK or 4-QAM

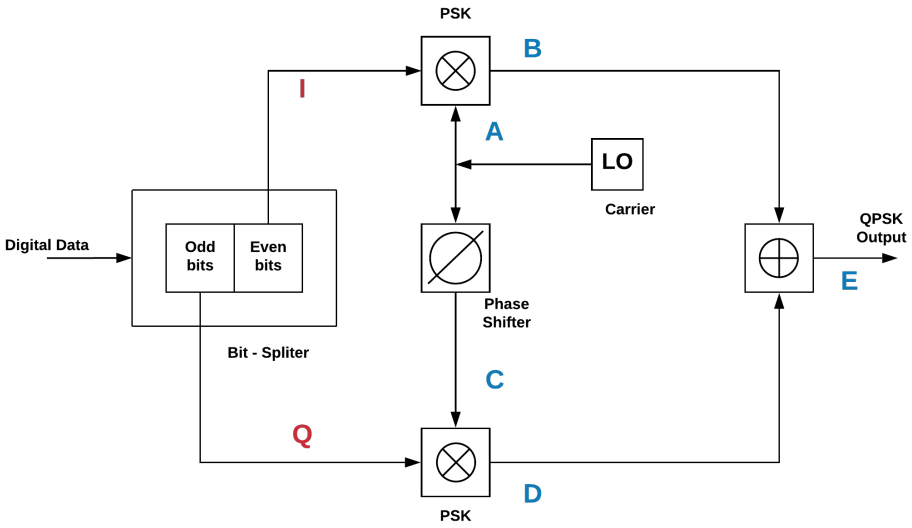

Figure 2.2: QPSK modulator.

At the input of the modulator, the digital data is separated into two channels called I and Q - I/Q Modulator by a "bit-splitter". In an I/Q Modulator, two bits are transmitted simultaneously, one per channel wherein each channel modulates a carrier (two carrier frequencies are the same). Thus, the two carriers are simply added together for transmission and, as they have the same carrier frequency, they occupy the same portion of the radio frequency spectrum. Hence, the two sets of signals would be irretrievably mixed and, in the reception, the recovery of the signal would be complicated. Therefore, the required ninety degrees of

phase separation between the carriers allows the sidebands to be separated by the receiver using phase discrimination, as shown in figure 2.2.

In the QPSK modulation, the carrier signal phase can take four possible values as

$$\varphi_i(t) = (2i-1)\frac{\pi}{4} \qquad i = 1, 2, 3, 4 \tag{2.2}$$

wherein the QPSK signal has four possible symbols, each of them carries two bits that are called dibits. These dibits and their corresponding signal phases are shown in table 2.1.

Information of dibits	Phase of QPSK signal
00	$\pi/4$
10	$3\pi/4$
11	$5\pi/4$
01	$7\pi/4$

Table 2.1: Signal space characteristic of QPSK.

Signals A, B, C and D of figure 2.2 can be written as

$$Signal_A = cos\Big[2\pi f_c t\Big] \tag{2.3}$$

$$Signal_B = \sqrt{\frac{2E_s}{T_s}} cos\Big[\varphi_i(t)\Big] cos\Big[2\pi f_c t\Big] \tag{2.4}$$

$$Signal_C = -sin\Big[2\pi f_c t\Big] \tag{2.5}$$

$$Signal_D = -\sqrt{\frac{2E_s}{T_s}} sin\Big[\varphi_i(t)\Big] sin\Big[2\pi f_c t\Big] \tag{2.6}$$

where E_s refers to transmitted signal energy per symbol, T_s refers to symbol duration and f_c is the carrier frequency.

Using equation 2.4 and equation 2.6, the QPSK signal can be expressed as

$$\begin{aligned} s_i(t) &= \sqrt{\frac{2E_s}{T_s}} cos\Big[\varphi_i(t)\Big] cos\Big[2\pi f_c t\Big] - \sqrt{\frac{2E_s}{T_s}} sin\Big[\varphi_i(t)\Big] sin\Big[2\pi f_c t\Big] \\ &= \sqrt{\frac{2E_s}{T_s}} cos\Big[(2i-1)\frac{\pi}{4}\Big] cos\Big[2\pi f_c t\Big] \\ &\quad -\sqrt{\frac{2E_s}{T_s}} sin\Big[(2i-1)\frac{\pi}{4}\Big] sin\Big[2\pi f_c t\Big] \qquad 0 \le t \le T_s, i = 1, 2, 3, 4 \end{aligned} \tag{2.7}$$

From equation 2.7 it is possible to construct the constellation which is the simple plot of the symbols on the rectangular space. The constellation shows the phases of the symbols

and their relationship to each other. The x-axis projection for each symbol is the I channel amplitude and the y-axis projection is the Q channel amplitude. The constellation diagram is always done at baseband, i.e. f_c=0, so the signal is just a point. For the first symbol, which lies in the first quadrant, the I and Q values are both +0.707107 (mean power of 1.0). The same goes for the others as shown in table 2.2 [26].

Symbol	Bits	s(t)	Phase (Deg.)	I	Q
S_1	00	$\sqrt{\frac{2E_s}{T_s}}cos\left[2\pi f_c t + \pi/4\right]$	45°	0.707107	0.70710
S_2	10	$\sqrt{\frac{2E_s}{T_s}}cos\left[2\pi f_c t + 3\pi/4\right]$	135°	-0.70710	0.70710
S_3	11	$\sqrt{\frac{2E_s}{T_s}}cos\left[2\pi f_c t + 5\pi/4\right]$	225°	-0.70710	-0.70710
S_4	01	$\sqrt{\frac{2E_s}{T_s}}cos\left[2\pi f_c t + 7\pi/4\right]$	315°	0.70710	-0.70710

Table 2.2: Mapping rules for QPSK.

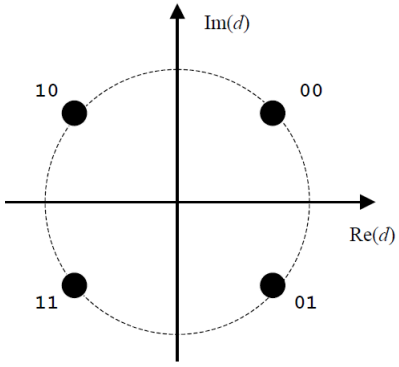

Figure 2.3: Diagram of a QPSK mapping [27].

Although the QPSK is considered as a constant envelope signal according to the literature, it is not technically a constant envelope signal because of its discontinuous phase shift, such as, 180° phase shift. This phase shift is the major problem of the QPSK, which means that, the larger transition is a source of trouble for the amplifier, which increases the spectral side lobe. Thus, to eliminate large transitions, some modulations have been created.

2.3.2 M-QAM (M>4)

Different from the QPSK modulation, where only the phase of the symbol varies, in the M-QAM modulation (M>4) not just the phase (red) of the symbol varies but also the amplitude (blue), as shown in equation 2.8. In the QPSK, all symbols sat in a circle so they all had the same amplitude. Here the points closer to the axes have lesser amplitudes and hence lesser energy than some others. We can compute the x and y axis values of the constellation depending on the total power we want. Now, we have M symbols in the constellation, each one with log2(M) bits.

$$s(t) = \sqrt{\frac{2E_s}{T_s}}cos\left[\theta(t)\right]cos\left[2\pi f_c t\right] - \sqrt{\frac{2E_s}{T_s}}sin\left[\theta(t)\right]sin\left[2\pi f_c t\right] \qquad 0 \leq t \leq T_s \quad (2.8)$$

2.3.2.1 16-QAM

As it was previously stated, there is not only phase modulation but also amplitude modulation. In this implementation, the constellation has 16 symbols, each one of them with 4 bits (log2(16)), figure 2.4, that are transmitted in parallel.

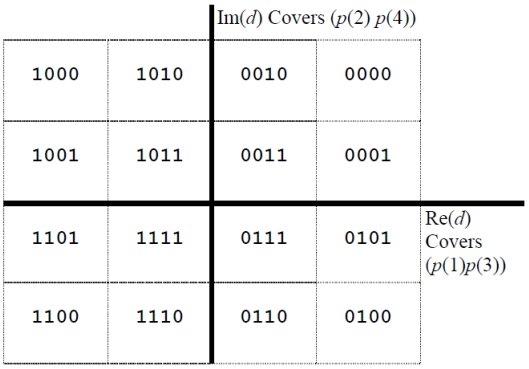

Figure 2.4: Diagram of a 16-QAM mapping [27].

Bits	I	Q
0000	0.9487	0.9487
0001	0.9487	0.3162
0010	0.3162	0.9487
0011	0.3162	0.3162
0100	0.9487	-0.9487
0101	0.9487	-0.3162
0110	0.3162	-0.9487
0111	0.3162	-0.9487
1000	-0.9487	0.9487
1001	-0.9487	0.3162
1010	-0.3162	0.9487
1011	-0.3162	0.3162
1100	-0.9487	-0.9487
1101	-0.9487	-0.3162
1110	-0.3162	-0.9487
1111	-0.3162	-0.3162

Table 2.3: Mapping rules for 16-QAM (mean power of 1.0).

2.3.2.2 64-QAM

The 64-QAM modulation is implemented in the same way as the 16-QAM, where the only difference resides in the number of the bits that can be transmit in parallel, i.e the constellation of the 64-QAM modulation has 64 symbols, each one of them with 6 bits (log2(64)), figure 2.5. With this implementation, it is possible to send more information than with the previous

modulations, but the distance between symbols in the constellation is shorter than before, contributing to the increase of errors when the calculation of the BER is in the receiver.

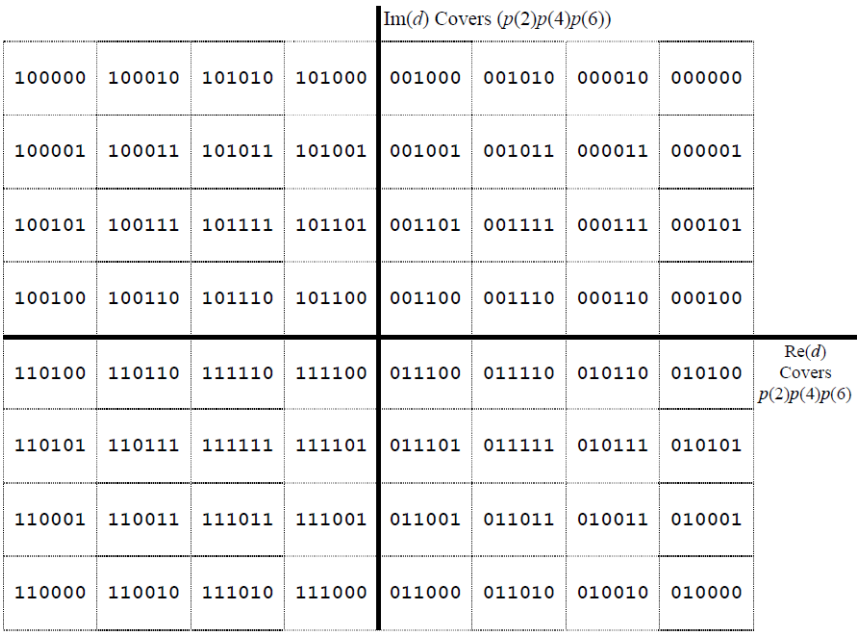

Figure 2.5: Diagram of a 64-QAM mapping [27].

Modulation	Bit Rate (bit/sec)	Bandwidth (Hz)	Spectral Efficiency (bit/sec/Hz)
QPSK	$2/T_s$	$1/T_s$	2
16-QAM	$4/T_s$	$1/T_s$	4
64-QAM	$6/T_s$	$1/T_s$	6

Table 2.4: Comparison between QPSK, 16-QAM and 64-QAM modulation.

According to table 2.4 we can see that with the increase in the number of symbols in the constellation, the bit rate increases, which in turn increases the spectral efficiency. Thus, in the 64-QAM we have a higher bit rate, being able to send 6 bits simultaneously. On the other hand, the fact that symbols are closer together causes the probability of error in the receiver to be greater.

Equation 2.1 proves this. As the distance between symbols d_{min} increases, power efficiency increases, which tells us that the probability of error is lower. The same thing happens in reverse: decreasing the distance between symbols decreases power efficiency and in turn increases the probability of error.

Since the bandwidth used for three modulations was the same, the bandwidth efficiency will be quantified by the spectral efficiency, as we have seen, the larger the number of symbols present in the constellation, the larger the spectral efficiency.

2.4 OFDM Modulator

In recent 4G systems, one of the most important points in the physical layer of a wireless communication system is the technique used to perform data allocation along the radio frequency resources. In LTE downlink, the technology used to modulate the radio frequency resources with input data is called OFDM.

OFDM is not only a simple scheme used as a digital Multi-Carrier Modulation (MCM) method, where a single data stream is transmitted over a number of lower rate sub-carriers, but it is also one of the most popular and effective technologies used in current communication systems [28].

2.4.1 Origin of OFDM

Throughout the years, several techniques has been used for the transmission of data, always with the aim of transmitting the greatest number of data in the shortest possible time. Initially in a Single-Carrier Modulation (SCM) system a high bit rate sequence of input is used to modulate just one carrier, occupying all available spectrum. Thus, it is well known in this modulation that the sending of data is limited and not at all desired. The appearance of MCM culminates this failure, in which the high bit rate sequence of input is divided in several low bit rate sequences. Therefore, each one of these lower rate sequences is used to modulate a particular sub-carrier. In this way, the spectrum is divided equally by the sub-carriers.

Figure 2.6 compares an SCM and an MCM, where B_{SCM} and B_{MCM} denote the bandwidths of transmitted SCM and MCM signals, respectively. Furthermore, in MCM f_k, $F_k(f;t)$, N_{SC} and $\triangle f$ represent the frequency of the kth sub-carrier, the frequency spectrum of pulse waveform of the kth sub-carrier, the total number of sub-carriers, and the sub-carrier separation, respectively.

From figure 2.6 and figure 2.7 it can be seen that, as the symbol rate increases, the signal bandwidth becomes larger. When the signal bandwidth becomes larger than the coherence bandwidth in the wireless channel, the link suffers from multipath fading leading to the Inter-Symbol Interference (ISI), further increasing the complexity of the equalizer to eliminate the ISI. So, in wireless communications the frequency limitation may arise because of the multipath fading which causes frequency selectivity. As a result, MCM has good performance in frequency selective fading channels. Moreover, MCM has low complexity of baseband receiver because it requires simple equalizers in frequency domain, good spectral properties and is compatible with multiple antenna technologies, whereas SCM requires complicated adaptive equalization.

It has been seen here that MCM has great advantages compared to SCM. However, channels must be separated by strips of unused bandwidth to prevent inter-channel cross talk. The previous solution is classical FDMA, represented in figure 2.8(a).

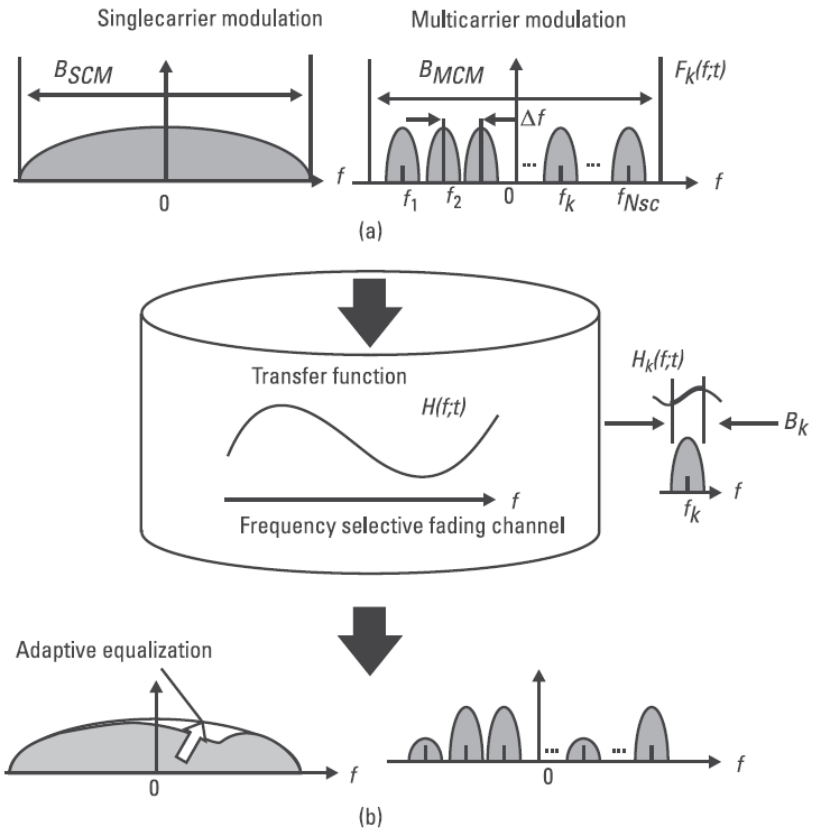

Figure 2.6: Comparison of SCM and MCM: a) frequency spectra of transmitted signals; and b) frequency spectra of received signals [29].

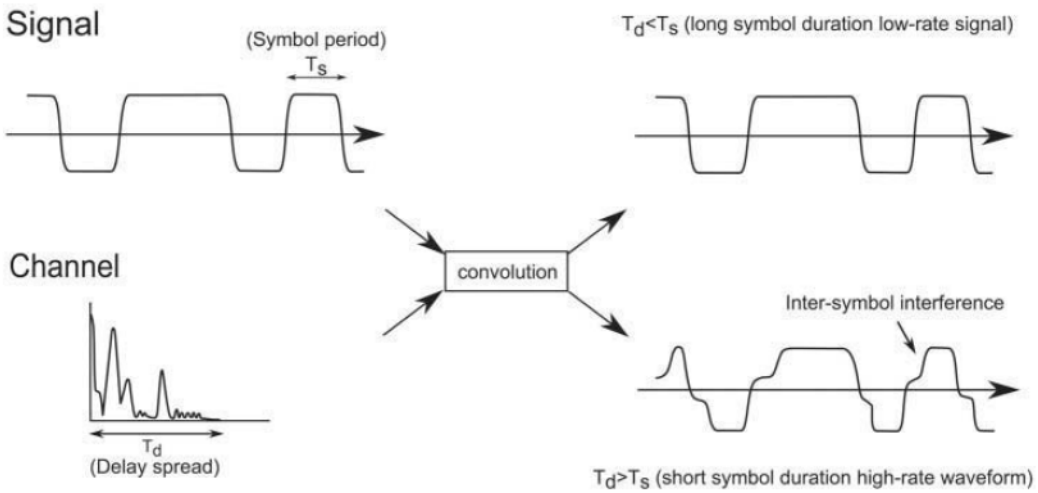

Figure 2.7: Effect of channel on signals with short and long symbol duration [30].

where T_s and T_d denote the symbol period and the delay spreed, respectively.

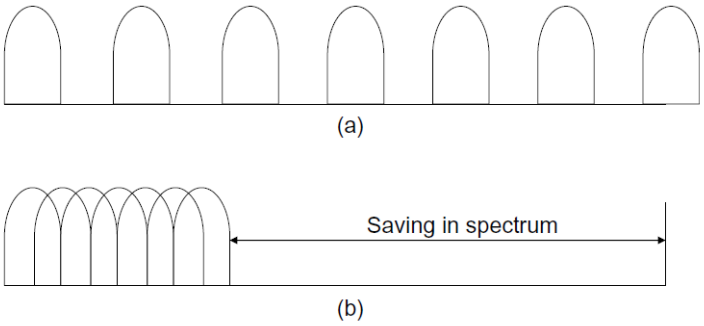

Figure 2.8: Spectral efficiency of OFDM compared to classical multicarrier modulation: (a) classical multicarrier system spectrum; (b) OFDM system spectrum [30].

So, inserting unused bandwidth in this implementation has one problem when the number of sub-carriers increases, because the total bandwidth increase, consequently decreases the spectral efficiency. The processing power of modern Digital Signal Processors (DSPs) has increased remarkably, opening the way for OFDM to be used in the LTE downlink, where not only the receivers have low complexity but also the ability of OFDM to be adapted in a straightforward manner to operate in different channel bandwidths according to spectrum availability [30]. Figure 2.8 shows the difference between a Frequency Division Multiplexing (FDM) system, figure 2.8(a), and an OFDM system, figure 2.8(b), where the channels are orthogonal [31] to each other.

2.4.2 OFDM Principles

According to the authors' best knowledge, the first OFDM scheme dates back to 1960 when Robert W. Chang published his pioneering work on the synthesis of band-limited orthogonal signals for multi-channel data transmission [32], although before that other systems for military applications such as KINEPLEX [33] and KATHRYN [34], were developed. While in these systems non-overlapped band-limited orthogonal signals were used because they did not have the capacity to control frequencies of sub-carriers local oscillators and the detection of sub-carrier signals with analog filters, in OFDM this problem has been solved and uses overlapped band-limited orthogonal signals.

As was previously stated, a high rate data stream typically faces the problem of having a symbol period T_s much smaller than the channel delay spread T_d if it is transmitted serially. This generates ISI which can only be undone by means of a complex equalization procedure. Ordinarily the equalization complexity grows with the square of the channel impulse response length.

Because of that, in OFDM the high rate stream of data symbols Serial-to-Parallel (S/P) is converted for modulation of the parallel sub-carriers. This increases the symbol duration on each sub-carrier by a factor of approximately the number of sub-carriers, such that it becomes significantly longer than the channel delay spread.

OFDM transmitter principle is represented in figure 2.9. After the S/P conversion, each sub-carrier is modulated on one different frequency. Separation between frequencies is equal to the total bandwidth of the single carrier divide by the number os sub-carriers. If this separation is less than the coherence band, it can be said that the channel is flat fading, no

ISI.

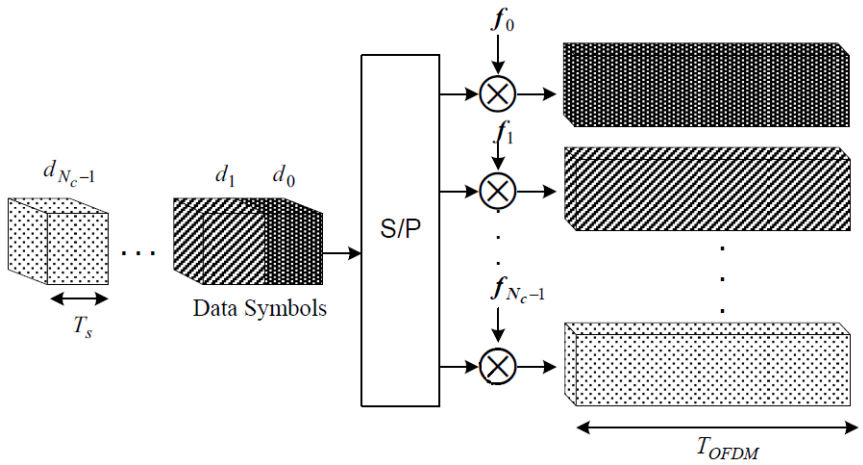

Figure 2.9: OFDM principle [35].

Considering that N_c is the number of sub-carriers, T_s is the symbol period, Δf_c is the separation between sub-carriers and T_{OFDM} is the OFDM symbol duration, you can write the following:

$$T_{OFDM} = N_c T_s \tag{2.9}$$

$$\Delta f_c = \frac{1}{T_{OFDM}} \tag{2.10}$$

$$f_k = f_c + k\Delta f \tag{2.11}$$

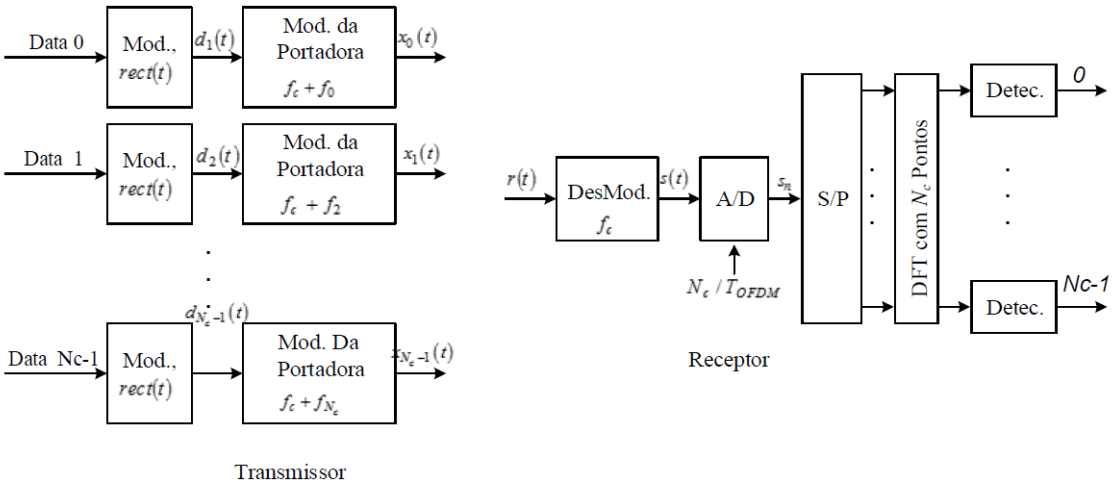

Figure 2.10: OFDM modulation and demodulation [35].

With the previous structure, the spectrum of each sub-carrier can be overlapping with another sub-carrier, as is possible to see in figure 2.8(b). OFDM principle inserts the orthogonality between sub-carriers, allowing it to send more information on a smaller bandwidth, but this implementation which resorts to a bank of modulators is quite complex, figure 2.10. In the next point, the way to work around this problem will be presented, using the Fast Fourier Transform (FFT) and Inverse Fast Fourier Transform (IFFT) algorithm.

2.4.2.1 OFDM Modulation and Demodulation

Considering that $X_l[k]$ denote the lth transmit symbol at the kth sub-carrier, l = 0,1,2,..., k=0,1,2,...,N-1. Let $\psi_{l.k}(t)$ denote the lth OFDM signal at the kth sub-carrier, which is given as

$$\psi_{l.k}(t) = \begin{cases} e^{j2\pi f_k(t-lT_{OFDM})}, & 0 < t \leq T_{OFDM} \\ 0, & \text{elsewhere} \end{cases} \tag{2.12}$$

Then the passband and baseband OFDM signals in the continuous-time domain can be expressed respectively as

$$x_l(t) = \text{Re}\left(\frac{1}{T_{OFDM}} \sum_{l=0}^{\infty} \left(\sum_{k=0}^{N_c-1} X_l[k]\psi_{l.k}(t) \right) \right) \tag{2.13}$$

So, $x_l(t)$ can be written as

$$x_l(t) = \sum_{l=0}^{\infty} \sum_{k=0}^{N_c-1} X_l[k] e^{j2\pi f_k(t-lT_{OFDM})} \tag{2.14}$$

If the continuous-time baseband OFDM signal, equation 2.14, is sampled at t = lT_{sym} + nT_s with $T_s = T_{sym}$/N and f_k = k/T_{sym}, a discrete-time OFDM symbol is produced as

$$x_l[n] = \sum_{k=0}^{N_c-1} X_l[k] e^{j2\pi kn/N} \quad \text{for} \quad n = 0, 1, ..., N_c - 1 \tag{2.15}$$

From equation 2.15 it is possible to conclude that the OFDM modulation is the same as doing the N-point Inverse Discrete Fourier Transform (IDFT) of data symbols $\left(X_l[k] \right)_{k=0}^{N_c-1}$ and can be computed efficiently by using the IFFT algorithm, figure 2.11(b).

Now, considering that the received baseband OFDM symbol

$$y_l(t) = \sum_{k=0}^{N_c-1} X_l[k] e^{j2\pi f_k(t-lT_{OFDM})}, \quad lT_{OFDM} < t \leq lT_{OFDM} + nT_s, \tag{2.16}$$

from which the transmitted symbol X_l[k] can be reconstructed by the orthogonality among the sub-carriers, the following is true.

$$
\begin{aligned}
Y_l[k] &= \frac{1}{T_{OFDM}} \int_{-\infty}^{+\infty} y_l(t) e^{-j2\pi k f_k (t - lT_{OFDM})} dt \\
&= \frac{1}{T_{OFDM}} \int_{-\infty}^{+\infty} \left(\sum_{i=0}^{N_c-1} X_l[i] e^{j2\pi f_i (t - lT_{OFDM})} \right) e^{-j2\pi f_k (t - lT_{OFDM})} dt \\
&= \sum_{i=0}^{N_c-1} X_l[i] \left(\frac{1}{T_{OFDM}} \int_{0}^{T_{OFDM}} e^{j2\pi (f_i - f_k)(t - lT_{OFDM})} \right) = X_l[k]
\end{aligned} \tag{2.17}
$$

where the effects of channel and noise are not taken into account. Let $\left(y_l[n] \right)_{n=0}^{N_c-1}$ be the sample values of the received OFDM symbol y_l(t) at t = lT_{OFDM} + nT_s. Then, the integration in the modulation process of equation 2.17 can be represented in the discrete time as follows:

$$
\begin{aligned}
Y_l[k] &= \sum_{n=0}^{N_c-1} y_l[n] e^{-j2\pi kn/N} \\
&= \sum_{n=0}^{N_c-1} \left(\frac{1}{N} \sum_{i=0}^{N_c-1} X_l[i] e^{j2\pi in/N} \right) e^{-j2\pi kn/N} \\
&= \frac{1}{N} \sum_{n=0}^{N_c-1} \sum_{i=0}^{N_c-1} X_l[i] e^{j2\pi (i-k)n/N} = X_l[k]
\end{aligned} \tag{2.18}
$$

Note that equation 2.18 is the N-point Discrete Fourier Transform (DFT) of $\left(y_l[n] \right)_{n=0}^{N_c-1}$ and can be computed efficiently by using the FFT algorithm.

Figure 2.12(a) shows an example of OFDM modulation and demodulation for 6 sub-carriers. Note that the original symbol X[k] has a duration of T_s, but its length has been extended to $T_{OFDM} = NT_s$ by transmitting N symbols in a parallel way. Figure 2.12(b) illustrates a typical realization of orthogonality among all sub-carriers.

According to the above discussion, it is possible to conclude that this multi-carrier modulation can be implemented by IFFT and FFT in the transmitter and receiver, respectively. With this technique it is possible to reduce complexity and increase efficiency.

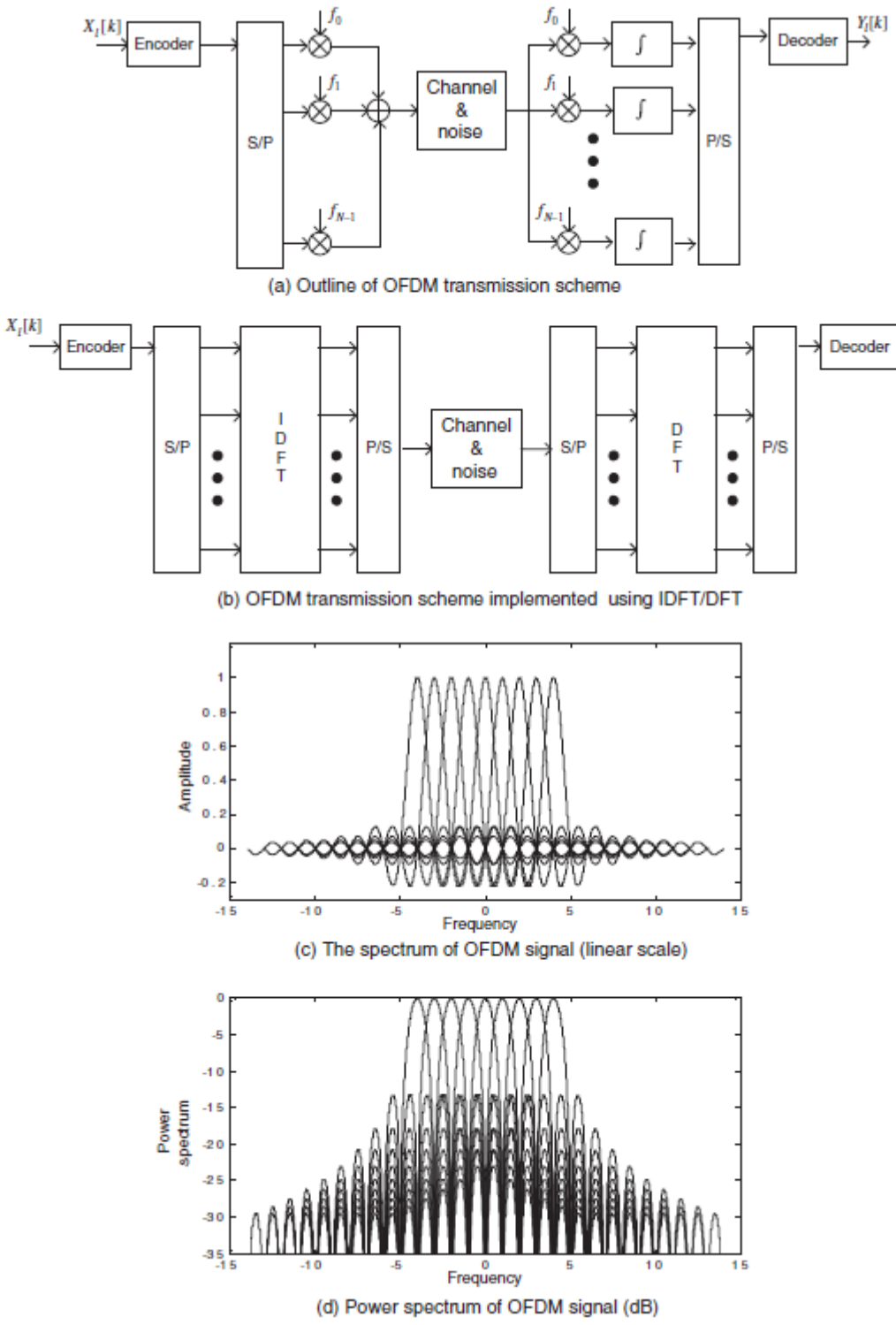

Figure 2.11: Structure and spectral characteristic of OFDM transmission scheme [31].

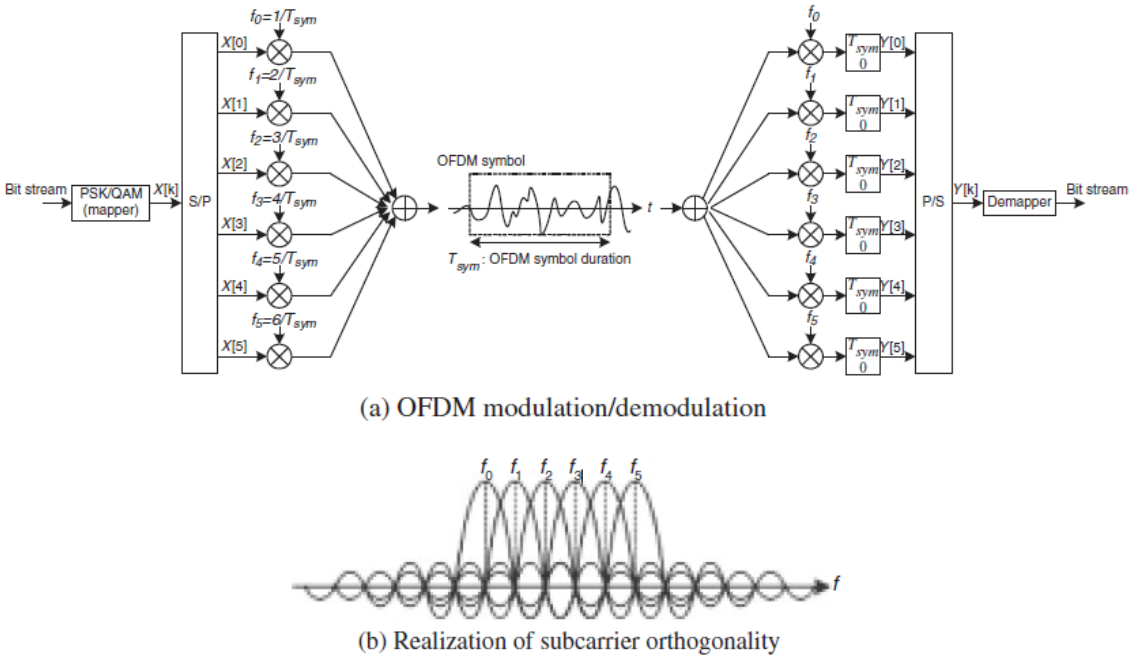

Figure 2.12: Illustrative block diagram of OFDM modulation and demodulation (N_c=6) [31].

2.4.2.2 OFDM Cyclic Prefix (CP)

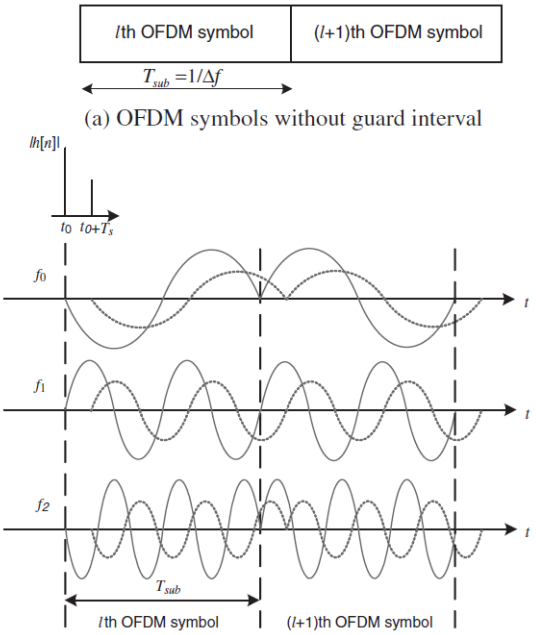

Figure 2.13: Effect of a multipath channel on the received signal without guard interval [31].

The next key operation in the generation of an OFDM signal is the creation of a guard period at the beginning of each OFDM symbol to eliminate the remaining impact of ISI caused by multipath propagation. In order to understand an ISI effect of the multipath channel, figure 2.13 is placed.

Figure 2.13 illustrates an ISI effect of the multipath channel over two consecutive OFDM symbols. Although the effect of the multipath fading channel is greatly reduced on the OFDM symbol, as it was seen before, its effect still remains as a harmful factor that may break the orthogonality among the sub-carriers. As shown in figure 2.13(b), the first received symbol is mixed up with the second received symbol, which is subject to the ISI. So, it is obvious that all sub-carriers are no longer orthogonal over the duration of each OFDM symbol.

To solve this problem, there are two possibilities: one is the Zero Padding (ZP) that pads the guard interval with zeros, and the other is the cyclic extension of the OFDM symbol with Cyclic Prefix (CP). In this work the CP is used.

So, if the channel has multipath then the transmitted OFDM symbols will not be confined to the slot of duration OFDM (T_{OFDM}) but will spread up to $T_{OFDM} + \tau_{max}$, where τ_{max} represents the max path delay, shown in figure 2.14.

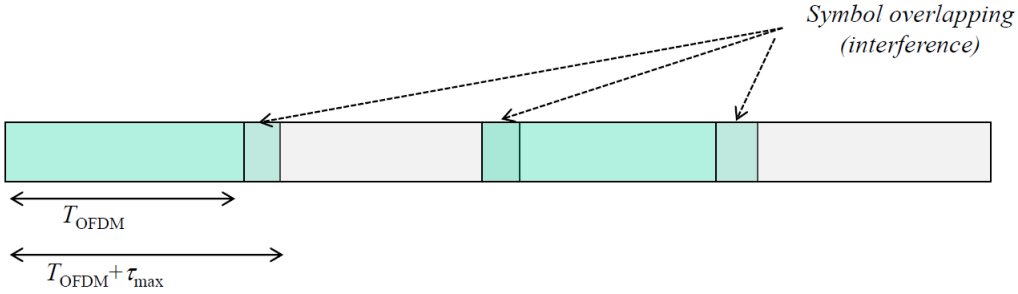

Figure 2.14: Overlapping of OFDM symbols [35].

Therefore in order to insure that there is no ISI it is necessary to ensure that the length of CP (T_G) is greater than the max path delay (τ_{max}).

The CP takes an extension of the OFDM symbol, by placing a copy of the last samples at the beginning, shown in figure 2.15.

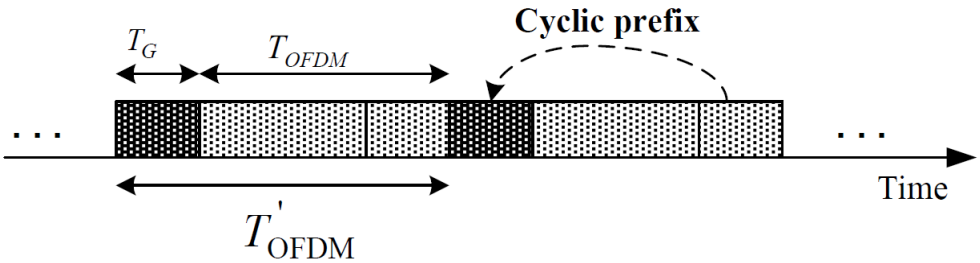

Figure 2.15: OFDM Cyclic Prefix (CP) insertion [35].

Figure 2.16(a) shows two consecutive OFDM symbols, each of which has the CP length

of T_G, while illustrating the OFDM symbol of length $T_{sym} = T_{sub} + T_G$. Meanwhile, figure 2.16(b) illustrates them jointly in the time and frequency domains. Figure 2.16(c) shows the ISI effects of a multipath channel on some sub-carriers of the OFDM symbol. This figure shows that if the length of the guard interval CP is set longer than or equal to the maximum delay of a multipath channel, the ISI effect of an OFDM symbol on the next symbol is confined within the guard interval so that it may not effect the FFT of the next OFDM symbol, taken for the duration T_{sub}. This implies that the guard interval longer than the maximum delay of the multipath channel allows for the preservation of the orthogonality among the sub-carriers. As the continuity of each delayed sub-carrier has been warranted by the CP, its orthogonality with all other sub-carriers is maintained over T_{sub}.

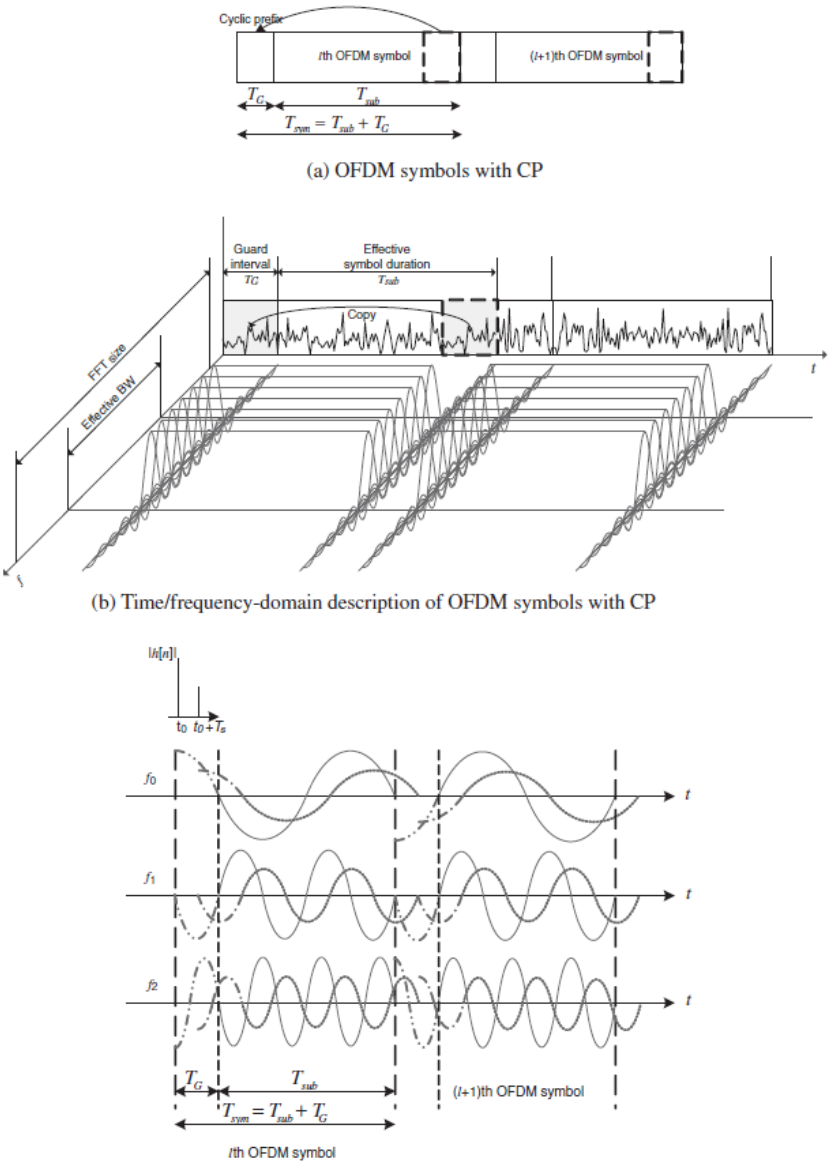

(a) OFDM symbols with CP

(b) Time/frequency-domain description of OFDM symbols with CP

(c) ISI effect of a multipath channel for each subcarrier

Figure 2.16: Effect of a multipath channel on OFDM symbols with CP [31].

On the other hand, figure 2.17 shows that even if the length of CP is set longer than the maximum delay of the multipath channel, ISI and/or InterCarrier Interference (ICI) may occur depending on the timing of the FFT window starting point.

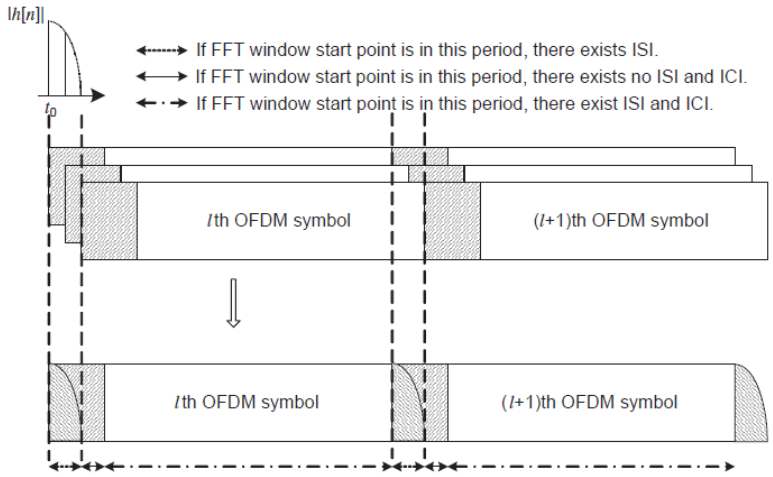

Figure 2.17: ISI/ICI effect depending on the FFT window start point [31].

More specifically, if the FFT window starting point is earlier than the lagged end of the previous symbol, ISI occurs; if it is later than the beginning of a symbol, not only ISI (caused by the next symbol), but ICI also occurs.

2.4.2.3 OFDM representation in frequency domain

Now let us consider the ideal conditions: CP length is set not shorter than the maximum delay of the channel and the FFT window starting point of an OFDM symbol is determined within its CP interval (i.e. unaffected by the previous symbol). Then the OFDM receiver takes the FFT of the received samples $\left(y_l[n]\right)_{n=0}^{N_c-1}$ to yield

$$\begin{aligned}
Y_l[k] &= \sum_{n=0}^{N_c-1} y_l[n] e^{-j2\pi kn/N} \\
&= \sum_{n=0}^{N_c-1} \left(\sum_{m=0}^{+\infty} h_l[m] x_l[n-m] + z_l[n] \right) e^{-j2\pi kn/N} \\
&= \sum_{n=0}^{N_c-1} \left(\sum_{m=0}^{+\infty} h_l[m] \left(\frac{1}{N} \sum_{i=0}^{N_c-1} X_l[i] e^{j2\pi i(n-m)/N} \right) \right) e^{-j2\pi kn/N} + Z_l[k] \\
&= \frac{1}{N} \sum_{i=0}^{N_c-1} \left(\left(\sum_{m=0}^{+\infty} h_l[m] e^{-j2\pi im/N} \right) X_l[i] \sum_{n=0}^{+\infty} e^{-j2\pi(k-i)n/N} \right) e^{-j2\pi kn/N} + Z_l[k] \\
&= H_l[k] X_l[k] + Z_l[k] \qquad (2.19)
\end{aligned}$$

where $X_l[k]$, $Y_l[k]$, $H_l[k]$ and $Z_l[k]$ denote the kth sub-carrier frequency components of the lth transmitted symbol, received symbol, channel frequency response, and noise in the frequency domain, respectively.

From equation 2.19 it is possible to conclude that the OFDM system can be simply thought of as multiplying the input symbol by the channel frequency response in the frequency domain.

Equation 2.19 can be equivalently represented as in figure 2.18. Since $Y_l[k] = H_l[k]X_l[k]$ under no noise condition, the transmitted symbol can be detected by one-tap equalization, which simply divides the received symbol by the channel ($X_l[k] = Y_l[k]/H_l[k]$). Note that $Y_l[k] \neq H_l[k]X_l[k]$ without CP. Insertion of CP in the transmitter makes the transmitted samples circularly-convolved with the channel samples, which yields $Y_l[k] = H_l[k]X_l[k]$ as desired in the receiver.

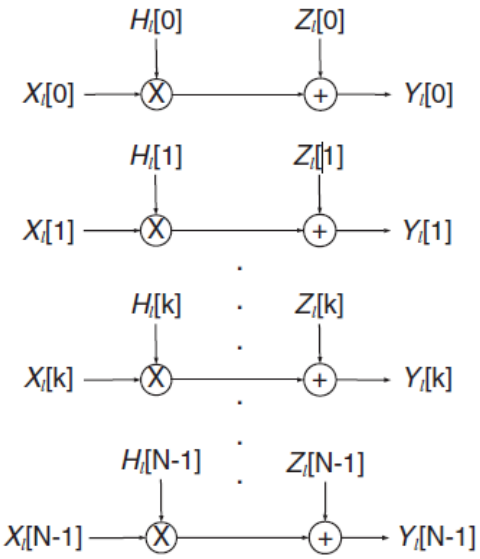

Figure 2.18: Frequency-domain equivalent model of OFDM system [31].

To understand the effect that type of modulation has on the BER, two types of channels will be shown next.

2.5 Channel

At this point, two channel configurations are described and compared in terms of probability of error [35][36].

2.5.1 AWGN Channel

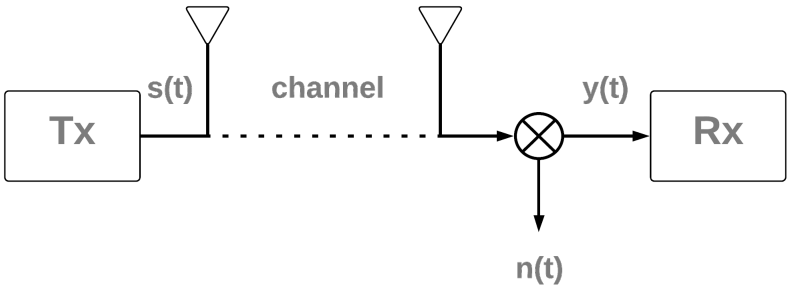

Figure 2.19: AWGN channel model.

The AWGN channel is considered a SISO link without channel multipath fading, pass loss or shadowing. The only perturbation in this channel is the white noise $n(t)$ with a Gaussian distribution of mean 0. The white noise has a constant Power Spectral Density (PSD), that is considered equal to $N_0/2$ watts/Hz.

$$y(t) = s(t) + n(t) \tag{2.20}$$

Considering a M-ary signal, and assuming that the symbol energy E_s is divided equally among the bits and that Gray encoding is used, it is possible to write the following relations.
SNR per bit:

$$SNR_b = \frac{SNR_s}{log_2(M)} \tag{2.21}$$

Probability of error per bit:

$$P_{e,b} \approx \frac{P_{e,s}}{log_2(M)} \tag{2.22}$$

where SNR_s, $P_{e,s}$ and M represent SNR per symbol, probability of error per symbol and size of constellation, respectively.
Now, for the QPSK modulation it is possible to write

$$P_{e,s} = 2Q\Big(\sqrt{SNR_s}\Big) \tag{2.23}$$

$$\begin{aligned} P_{e,b} &\approx \frac{P_{e,s}}{2} \\ &= Q\Big(\sqrt{SNR_s}\Big) \end{aligned} \tag{2.24}$$

where function Q(...) declines very fast with increasing SNR as illustrated below.

$$Q(x) = \frac{1}{\sqrt{2\pi}} \int_{x}^{\infty} e^{-t^2/2} dt \tag{2.25}$$

For a general M-ary with a square signal constellation, we get

$$P_{e,b} \approx \psi Q\left(\sqrt{\beta SNR_s}\right) \tag{2.26}$$

$$\beta = \frac{3}{M-1} \tag{2.27}$$

$$\psi = \frac{4}{log_2 M}\left(1 - \frac{1}{\sqrt{M}}\right) \tag{2.28}$$

From equation 2.24 and equation 2.26 it is possible to conclude that, in these two kinds of modulations, the error probability declines exponentially with SNR for high SNR regime.

2.5.2 Rayleigh Flat Fading Channel

Let us now consider that the received signal is not only affected by AWGN noise at the receiver antenna, but also by the multipath fading channel, resulting in a h coefficient (fading coefficient) different from 1, defined as the sum of the various multipath components, each one of them with an amplitude, phase, and delay. The amplitude follows a Rayleigh distribution.

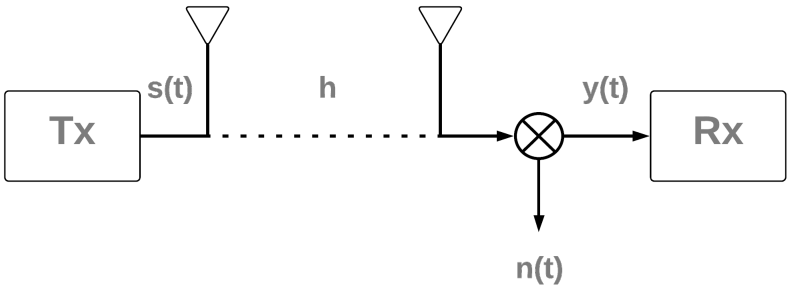

Figure 2.20: Rayleigh flat fading channel model.

$$y(t) = h(t)s(t) + n(t) \tag{2.29}$$

Assuming the average power of the fading is equal to 1, the instantaneous SNR is given by

$$SNR(h) \quad = \quad |h|^2 SNR \tag{2.30}$$

where SNR is the average signal to noise ratio. Now, the probability of error conditioned on h is

$$\begin{aligned} P_{e,b} &\approx \psi Q\Big(\sqrt{\beta SNR_s(h)}\Big) \\ &= \psi Q\Big(|h|^2 \beta SNR_s\Big) \\ &\Rightarrow \begin{cases} |h|^2 SNR \gg 1, & error \quad probability \quad is \quad very \quad small \\ |h|^2 SNR < 1, & error \quad probability \quad is \quad large \end{cases} \end{aligned} \tag{2.31}$$

Therefore, one expects that the probability of error will be mainly dictated by low values of SNR, i.e., broadly speaking it is possible to say

$$P_e \quad \propto \quad Prob(SNR(h)_{low}), \qquad |h|^2 < \frac{1}{SNR} \tag{2.32}$$

Based on the previous definition, we can rewrite it as

$$Prob(SNR(h)_{low}) \quad = \quad Prob(|h|^2 SNR < 1) \geq \frac{1}{SNR} \tag{2.33}$$

which corresponds to Markov inequality. Thus, we have to expect that the behavior in the probability of error will never decline faster than 1/SNR. When h is Gaussian this is verified with the following equality

$$\begin{aligned} P_e &\approx P\Big[|h|^2 SNR < 1\Big] \\ &\approx \frac{1}{SNR} \end{aligned} \tag{2.34}$$

From equation 2.34 we can see that the probability of error declines inversely proportional to the SNR for high SNR regime.

Thus, there must be a tradeoff between spectral efficiency and probability of error so that we have a high bit rate without corrupting the signal to be transmitted.

So, if the channel is good, we may opt for the 64-QAM modulation that has the highest spectral efficiency and, due to its advantage, it does not prevent the transmission. On the other hand, if the channel is bad, a QPSK modulation despite having less spectral efficiency it allows the signal to reach the receiver virtually uncorrupted.

In other words, if it were possible to change the modulation according to the state of the channel, the system behavior would be better.

2.6 Multiple Antenna System

Up to then, the effect that the type of modulation and channel has on the probability of error, calculated in the receiver, has been studied for a SISO system. This section shows a simple case of a MISO system, Alamouti 2x1, introducing the concept of diversity.

2.6.1 Introduction

Multiple antenna techniques can be classified into two main categories: spacial multiplexing techniques and diversity techniques [37]. Essentially, diversity techniques are aimed at sending the same information through different independent paths. Combining techniques are employed at the receiver to exploit multipath propagation characteristics of a channel. So, diversity techniques are used to combat degradation in the error performance due to unstable wireless fading channels mostly caused by multipath fading. So, the probability that multiple statistically independent fading channels simultaneously experience deep fading is very low.

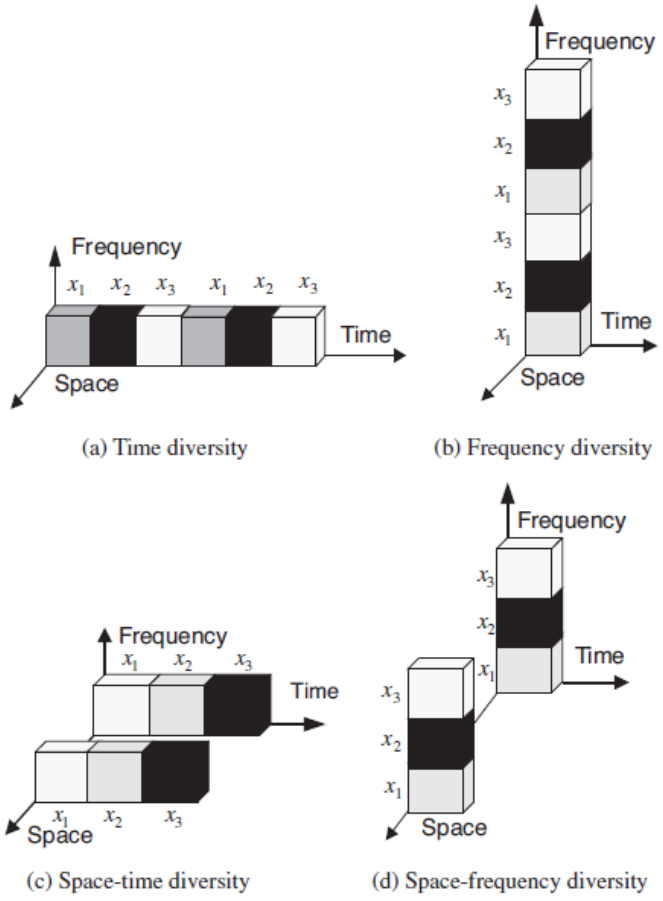

Figure 2.21: Illustration of time, frequency, and space diversity techniques [31].

There are various ways we can create diversity gain: time diversity, frequency diversity and spatial diversity. These techniques are illustrated in figure 2.21. Time diversity can be achieved by sending the same information at different times if they are separated by much more than the coherence time. Frequency diversity can also be achieved by transmitting the same narrow-band signal at different carriers, where the carriers are separated by the coherence bandwidth of the channel. It is evident that time diversity and frequency diversity techniques require additional time resources and frequency resources, respectively. How-

ever, spatial diversity techniques do not require any additional time, frequency resources or power. Figure 2.21(c) illustrates a concept of the space-time diversity that employs multiple transmit antennas, which do not require additional time resources as opposed to the one in figure 2.21(a). Similarly, figure 2.21(d) illustrates a concept of the space-frequency diversity that employs multiple transmit antennas, not requiring additional frequency resources as opposed to the one in figure 2.21(b).

In this section, we will study the basic concepts of antenna diversity techniques. Today there are different types of antenna diversity techniques such as transmit and receive diversity. The transmit diversity technique has been widely adopted for downlink, since it is useful in reducing the complexity of the receiver and it requires multiple antennas only on the transmitter side. In this section, the space-time coding technique illustrated is Alamouti 2x1, two antennas on the transmitter and one antenna on the receiver.

2.6.2 Space-Time Block Code (STBC)

The very first and most well-known Space-Time Block Code (STBC) is the Alamouti code, which is a complex orthogonal space-time code [38] that can be used for two transmit antennas and N_r receive antennas.

2.6.2.1 Alamouti 2x1 Technique

A complex orthogonal space/time block code for two transmit antennas was developed by Alamouti [39]. The idea of Alamouti was as follows: two consecutive symbols s_1 and s_2 are encoded with the space-time codeword matrix, represented in figure 2.22 and figure 2.23. Now, the Alamouti encoded signal is transmitted from the two transmit antennas over two symbol periods. Throughout the first symbol period, s_1 and s_2 are simultaneously transmitted from the two transmit antennas. On the other hand, during the second period symbol, s_1 and s_2 are transmitted again but in a different way: symbol $-s_2^*$ is transmitted from the first transmit antenna and symbol s_1^* is transmitted from the second transmit antenna.

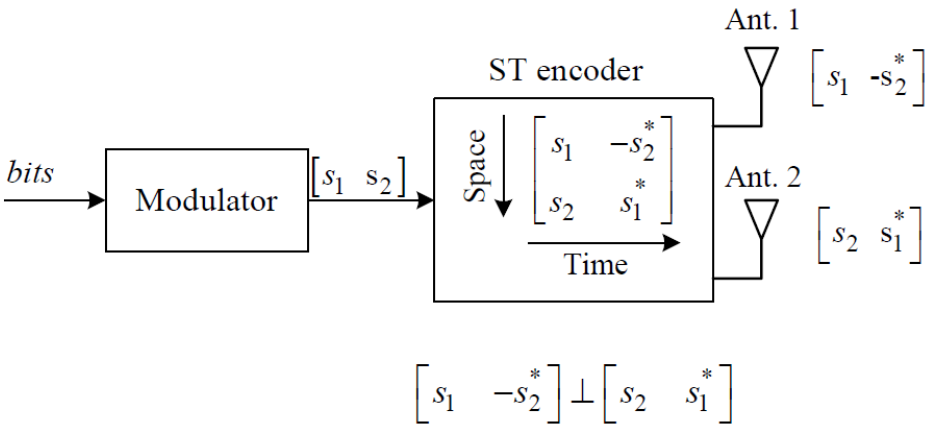

Figure 2.22: Block diagram of the Alamouti 2x1 Space-Time Encoder [35].

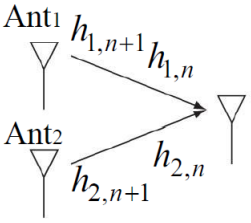

time/frequency	Ant1	Ant 2
n	s_n	s_{n+1}
$n+1$	$-s^*_{n+1}$	s^*_n

Figure 2.23: Alamouti 2x1 coding [35].

where $h_{x,n}$ denote a fading coefficient of the channel x that affect the symbol n and $h_{x,n+1}$ denote a fading coefficient of the channel x that affect the symbol $n+1$.

Therefore, the received signals at time/frequency n and n+1 are given by

$$\begin{cases} y_n = \frac{1}{\sqrt{2}} h_{1,n} s_n + \frac{1}{\sqrt{2}} h_{2,n} s_{n+1} + n_n \\ y_{n+1} = -\frac{1}{\sqrt{2}} h_{1,n+1} s^*_{n+1} + \frac{1}{\sqrt{2}} h_{2,n+1} s^*_n + n_{n+1} \end{cases} \tag{2.35}$$

wherein $\frac{1}{\sqrt{2}}$ represents the power constraint in order to normalize the power per symbol to one.

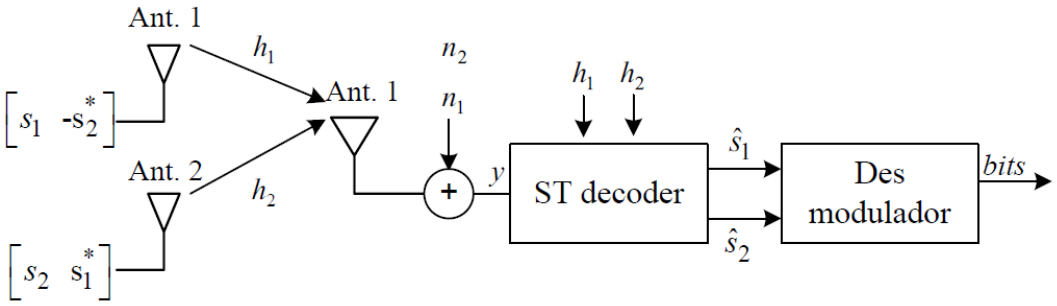

Figure 2.24: Complete Alamouti 2x1 scheme [35].

Now, it is necessary to decode the signal on the receiver:

$$\begin{cases} \hat{s}_n = \frac{1}{\sqrt{2}} h^*_{1,n+1} y_n + \frac{1}{\sqrt{2}} h_{2,n} y^*_{n+1} \\ \hat{s}_{n+1} = \frac{1}{\sqrt{2}} h^*_{2,n+1} y_n - \frac{1}{\sqrt{2}} h_{1,n} y^*_{n+1} \end{cases} \tag{2.36}$$

The soft decision of data symbol s_n is given by:

$$\hat{s}_n = \frac{1}{2}\left(h^*_{1,n+1} h_{1,n} + h_{2,n} h^*_{2,n+1} \right) s_n + \frac{1}{\sqrt{2}} h^*_{1,n+1} n_n + \frac{1}{\sqrt{2}} h_{2,n} n^*_{n+1} \tag{2.37}$$

where it is notorious that interference caused by data symbol n+1 has been fully eliminated.

As in most OFDM systems the channels between adjacent carriers are correlated, it can be assumed that h_n=h_{n+1}. So, the previous expression is reduced to

$$\hat{s}_n = \frac{1}{2}\left(|h_{1,n}|^2 + |h_{2,n}|^2 \right) s_n + \frac{1}{\sqrt{2}} h^*_{1,n+1} n_n + \frac{1}{\sqrt{2}} h_{2,n} n^*_{n+1} \tag{2.38}$$

The SNR is given by

$$SNR = \frac{1}{2} \frac{\left(|h_1|^2 + |h_2|^2 \right)}{\sigma^2} \tag{2.39}$$

From equation 2.38 it is possible to conclude that if the channels between two adjacent frequencies or instants are highly correlated, where there is no gain with Alamouti 2x1, so the system would have the same performance as an SISO system having the disadvantage that the transmitter has one more antenna.

Chapter 3

Simulation Platform

3.1 Introduction

In Chapter 2 we analyzed the main blocks of a wireless communications system as well as its performance for three different data modulations, modulated in OFDM, and for two types of channel. This performance did not take into account the effect of PA normally present in these systems. Thus, to study the impact that a PA has on the performance of a 5G system, a platform that allows simulating its performance has been created.

The platform developed will allow us to choose the type of desired configuration, the model of the PA, the modulation, as well as the signal bandwidth to be applied to the chosen PA, as shown in figure 3.1.

This chapter begins with the circuit simulation of PAs where their basic characteristics are presented. After that, the system simulation is explained by referring to the concepts discussed in Chapter 2. After presenting the two types of analysis that will be addressed, in the following section we will create the global simulation platform linking these two domains.

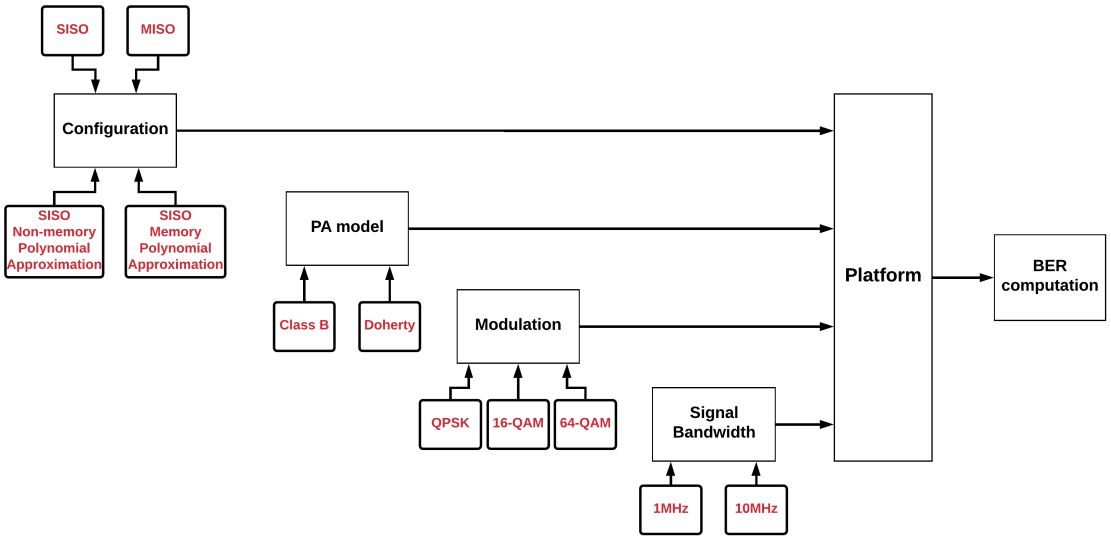

Figure 3.1: Global platform schematic.

3.2 Circuit Simulation

As one of the objectives with the creation of the platform is to be able to use it to visualize the impact that a PA has on a wireless communications system, it is necessary to initially present the basic characteristics of the PAs that are used. This characteristics will be important in the observation and discussion of the results obtained in the simulations. Thus, in this section the basic characteristics of two off-the-shelf PAs are presented: a 5GHz Class B PA and a 900MHz Doherty PA.

Since the main source of nonlinearities is the active device, the choice of PAs took into account the number of active devices present in them: whereas the Class B PA, which has an active device, incurs in a significant degradation of energy efficiency in favor of greater linearity, the Doherty PA, which has two active devices, improves the linearity/efficiency trade off. In this way, it is possible to analyze two different PA configurations. For more details consult [40][41][42].

So, in this section the study of both amplifiers is done applying 1 tone to the input and doing a harmonic balance analysis. For this purpose, a description of the following characteristics is given:

- AM-AM measurement: defined by the modulation in amplitude of the output signal in function of the amplitude of the input signal.

- Gain: defined by the ratio between output power (P_{out}) and input power (P_{in}) and is one of the main figures of merit of an amplifier:

$$Gain = \frac{P_{out}}{P_{in}} \tag{3.1}$$

- Power Added Efficiency PAE: defined as the subtraction of the input power from the output power, taking into account only the fraction of the output power that was obtained through the Direct Current (DC) supply (P_{dc}):

$$PAE = \frac{P_{out} - P_{in}}{P_{dc}} \tag{3.2}$$

- Drain Efficiency n: defined as the ratio between the RF output power and the DC power provided by the source:

$$n = \frac{P_{out}}{P_{dc}} \tag{3.3}$$

- AM-PM measurement: defined by phase distortion of the output signal in function of the amplitude of the input signal.

Figure 3.2 shows the results of the harmonic balance analysis for Class B PA. As a PA is not linear, the results obtained are analyzed at 1 dB compression point [43], as shown in table 3.1.

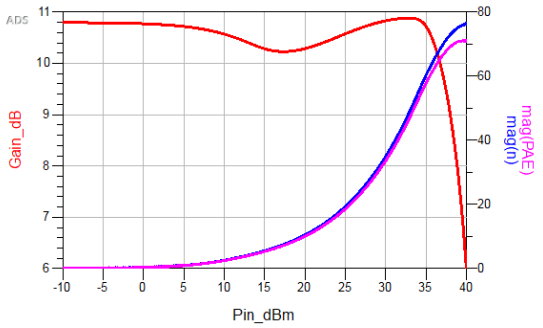

(a) Gain, PAE and n measurement.

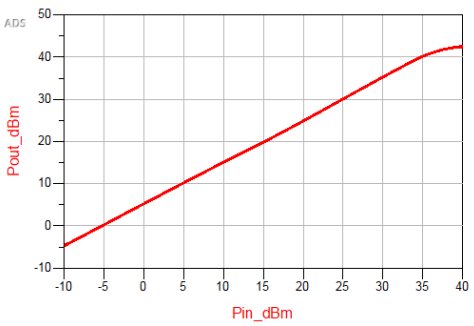

(b) Power Delivered to the load measurement.

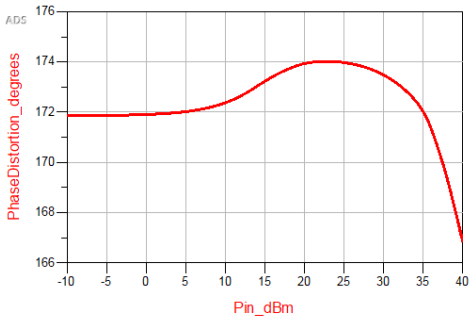

(c) AM-PM measurement.

Figure 3.2: Class B PA - Harmonic Balance results.

Gain (dB)	PAE (%)	n (%)	P_{out} (dBm)	PhaseDistortion (degrees)
9.2	68.7	72.3	41.9	169.6

Table 3.1: Class B PA - Harmonic Balance results at 1dB compression point.

At this point the Class B PA has $Gain$, PAE, n and power delivered to the load (P_{out}) equal to 9.2dB, 68.7%, 72.3% and 41.9dBm, respectively. In addition, over the entire range of input power (P_{in}) the phase distortion has a phase variation of 7 degrees, as shown in figure 3.2(c).

As for the Class B PA, figure 3.3 shows the results of the harmonic balance analysis for Doherty PA. In addition, table 3.2 shows the results obtained at 1dB compression point.

Gain (dB)	PAE (%)	n (%)	P_{out} (dBm)	PhaseDistortion (degrees)
11.1	84.9	78.4	44.7	81.2

Table 3.2: Doherty PA - Harmonic Balance results at 1dB compression point.

Thus, at this point, the Doherty PA has $Gain$, PAE, n and power delivered to the load (P_{out}) equal to 11.1dB, 84.9%, 78.4% and 44.7dBm, respectively. Concerning the phase distortion it is found that throughout the input power P_{in} range the phase distortion has a phase variation of approximately 50 degrees as shown in figure 3.3(c).

So, applying 1 tone to the input and doing a harmonic balance analysis, it can be verified

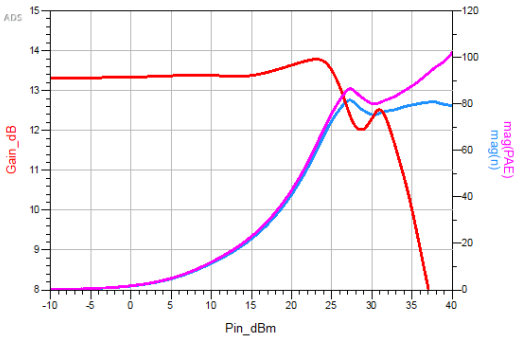

(a) Gain, PAE and n measurement.

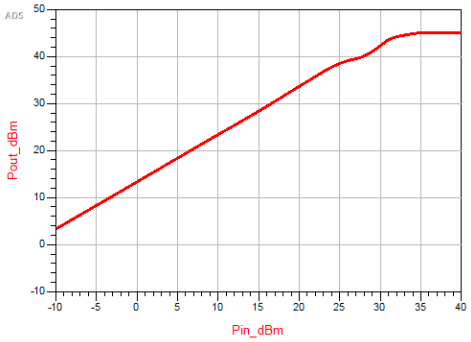

(b) Power Delivered to the load measurement.

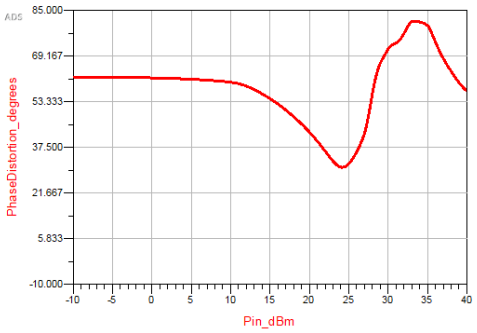

(c) AM-PM measurement.

Figure 3.3: Doherty PA - Harmonic Balance results.

at 1 dB compression point that the Doherty PA has higher $Gain$, higher PAE, higher n, higher power delivered to the load (P_{out}) and higher phase variation compared to Class B PA.

3.3 System Simulation

In this section two system configurations are discussed: SISO system and later a particular case of a MISO system, the Alamouti 2x1.

3.3.1 SISO Simulation

To simulate a wireless communication system typically a diagram like the one discussed in Chapter 2 is used. In this work the system simulation is done taking into account the OFDM modulation, present in the 4G systems, three types of modulation and two types of channel model, as shown in the blocks of figure 3.4.

The following is a brief explanation of what was done in each of the main blocks, including some relevant characteristics and implementation details of the elements belonging to these blocks.

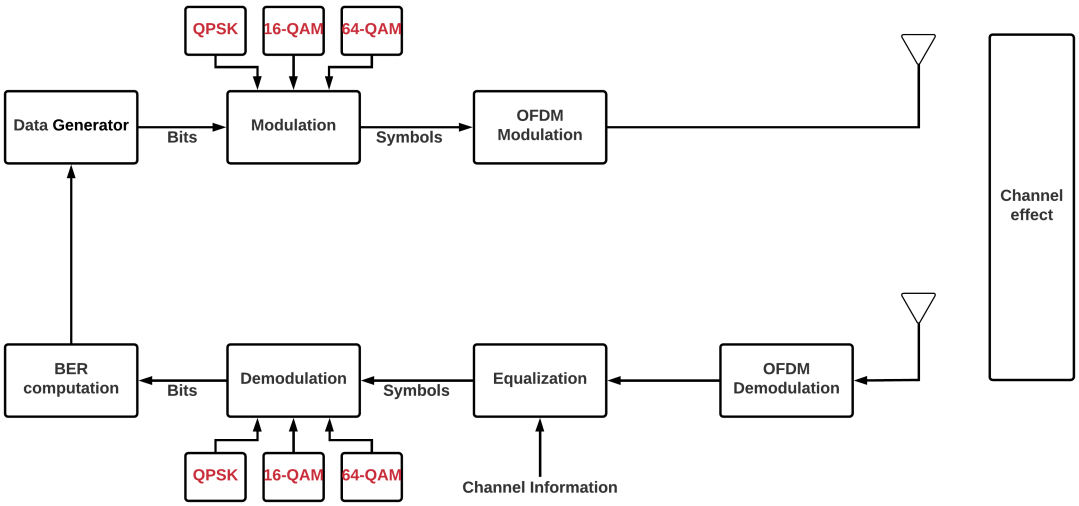

Figure 3.4: Main blocks of the SISO wireless communication system.

Modulation As reasoned in section 2.3, for band-limited communications systems, M-QAM techniques are more appropriate due to their higher spectral efficiency. But, if the channel is bad, good spectral efficiency does not guarantee correct data transmission - so depending on the channel there are better techniques than others. Here three modulation techniques are compared, like in section 2.3. It has also been said that the rectangular constellation was used. We know that the error rate performance of a system is determined primarily by the minimum distance between the symbols. The farther the symbols are from each other, the lower the probability error. Thus, constellations with the same minimum distance between the symbols achieve the same performance. In addition, the transmitted power is a limiting factor in system designs, often limited by the Federal Communications Commision (FCC) regulations to a certain threshold inside and outside the band of interest. Furthermore, in mobile applications, low-power signals are required. Hence, for a given minimum distance, an optimum constellation is one that has the least power. With the above discussion, to meet certain requirements on power and minimum distance, we are limited to a few constellation choices. For these reasons the constellation used was the rectangular constellation.

After that, the signal is modulated in OFDM as in section 2.4.

Channel To study the effect of two channel types mentioned in section 2.5, two blocks were considered, as shown in figure 3.5. AWGN block picks up the transmitted signal and adds it to the noise that is generated with a Gaussian variable with zero mean and variance σ^2. The noise variance depends on the E_b/N_0 ratio used in the simulation, the received signal power (P_r) and the modulation scheme considered (m), as shown in equation 3.4.

$$\sigma^2 = P_r \times 10^{(-E_b N_0(dB)/10)}/(log2(m)) \tag{3.4}$$

On the other hand, Rayleigh block shows that the transmitted signal goes through a multipath block and is added to the noise variable. Multipath block should be based on the Power Delay Profile (PDP) present in table 3.3, normally used in LTE. This block performs

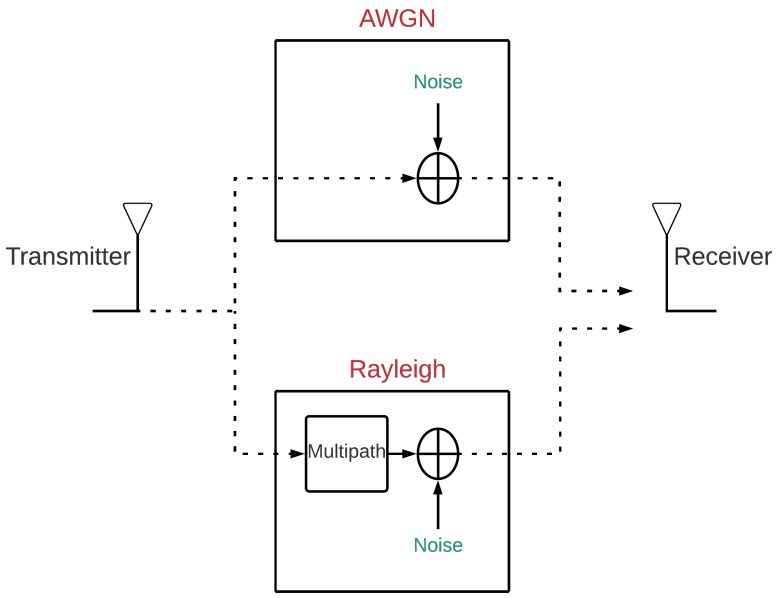

Figure 3.5: AWGN and Rayleigh channel blocks.

the impulsive response and the frequency response of the channel and, then the convolution of the transmitted signal with the impulsive response of the channel.

Delay (ns)	Average Power (dB)
0	-1
50	-1
120	-1
200	0
230	0
500	0
1600	-3
2300	-5
5000	-7

Table 3.3: LTE extended typical urban channel model (ETU) [35].

Equalization On the receiver, when the effect of the channel used is Rayleigh, it is necessary to implement the equalization in order to reverse the distortion introduced by the channel in the signal. There are different types of equalization, the one performed as a Zero-Force Combining (ZFC) as shown in equation 3.5.

$$g_l = \frac{h_l^*}{|h_l|^2} \qquad , l = 0, ..., N_c \tag{3.5}$$

where (*) is the conjugate of the channel in the frequency domain, obtained from the frequency response (h_l) of the channel.

Demodulation After OFDM demodulation and equalization is done, the QPSK, or 16-QAM or 64-QAM demodulation is made. Now, having the output data sequence we can calculate the BER relating this sequence to the input sequence.

After the main blocks of a wireless communications system and its characteristics were known, the system is simulated using the MATLAB software as support. At this point, the system performance is analyzed in terms of BER curves.

Figure 3.6 shows the effect of modulation type considering the AWGN channel, where EbN0 (Eb/N0[dB]) is a normalizes SNR measure. As it was expected from conclusions of the Chapter 2, the higher the number of symbols in the constellation the greater the probability of error. The GAP between the 16-QAM and the QPSK modulation is 4dB.

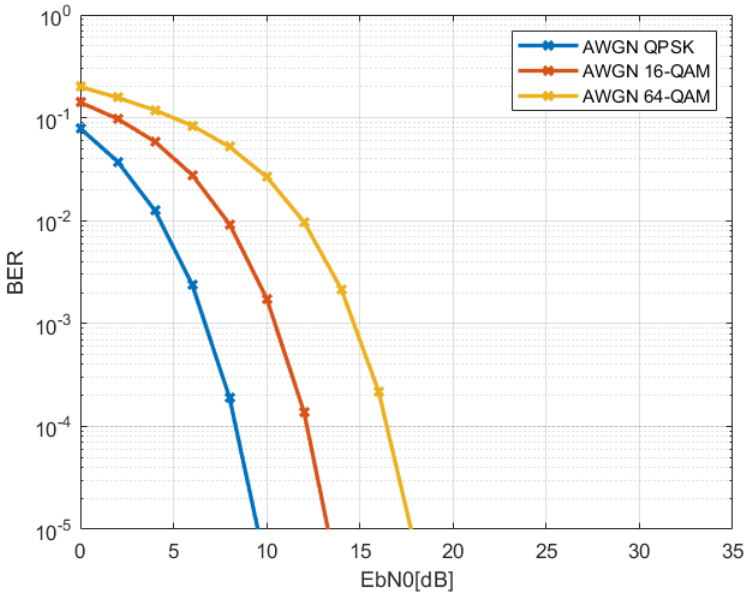

Figure 3.6: Effect of AWGN channel on the probability of error.

Considering now that the signal transmission is also affected by the Rayleigh channel. Figure 3.7 shows the results for this two channel model types. It is possible to conclude that there is a degradation of the BER with the increase of number of bits sent simultaneously in both channel models. While the AWGN channel curves drops exponentially with SNR, the Rayleigh channel curves falls inversely with SNR, as was concluded in Chapter 2. Thus, it is notorious that the Rayleigh channel curves falls more slowly than the AWGN channel curves.

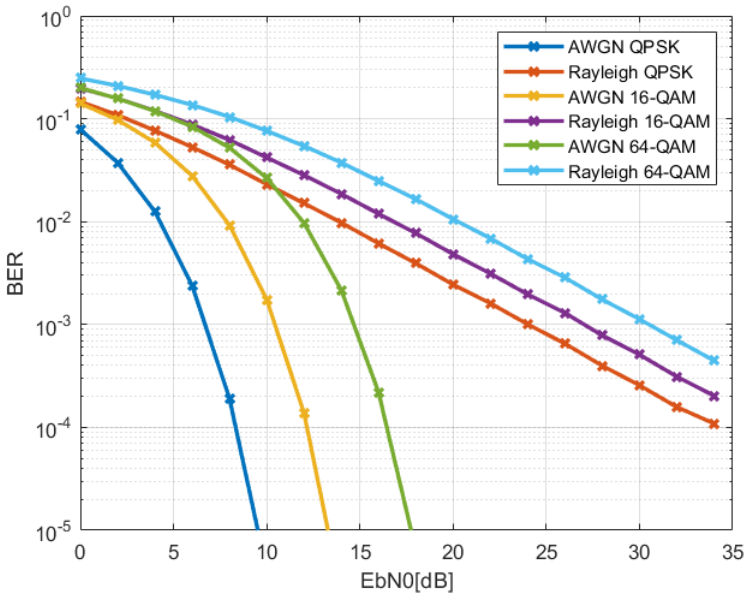

Figure 3.7: Effects of AWGN and Rayleigh flat fading channel on the probability of error.

3.3.2 Alamouti 2x1 Simulation

At the end of Chapter 2 the concept of a multiple antenna system was introduced in which a particular case of the MISO configuration, more specifically the Alamouti 2x1, was studied.

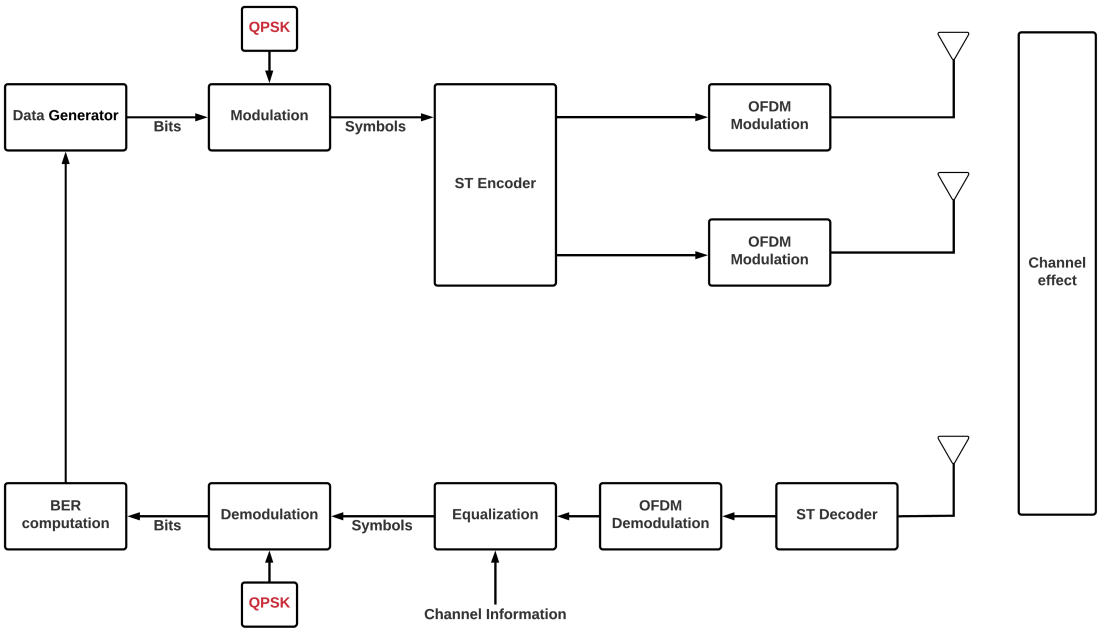

Figure 3.8: Main blocks of the Alamouti 2x1 wireless communication system.

Figure 3.8 shows the main blocks of the Alamouti 2x1 wireless communications system. The main difference is that there are two antennas in the transmitter allowing the introduction of the concept of diversity. For this a new block in the transmitter (Space Time Encoder) and a new block in the receiver (Space Time Decoder) were added having its characteristics explained in Chapter 2.

In order to visualize the impact that diversity has on the BER curves, the figure 3.9 shows comparison between SISO implementation with QPSK modulation and Alamouti 2x1 MISO implementation, with the same modulation. From there we can see that, as concluded earlier, adding diversity is one way to improve the BER affected by a Rayleigh fading wireless channel.

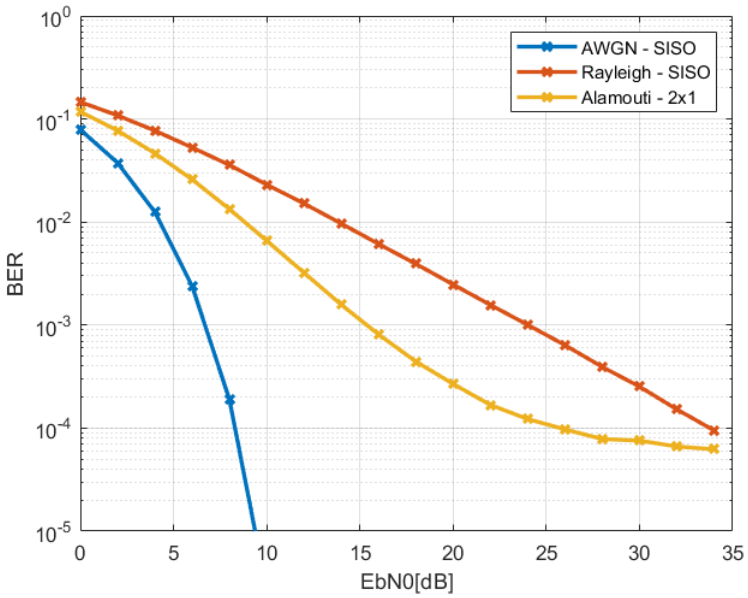

Figure 3.9: Effect of the Alamouti 2x1 technique on the probability of error of QPSK modulation.

3.4 Global Simulation

As in the future simulations a OFDM modulated signal will be applied to the input of the PA, then the impact of this modulated signal on the behavior and characteristics of the PA seen in the circuit simulation section is analyzed before the creation of the platform configurations [44][45][46][47][48].

3.4.1 Power Amplifier Modulated Signal Test

At times PAs are forced to operate much beyond their linear range of operation to improve overall efficiency of the transmission. Due to the nonlinear behavior of PA, along with power amplification in the main channel some power leaks into the adjacent channel, mainly due to intermodulation distortion. This spectral leakage is quantified through Adjacent Channel Power Ratio (ACPR) defined as the ratio between the total power adjacent channel (intermodulation signal) to the main channel's power (signal).

In this subsection the study of both amplifiers applying one OFDM modulated signal to the input is done. For this, it is necessary to control the amplitude of the input signal of how to reach the 1 dB compression point, in the same conditions as in the circuit simulation. For this, a gain constant K is placed in order to reach this point, as shown in figure 3.10. In addition, it is necessary to define the bandwidth of the signal to be applied. In this context, two different bandwidths are tested: one of 1MHz and one of 10MHz.

For the following simulations the OFDM modulated signal is generated in MATLAB software and later introduced in the simulation of the PA in ADS circuit simulation software, where the graphs are obtained.

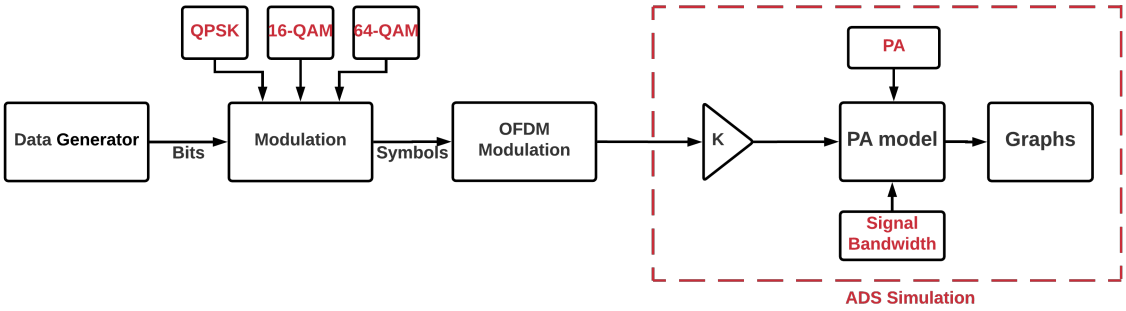

Figure 3.10: Test configuration of a OFDM modulated signal.

In order to reach the 1 dB compression point, the gain constant K used in Class B PA is 4000.

Figure 3.11(a) and 3.11(b) shows the impact that the bandwidth of the OFDM modulated signal has on the performance of the Class B PA. As can be seen, the spectrum of the 10MHz bandwidth signal is more degraded than the spectrum of the 1MHz bandwidth signal, where it is possible to see in the spectrum of the 10MHz bandwidth signal the intermodulation distortion [43]. Since the amplifier has been sized for a fixed frequency, without bandwidth, the larger the bandwidth of the signal to be applied, the greater the degradation of the signal spectrum. This phenomenon is proven with the values in table 3.4. It is seen that the ACPR of the signal after PA, ACPR_{out}, with 1MHz bandwidth is greater than the ACPR_{out} of the signal with 10MHz bandwidth.

Regarding the gain, it is seen that the increase of the bandwidth of the OFDM modulated signal causes a scattering in the curve giving the idea that the PA has "memory", [49]-section 9.6, as shown in figure 3.11(c). The same is true for the efficiency (figure 3.11(d)) and AM-PM curve (figure 3.11(e)).

As was done for Class B PA, to reach the 1 dB compression point the gain constant used in Doherty PA is 2300.

In the Doherty PA the impact that the bandwidth of the OFDM modulated signal has on the ACPR_{out} is not obvious (figure 3.12(a) and 3.12(b)), as shown by the values in table 3.4. However, the scattering verified in the gain (figure 3.12(c)), in the efficiency (figure 3.12(d)) and in the AM-PM curve (figure 3.12(e)) is a little more pronounced.

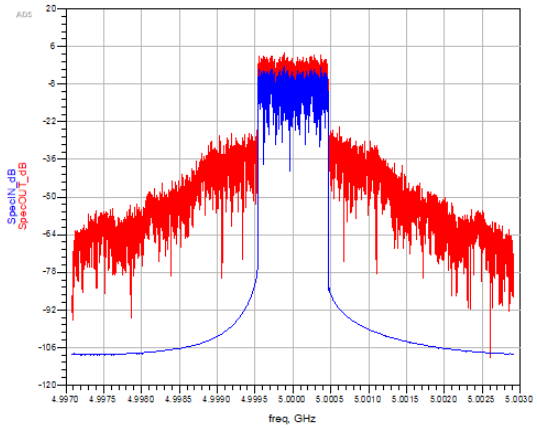

(a) Spectrum of 1MHz bandwidth signal.

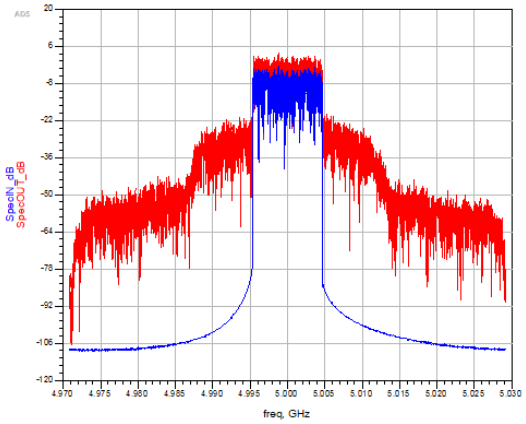

(b) Spectrum of 10MHz bandwidth signal.

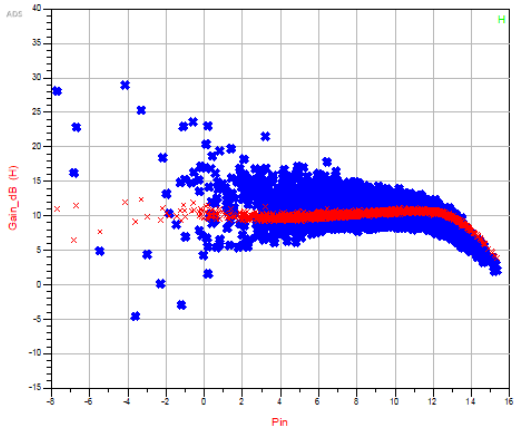

(c) Gain curve compare. Red: 1MHz bandwidth signal; Blue: 10MHz bandwidth signal.

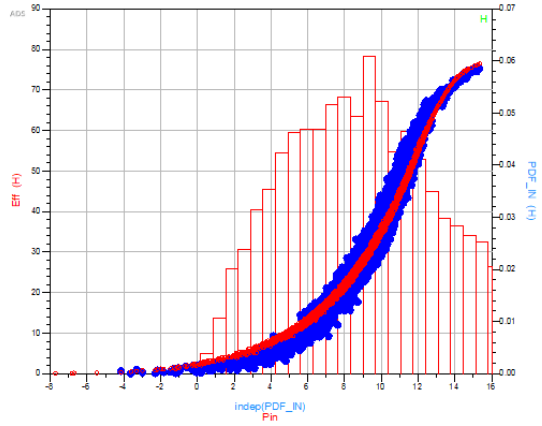

(d) Efficiency curve compare. Red: 1MHz bandwidth signal; Blue: 10MHz bandwidth signal and PDF histogram.

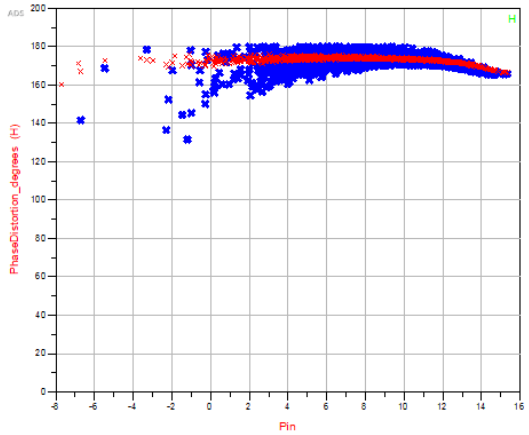

(e) AM-PM curve compare. Red: 1MHz bandwidth signal; Blue: 10MHz bandwidth signal.

Figure 3.11: Impact of the OFDM modulated signal in Class B PA.

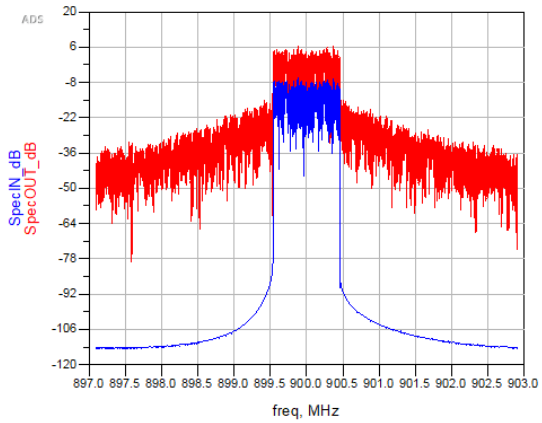

(a) Spectrum of 1MHz bandwidth signal.

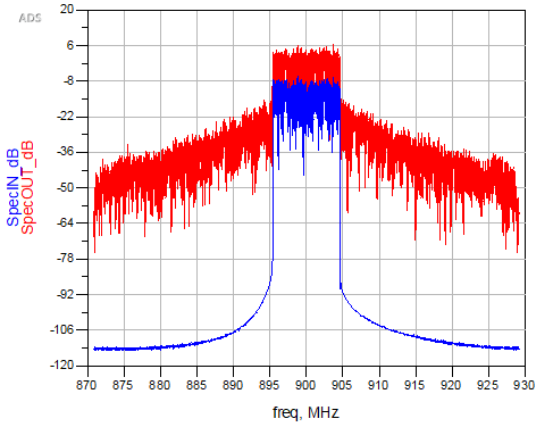

(b) Spectrum of 10MHz bandwidth signal.

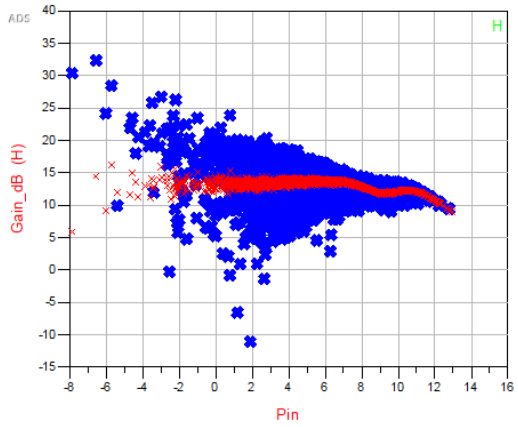

(c) Gain curve compare. Red: 1MHz bandwidth signal; Blue: 10MHz bandwidth signal.

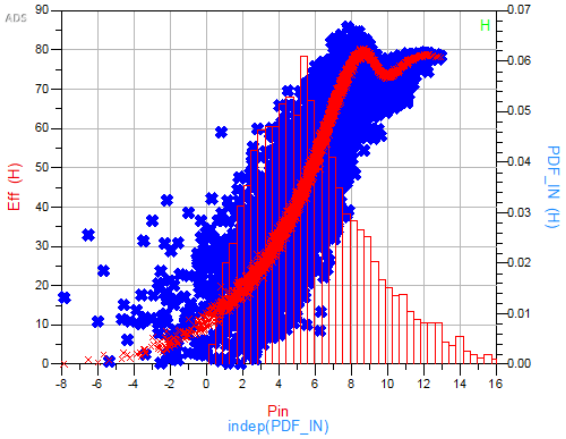

(d) Efficiency curve compare. Red: 1MHz bandwidth signal; Blue: 10MHz bandwidth signal and PDF histogram.

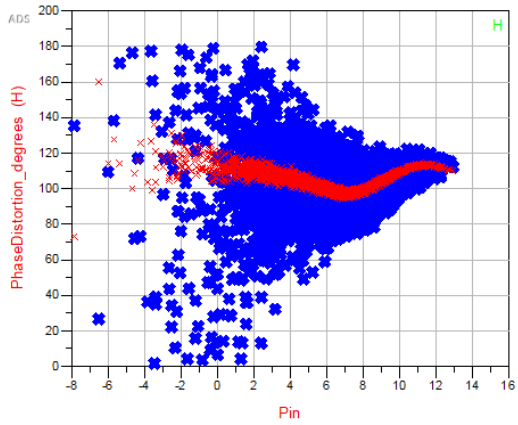

(e) AM-PM curve compare. Red: 1MHz bandwidth signal; Blue: 10MHz bandwidth signal.

Figure 3.12: Impact of the OFDM modulated signal in Doherty PA.

PA	ACPR$_{in}$ (dB)	ACPR$_{out}$ (dB)	Eff_{mean} (%)	$PowerAddedEfficiency$(PAE)$_{mean}$ (%)	PhaseDistortion (degrees)	$Gain_{mean}$ (dB)	PAPR
ClassB-1MHz	86.192	29.777	34.669	17.939	173.157	10.244	9.410
ClassB-10MHz	86.192	24.372	35.002	17.031	167.592	10.242	9.410
Doherty-1MHz	86.192	22.165	59.988	58.184	103.511	12.949	9.410
Doherty-10MHz	86.192	23.007	58.212	56.317	100.946	12.748	9.410

Table 3.4: Impact of a OFDM modulated signal on different PAs.

In relation to phase distortion, table 3.4 shows that there is no large variation in the mean of the phase distortion with the increase of the signal bandwidth in each of the PAs, being approximately 170 degrees and 100 degrees for the Class B PA and Doherty PA, respectively. This will be an important parameter to take into account in the future simulations because it will be necessary to compensate this phase distortion in order to allow for a demodulation of the correct signal in the receiver. Thus, in order to have an idea of how phase distortion affects the constellation of modulated symbols, the following subsection shows the constellations of three modulations that will be used.

3.4.2 Power Amplifier effect in the constellation

As already mentioned, because a PA is a non-linear device, [49]-Chapter 9, it has phase distortion that changes the arrangement of the symbols in the original constellation. In this way, and taking into account the three modulations mentioned in section 2.3 they will show the changes caused by the two PAs in their constellations.

According to figure 3.13, it can be seen that there are two different concepts to take into account: one already mentioned in the previous subsection, referring to the phase distortion of Class B PA that causes a rotation of the symbols in the constellation. The other result of the nonlinearities of the Class B PA is that it causes a scattering of the symbols around the central point.

By comparing the effect on the three modulations, it is possible to predict that the more symbols the constellation has, the closer they will be and, consequently, the greater the error in the decision. Thus, a larger error is expected in the 64-QAM modulation and a smaller error in the QPSK modulation.

In order to obtain a correct demodulation, after the passage of the OFDM modulated signal by the Class B PA, it is necessary to eliminate the effect of phase distortion. Thus, with the aid of the phase distortion values obtained in the previous subsection, table 3.4, it is possible to compensate this distortion, as shown in the graphs of figure 3.14, where it is seen that the symbols of the OFDM modulated signal are practically centered in the symbol without effect of the Class B PA, as was expected after the compensation effected.

As was done for the Class B PA case, figure 3.15 shows the effect of Doherty PA on the constellation of the three modulation types. There is also a phase rotation and scattering of the symbols, and it is possible to predict a larger error in the 64-QAM modulation due to the greater proximity of the symbols.

By compensating for phase distortion, figure 3.16 is obtained.

In short, in both PAs we can conclude that there is an increase of the error with the increase of the symbols in the constellation, as foreseen in Chapter 2, as well as the increase of the error with the increase of the signal bandwidth that will pass through the PA.

Thus, it is possible to measure the error obtained in the symbols received in relation to the symbols of the ideal constellation, through Error Vector Magnitude EVM:

$$EVM(\%) = \sqrt{\frac{P_{error}}{P_{reference}}} * 100 \tag{3.6}$$

where P_{error} is the root mean square amplitude of the error vector and $P_{reference}$ is the amplitude of the point in the reference signal constellation.

The mean values are presented in table 3.5 and the variance values are presented in table 3.6, where it is verified that with the phase compensation it is possible to reduce the error present in the symbols, allowing for a better data reception.

PA	Bandwidth Signal	Modulation	EVM_{mean} (%)
ClassB	1MHz	QPSK	3.7
ClassB	1MHz	16-QAM	4.9
ClassB	1MHz	64-QAM	5.3
ClassB	10MHz	QPSK	9.2
ClassB	10MHz	16-QAM	9.8
ClassB	10MHz	64-QAM	10.6
Doherty	1MHz	QPSK	9.1
Doherty	1MHz	16-QAM	10.7
Doherty	1MHz	64-QAM	11.9
Doherty	10MHz	QPSK	18.5
Doherty	10MHz	16-QAM	19.9
Doherty	10MHz	64-QAM	20.9

Table 3.5: Error Vector Magnitude mean values after phase distortion compensation.

PA	Bandwidth Signal	Modulation	EVM_{var} (%)
ClassB	1MHz	QPSK	4.3
ClassB	1MHz	16-QAM	14.4
ClassB	1MHz	64-QAM	28.6
ClassB	10MHz	QPSK	17.4
ClassB	10MHz	16-QAM	29.4
ClassB	10MHz	64-QAM	59.2
Doherty	1MHz	QPSK	24.2
Doherty	1MHz	16-QAM	51.5
Doherty	1MHz	64-QAM	116.1
Doherty	10MHz	QPSK	78.8
Doherty	10MHz	16-QAM	97.6
Doherty	10MHz	64-QAM	140.3

Table 3.6: Error Vector Magnitude variance values after phase distortion compensation.

After studying the OFDM modulated signal transmission with PA effect the platform creation is done.

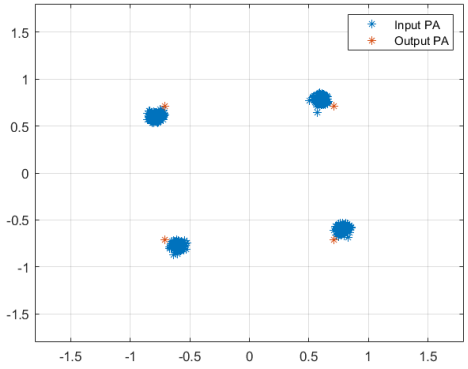

(a) QPSK signal modulated with 1MHz bandwidth.

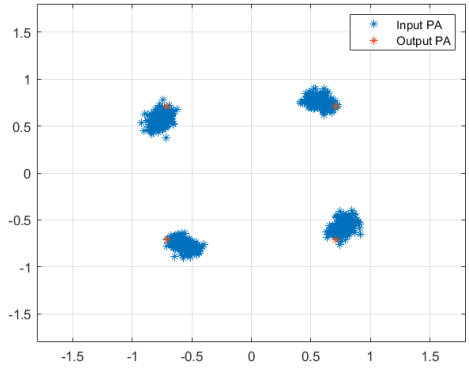

(b) QPSK signal modulated with 10MHz bandwidth.

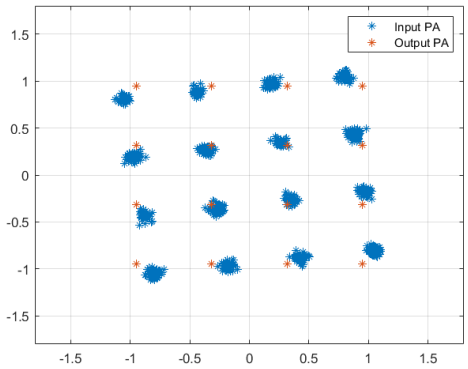

(c) 16-QAM signal modulated with 1MHz bandwidth.

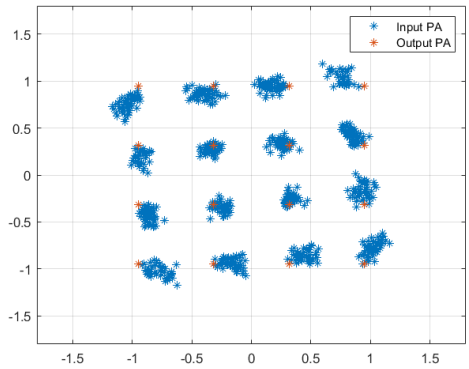

(d) 16-QAM signal modulated with 10MHz bandwidth.

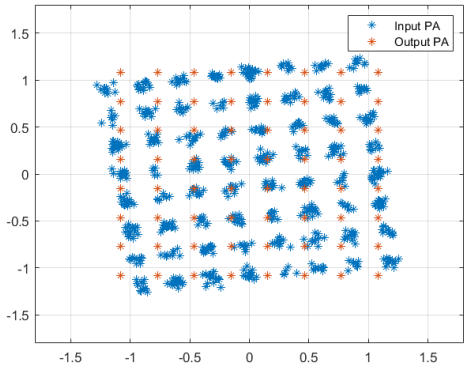

(e) 64-QAM signal modulated with 1MHz bandwidth.

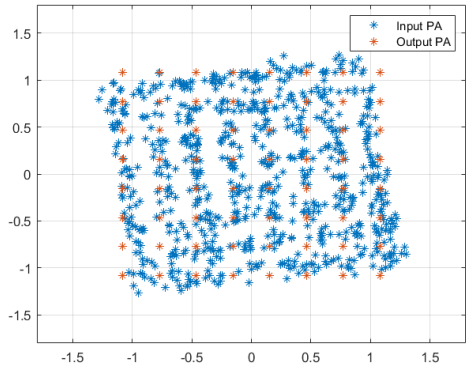

(f) 64-QAM signal modulated with 10MHz bandwidth.

Figure 3.13: Impact of Class B PA on the OFDM modulated signal constellation.

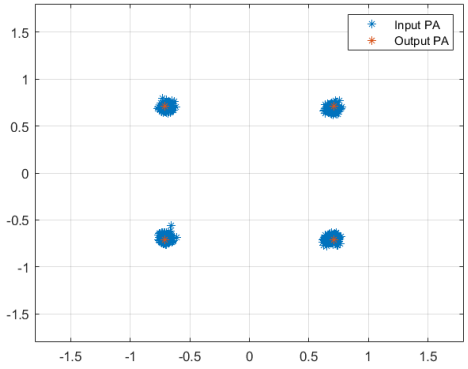

(a) QPSK signal modulated with 1MHz bandwidth.

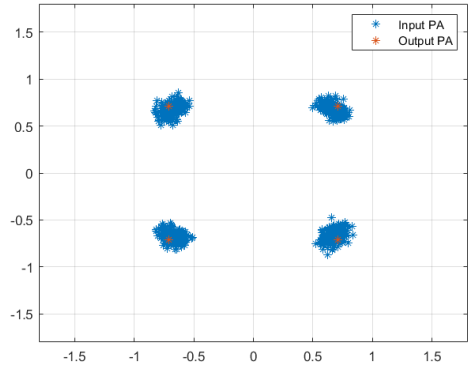

(b) QPSK signal modulated with 10MHz bandwidth.

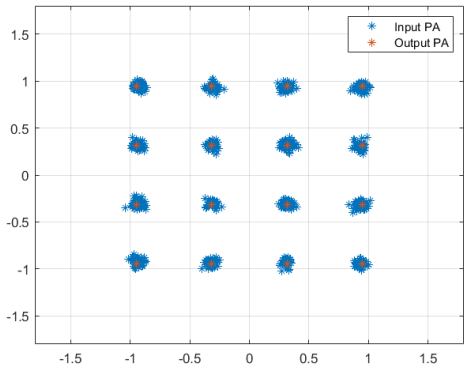

(c) 16-QAM signal modulated with 1MHz bandwidth.

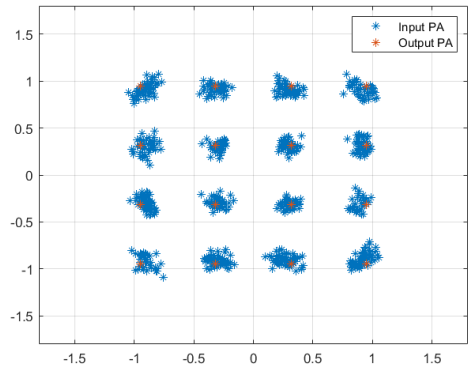

(d) 16-QAM signal modulated with 10MHz bandwidth.

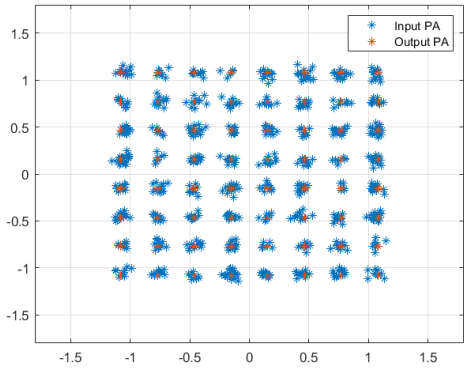

(e) 64-QAM signal modulated with 1MHz bandwidth.

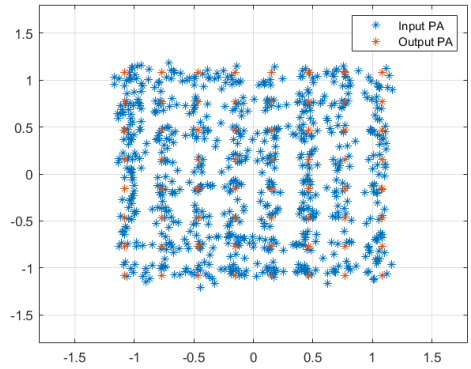

(f) 64-QAM signal modulated with 10MHz bandwidth.

Figure 3.14: Impact of Class B PA on the OFDM modulated signal constellation after phase distortion compensation.

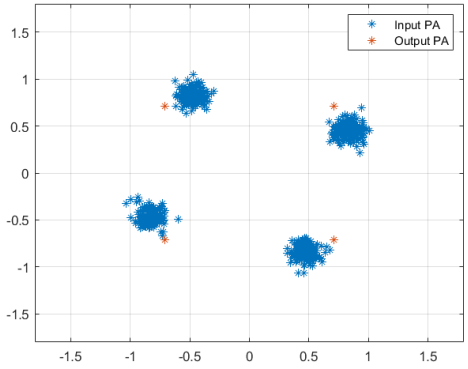

(a) QPSK signal modulated with 1MHz bandwidth.

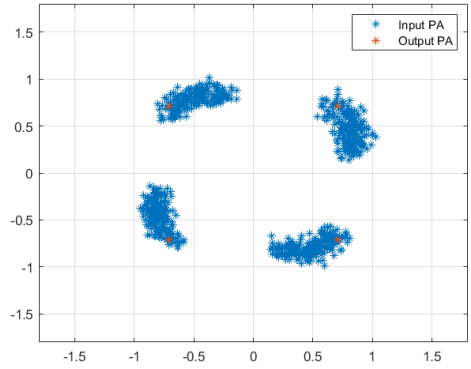

(b) QPSK signal modulated with 10MHz bandwidth.

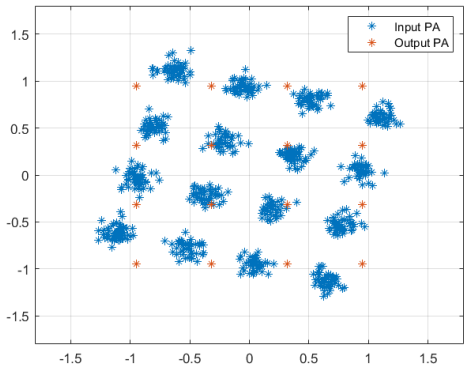

(c) 16-QAM signal modulated with 1MHz bandwidth.

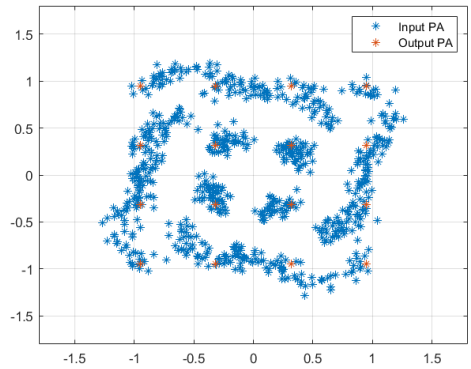

(d) 16-QAM signal modulated with 10MHz bandwidth.

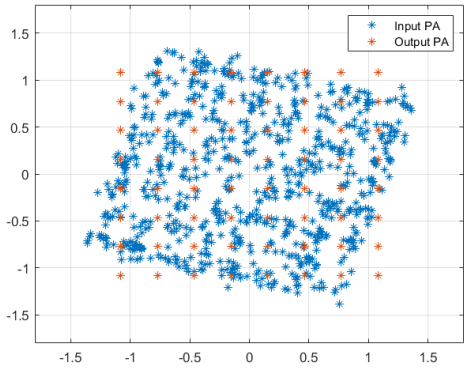

(e) 64-QAM signal modulated with 1MHz bandwidth.

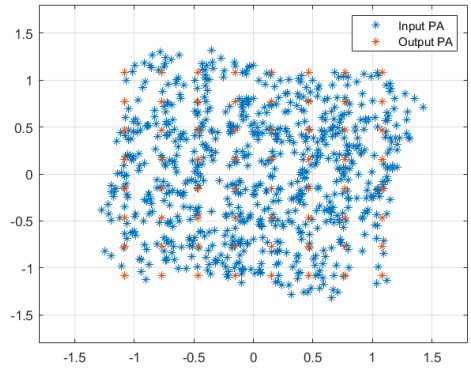

(f) 64-QAM signal modulated with 10MHz bandwidth.

Figure 3.15: Impact of Doherty PA on the OFDM modulated signal constellation.

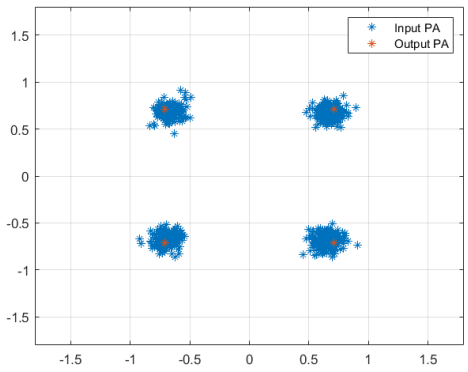

(a) QPSK signal modulated with 1MHz bandwidth.

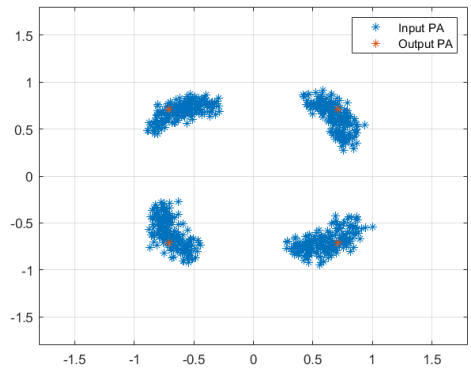

(b) QPSK signal modulated with 10MHz bandwidth.

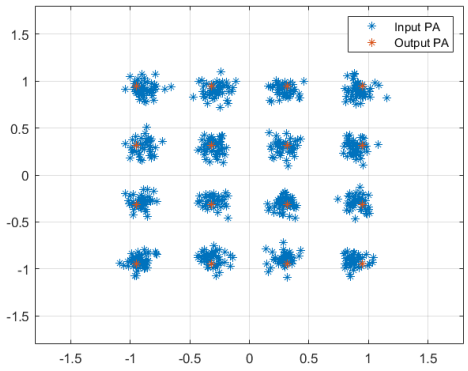

(c) 16-QAM signal modulated with 1MHz bandwidth.

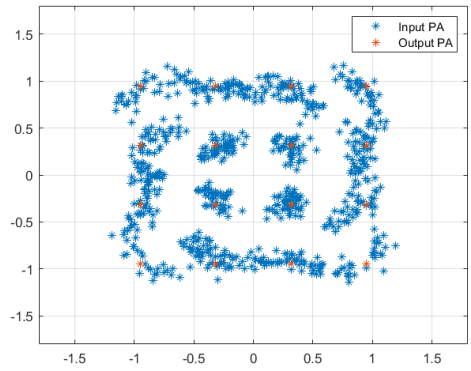

(d) 16-QAM signal modulated with 10MHz bandwidth.

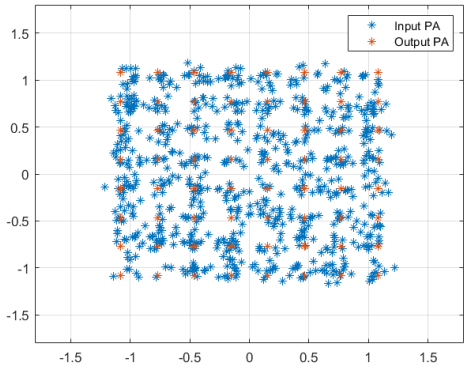

(e) 64-QAM signal modulated with 1MHz bandwidth.

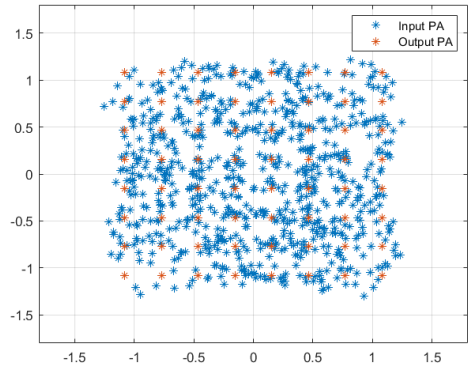

(f) 64-QAM signal modulated with 10MHz bandwidth.

Figure 3.16: Impact of Doherty PA on the OFDM modulated signal constellation after phase distortion compensation.

3.4.3 Platform Configurations

In system simulation section we studied the wireless communications system performance. However, in this system it lacks the effect that a PA present in the transmitter has on its performance. In this way, the first platform analyze the impact that a PA has on the overall performance of a SISO wireless communications system. Also in system simulation section, the reference to a particular case of a MISO system, i.e. the Alamouti 2x1 is made. In order to study the impact that a PA has on this system, a second platform is created in which the effect of a PA is added to each of the system inputs. Finally, as a way of introducing the concept of the polynomial approximation, the PA of the SISO system is replaced by a polynomial approximation, thus creating a third platform.

3.4.3.1 SISO Configuration

The SISO platform allows for the introduction of the effect of a PA in the wireless communications system analyzed in system simulation section. This effect is simulated in the ADS circuit simulation software while the remaining simulation is performed in MATLAB, as shown in figure 3.17. In this way, the interconnecting of the simulation softwares makes it is possible to analyze this effect.

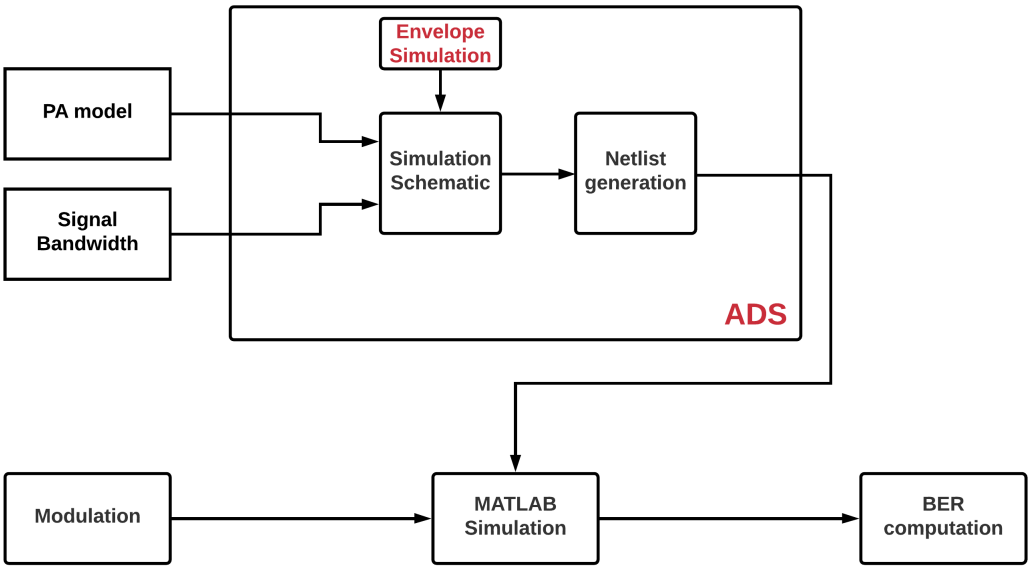

Figure 3.17: SISO platform.

Choosing the PA model and the OFDM modulated signal bandwidth to be simulated, the simulation schematic in ADS is constructed. As shown in figure 3.18, the ADS simulation schematic has in the input two readers of a .txt file, one for the real part I and another for the imaginary part Q of the OFDM modulated signal in time domain, that later are multiplied by a gain K (reason explained in the previous subsection). After that, the I and Q signals come together in a single ($TimedIQToCx$) and placed in the center frequency ($RFfreq$) of the PA that is used ($CxToTimed$). Then the signal pass through the PA envelope simulation, only the signal around the center frequency ($EnvOutSelector$) is chosen and afterwards the

signal is recovered and put back into a .txt file which will be read in MATLAB. In addition, in this simulation a Data Flow (DF) controller is used that allows us to define the simulation time as well as the step ($TstepData$) that is wanted for the signal samples (N).

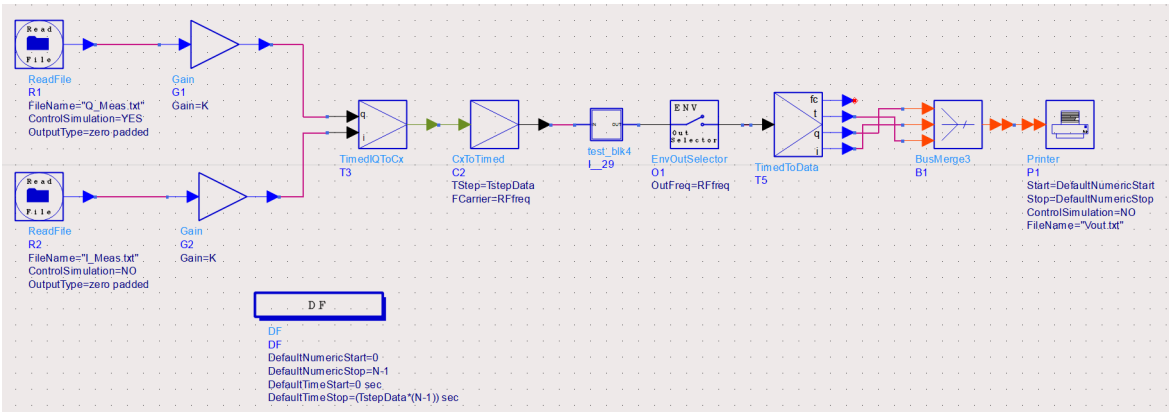

Figure 3.18: SISO platform - ADS simulation schematic.

Regarding the envelope simulation, this is done based on the selected PA model. In this way, figure 3.19 and figure 3.20 shows the envelope simulation for Class B PA and Doherty PA, respectively.

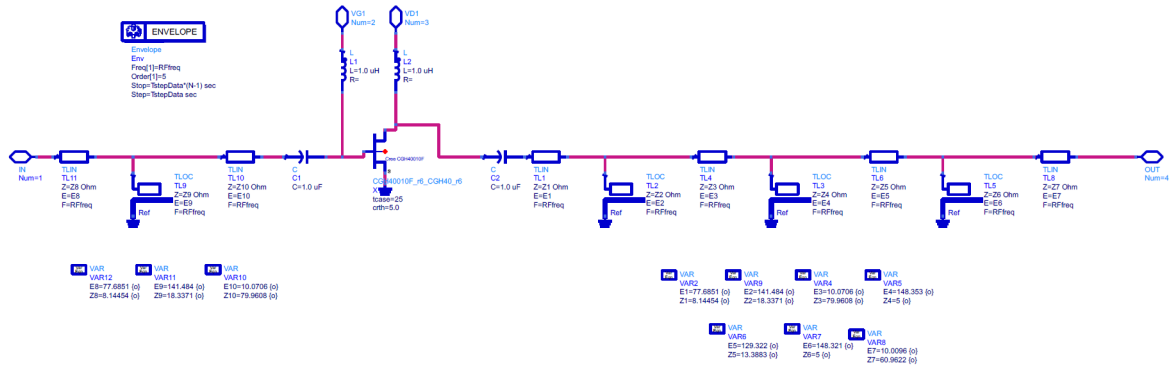

Figure 3.19: Class B PA - ADS envelope simulation.

Finally, after the ADS simulation schematic has the mentioned characteristics, a netlist that will be used in the MATLAB simulation is generated from this schematic, figure 3.18.

Thus, in MATLAB simulation it is necessary to insert the data corresponding to the I and Q signals into the .txt files, read the netlist generated in ADS and retrieve the signal placed in the .txt file at the ADS simulation output. In this way, we can analyze the wireless communications system affected by a PA, as shown in figure 3.21.

The MATLAB simulation block consists of a random data generator, followed by a modulator and an OFDM modulator. At this moment the signal is in the condition to pass through the PA, and for that the netlist created by ADS software is used. Then, the channel effect is applied to the signal, and in the receiver the phase compensation, OFDM demodulation, equalization and demodulation are performed. Here, the received bits are compared to the

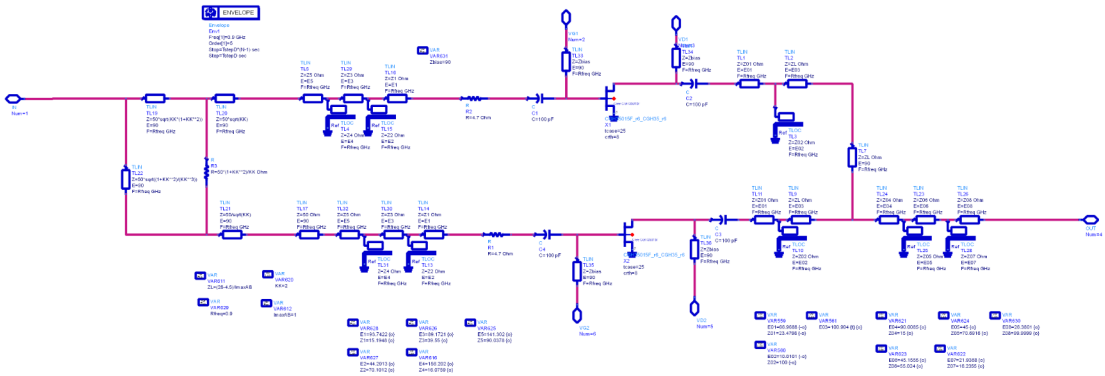

Figure 3.20: Doherty PA - ADS envelope simulation.

sent bits via BER, as shown in figure 3.21.

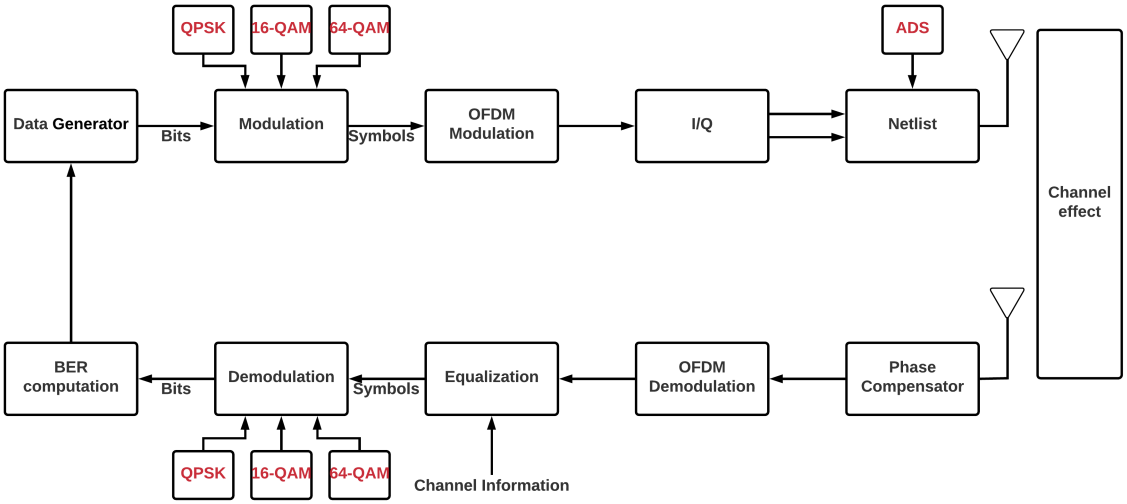

Figure 3.21: SISO platform - MATLAB simulation scheme.

3.4.3.2 MISO - Alamouti 2x1 Configuration

In this system, the difference in relation to the SISO system is that there are two antennas in the transmitter and therefore two PAs. In this way, the MISO platform analyze the effect of the introduction of two PAs on the overall performance of the MISO system - Alamouti 2x1. As in the SISO configuration, the MISO configuration use the ADS to simulate the PAs while the remaining simulation is done in MATLAB.

As shown in figure 3.22, the procedure is the same as in the previous case. The difference is that since we now have two signals to send, we must have a branch for each of them, knowing that in each branch an envelope simulation will be made.

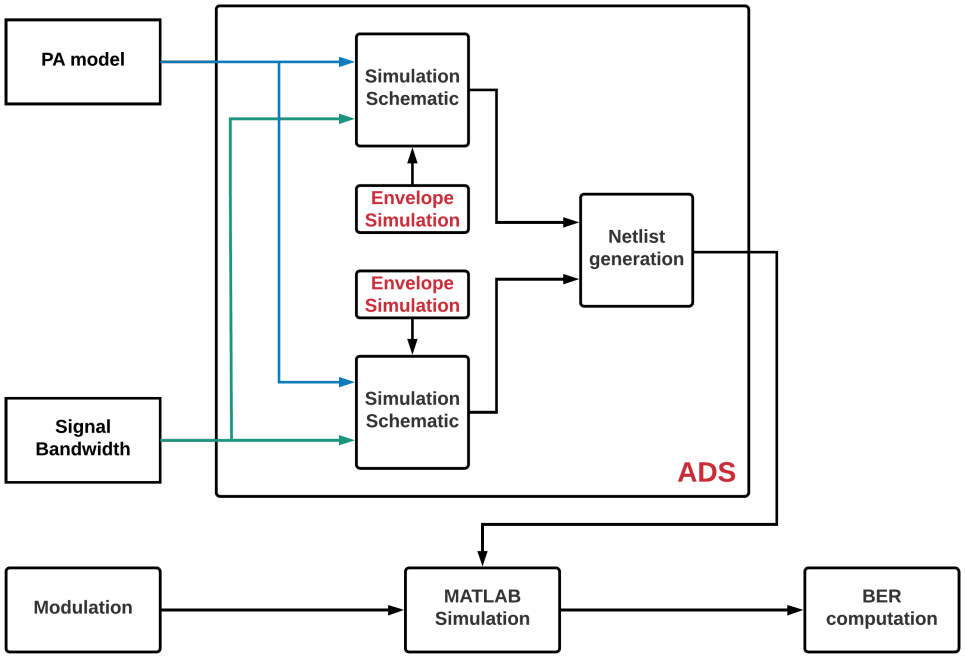

Figure 3.22: MISO - Alamouti 2x1 platform.

So, the netlist creation is based on the two branches of the transmitter, as shown in figure 3.23. After the netlist is created, the MATLAB simulation follows the scheme of figure 3.24.

Now, since we have two antennas in the transmitter the signals are generated from the space time block coding of the Alamouti 2x1. In the receiver, the signals being affected by the channel, the Alamouti 2x1 decoding is performed, the remaining process being equal to the SISO platform.

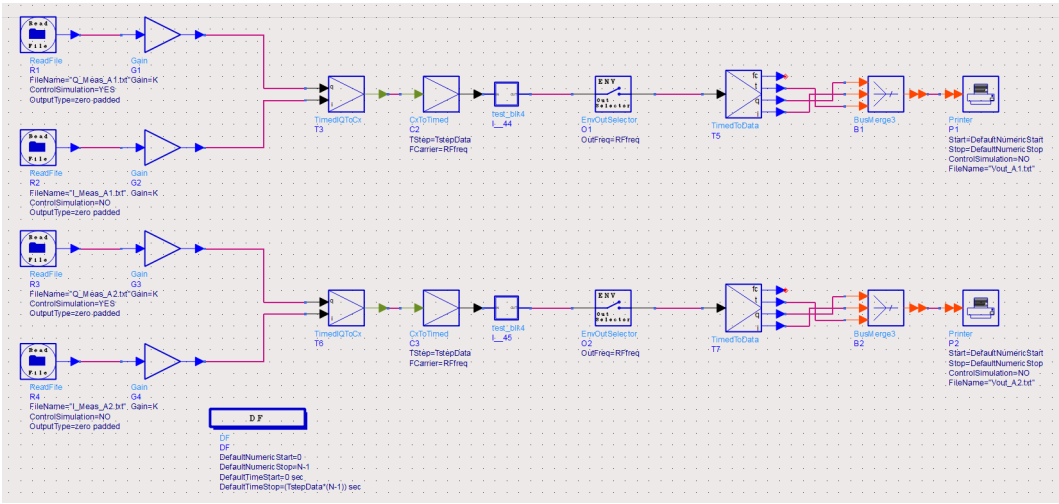

Figure 3.23: MISO Alamouti 2x1 platform - ADS simulation schematic.

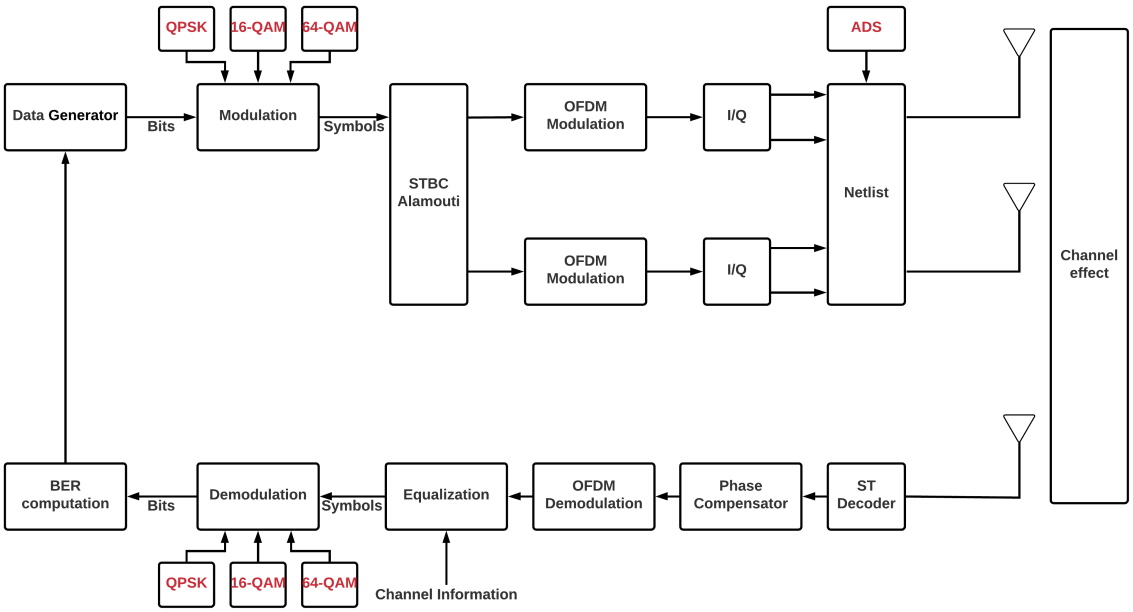

Figure 3.24: MISO Alamouti 2x1 platform - MATLAB simulation scheme.

3.4.3.3 Polynomial Approximation Configuration

In previous simulations, the simulation time (which depends on the number of simulated OFDM symbols and netlist reading time) is one of the major obstacles in the use of the system of simulations previously mentioned. Due to this, an alternative to the SISO configuration is presented using a polynomial that approximates the behavior of the PA [50][51][52]. Thus, the new simulation scheme is illustrated in figure 3.26. Here ADS software is only used to generate the polynomial: figure 3.25 shows how to achieve the input and output signal of the PA to create the polynomial, in which the whole simulation is performed in MATLAB.

As seen so far, a PA is a non-linear device that complicates the polynomial approximation. In an actual PA, the output depends not only on the input at that instant $x(n)$ but also on the excitation level of the previous instants $x(n-m_1)$. Because of this, it is necessary to use a polynomial that takes these two factors into account, as shown by equation 3.7 [53].

$$y(n) = \sum_{p=0}^{P-1} \sum_{m_1=0}^{M_1} h_{p,m_1} x(n-m_1) x(n-m_1)^p \tag{3.7}$$

where P is the order of the polynomial and M_1 is the memory depth (the oldest sample that still has an impact on the output signal).

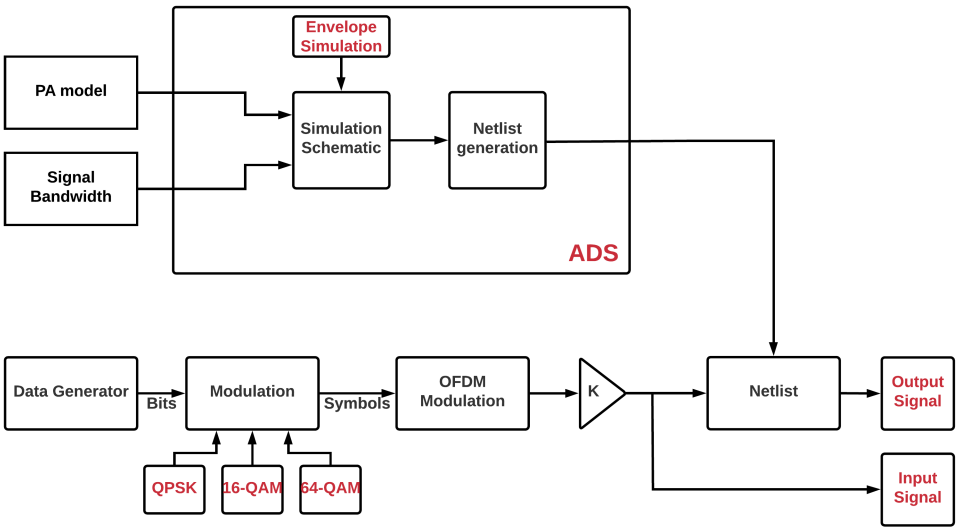

Figure 3.25: Input and output signal collect scheme.

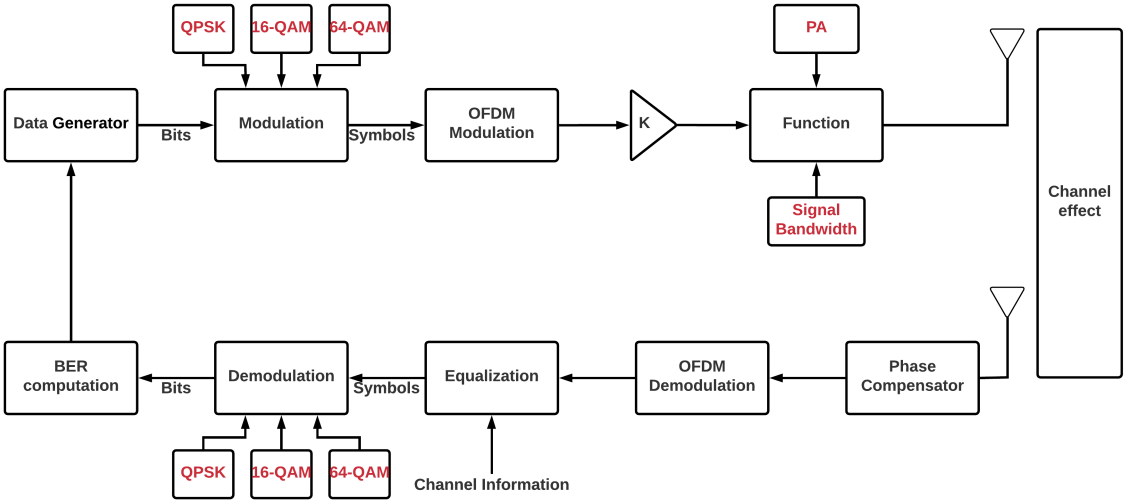

Figure 3.26: Polynomial Approximation platform.

In these simulations the construction of the polynomial approximation is made based on the equation 3.7 and considering two cases: one, that the output does not depend on samples of past instants ($M_1 = 0$) and another, that the output depends on samples of past instants ($M1$ other than 1 that minimizes Normalised Mean Square Error (NMSE)).

Chapter 4

Simulation Tests

4.1 System Performance Measurement - BER computation

4.1.1 SISO Configuration Simulation

After the characteristics of the simulation system blocks are known, figure 3.21, the simulations are carried out. For this, 10000 OFDM symbols are simulated to obtain a consistent mean of these values (since the generated signal is random). The results obtained are present in figure 4.1 for the case of Class B PA and in figure 4.2 for the case of Doherty PA. In addition, figure 4.3 compares both PAs performance.

By analyzing the effect that the Class B PA has on the BER curves, we can seen that in the QPSK modulation the impact that the signal bandwidth to apply has is not significant, as is verified in figure 4.1(a) and 4.1(b). On the other hand, in the 16-QAM modulation, with no PA effect, there is more BER than in the QPSK modulation, as concluded in Chapter 2. In addition, in the 16-QAM modulation, the increase of the signal bandwidth to be applied has a significant impact contrary to that observed in the QPSK modulation, as can be seen in figure 4.1(c) and 4.1(d): applying a 10MHz bandwidth signal, the BER curves begin to tend to a minimum for high SNR (high SNR regime). Finally, in the 64-QAM modulation, with no PA effect, it was concluded in Chapter 2 that it was the modulation that has a higher BER compared to those previously mentioned. With the PA effect, we see that the curves begin to tend to a minimum value, this value being lower in the case of the 1MHz bandwidth signal, as shown in figure 4.1(e) and 4.1(f). In this way, we can conclude that there is a great degradation of the signal with the increase of the data to be transmitted simultaneously, such as the 64-QAM modulation.

In relation to the effect that the Doherty PA has on the BER curves, it is possible to conclude that in the QPSK modulation the BER degradation is not significant, figure 4.2(a) and 4.2(b). On the other hand, in the 16-QAM modulation and the 64-QAM modulation it is verified that the curves begin to tend to a minimum value for high SNR values, the lowest minimum value for the 16-QAM modulation when applying a 1MHz bandwidth signal and higher for 64-QAM modulation by applying a 10MHz bandwidth signal, as shown in figure 4.2(c),4.2(d), 4.2(e) and 4.2(f).

Finally, in order to compare the performance of the PAs with the same modulation and the same bandwidth, figure 4.3 was added. As noted in section 3.2.2 and 3.2.3, Doherty PA further degrades the signal comparatively to Class B PA and thus has a higher BER. This conclusion coincides with that observed in the figure 4.3, where it is concluded that the BER

in Doherty PA is larger than the BER in Class B PA.

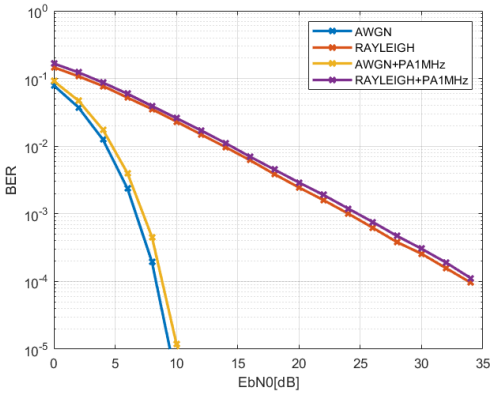

(a) BER for QPSK modulation and signal with 1MHz of bandwidth.

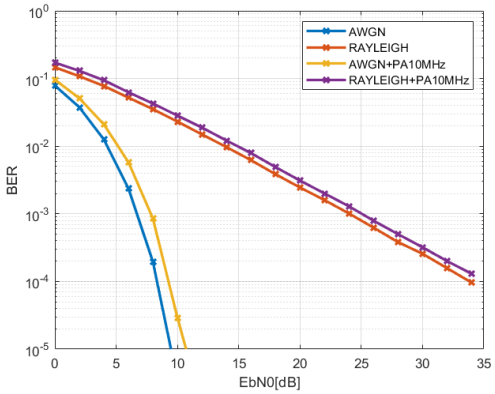

(b) BER for QPSK modulation and signal with 10MHz of bandwidth.

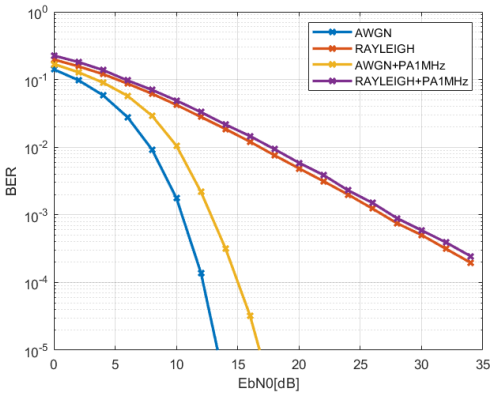

(c) BER for 16-QAM modulation and signal with 1MHz of bandwidth.

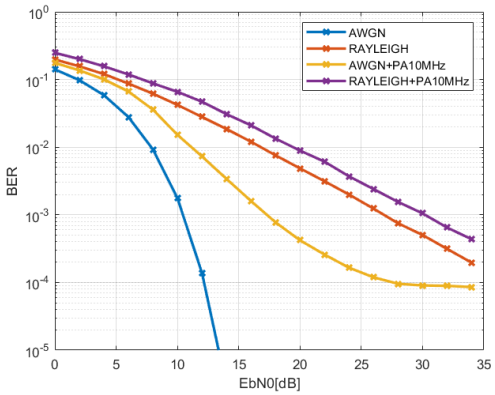

(d) BER for 16-QAM modulation and signal with 10MHz of bandwidth.

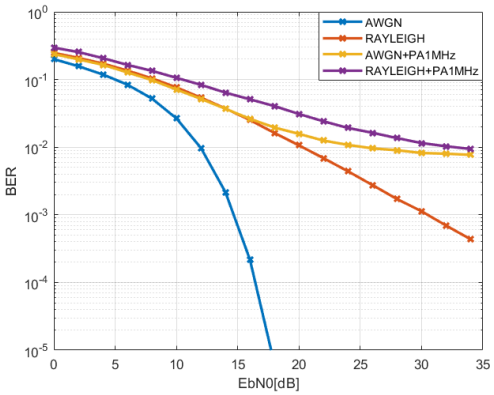

(e) BER for 64-QAM modulation and signal with 1MHz of bandwidth.

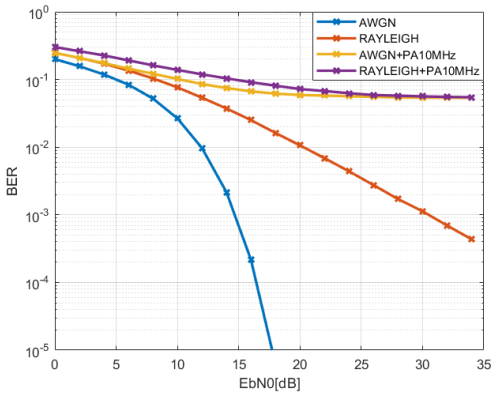

(f) BER for 64-QAM modulation and signal with 10MHz of bandwidth.

Figure 4.1: SISO simulation - Class B PA effect on the BER.

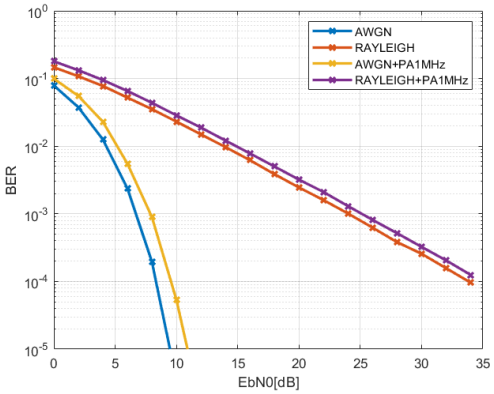

(a) BER for QPSK modulation and signal with 1MHz of bandwidth.

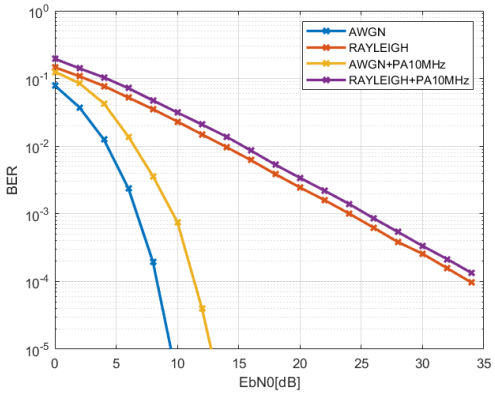

(b) BER for QPSK modulation and signal with 10MHz of bandwidth.

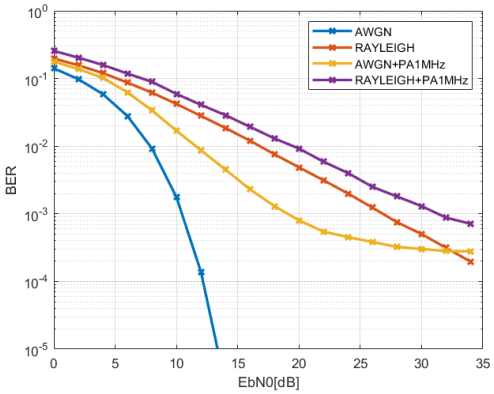

(c) BER for 16-QAM modulation and signal with 1MHz of bandwidth.

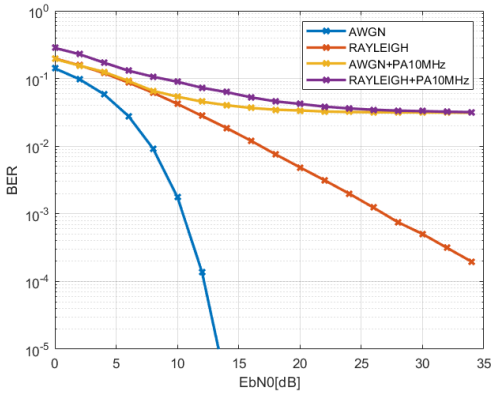

(d) BER for 16-QAM modulation and signal with 10MHz of bandwidth.

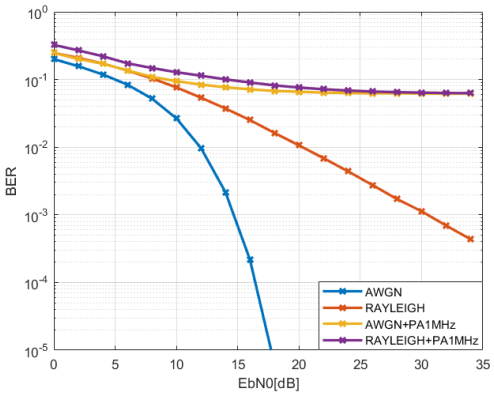

(e) BER for 64-QAM modulation and signal with 1MHz of bandwidth.

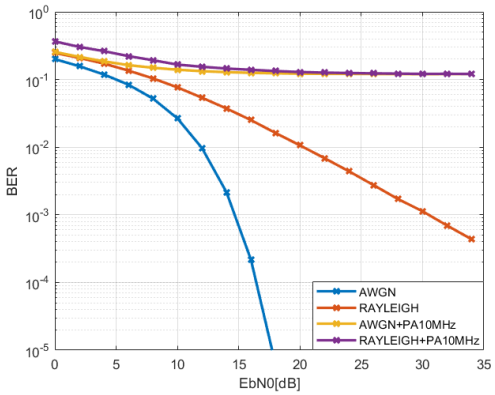

(f) BER for 64-QAM modulation and signal with 10MHz of bandwidth.

Figure 4.2: SISO simulation - Doherty PA effect on the BER.

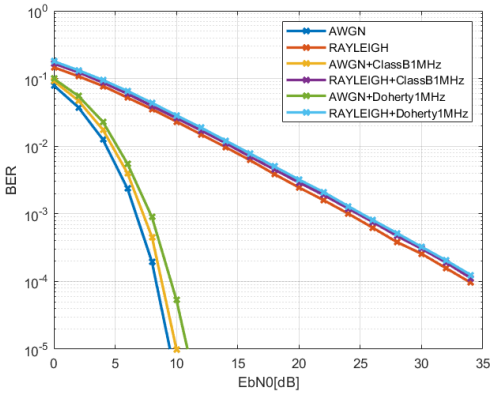

(a) BER for QPSK modulation and signal with 1MHz of bandwidth.

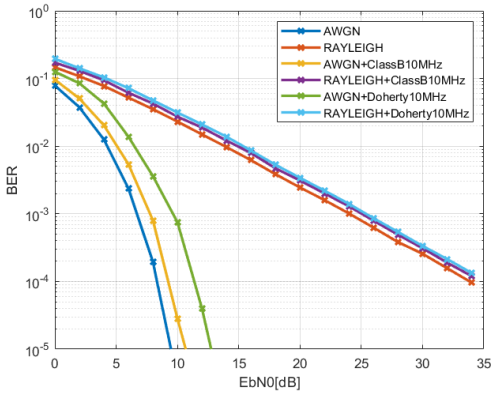

(b) BER for QPSK modulation and signal with 10MHz of bandwidth.

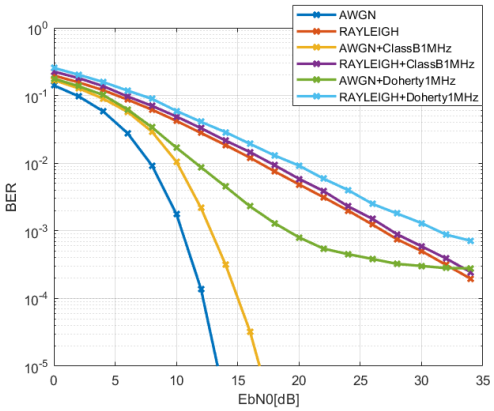

(c) BER for 16-QAM modulation and signal with 1MHz of bandwidth.

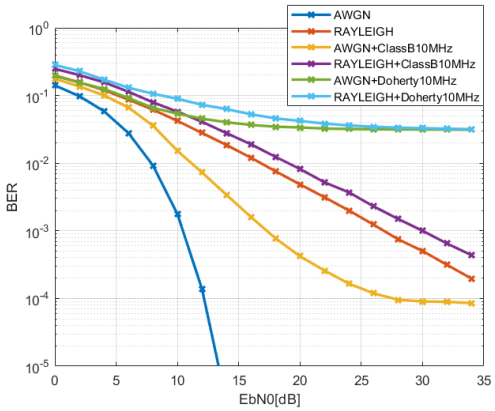

(d) BER for 16-QAM modulation and signal with 10MHz of bandwidth.

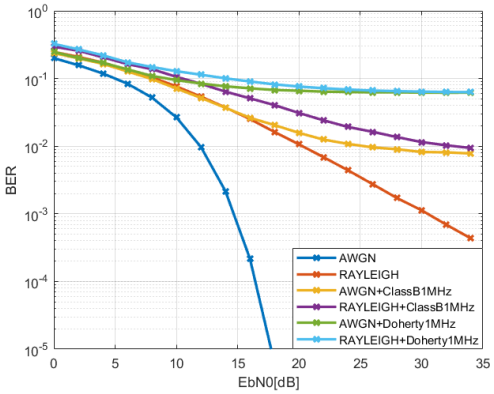

(e) BER for 64-QAM modulation and signal with 1MHz of bandwidth.

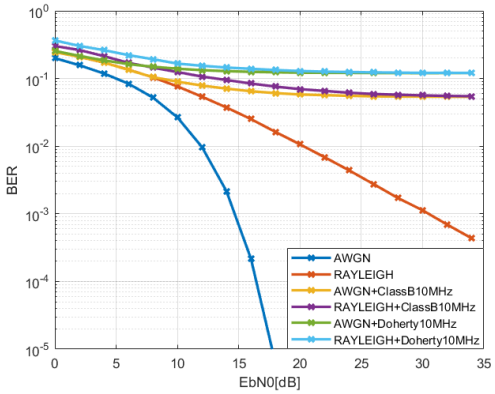

(f) BER for 64-QAM modulation and signal with 10MHz of bandwidth.

Figure 4.3: SISO simulation - PAs effect on the BER.

4.1.2 MISO - Alamouti 2x1 Configuration Simulation

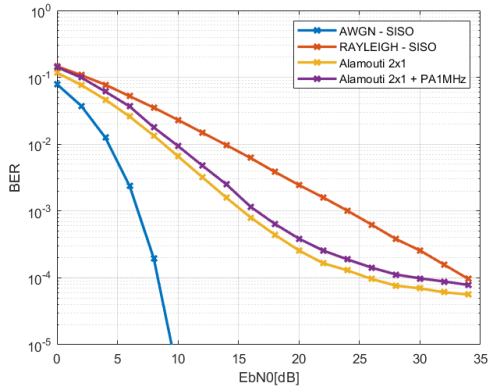

(a) Effect of Class B PA on the BER with 1MHz modulated signal bandwidth.

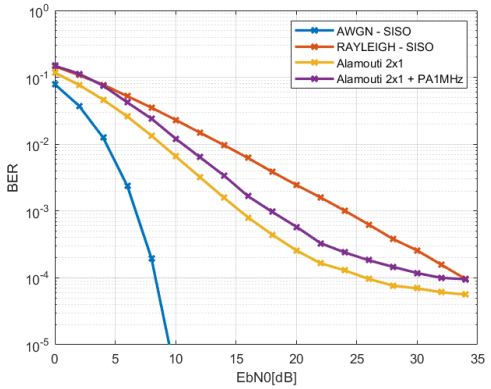

(b) Effect of Doherty PA on the BER with 1MHz modulated signal bandwidth.

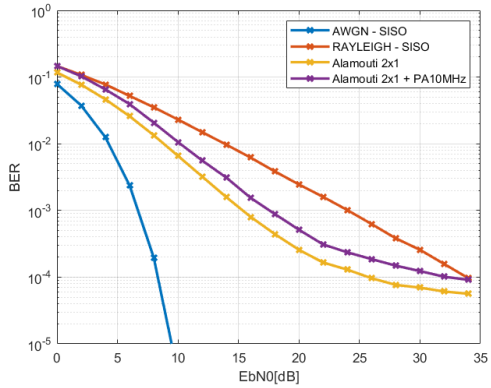

(c) Effect of Class B PA on the BER with 10MHz modulated signal bandwidth.

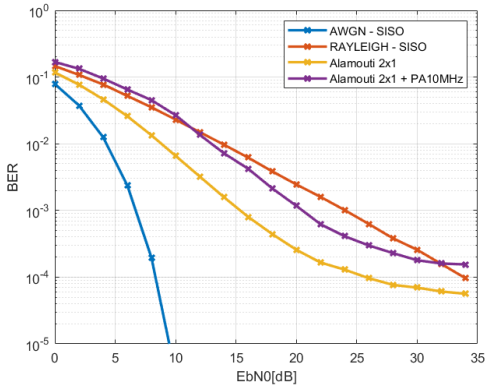

(d) Effect of Doherty PA on the BER with 10MHz modulated signal bandwidth.

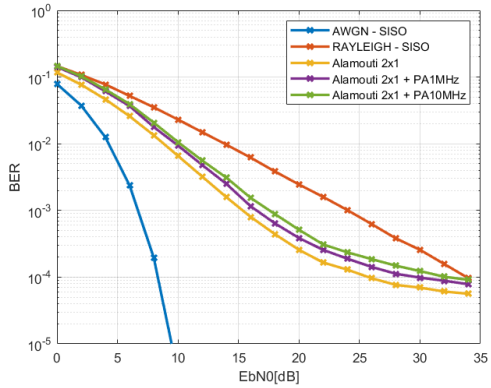

(e) Effect of Class B PA on the BER.

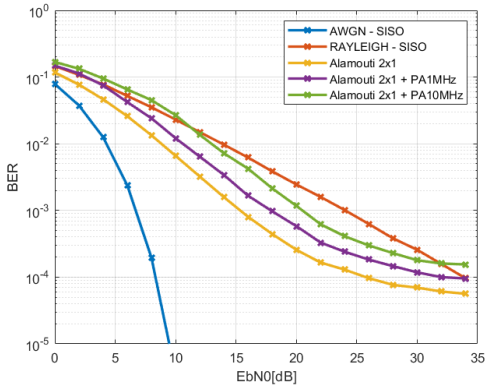

(f) Effect of Doherty PA on the BER.

Figure 4.4: Alamouti 2x1 simulation - PAs effect on the BER considering the QPSK modulation.

After having looked at the SISO configuration simulation, we will now study the Alamouti 2x1 which is a particular case of the MISO system. For this study, the SISO configuration scheme, figure 3.21, has to be changed, as shown in figure 3.24.

After the simulation is performed, the results are processed as shown in figure 4.4. Based on the figure we can see that in the case of the Doherty PA the increase of the 1MHz bandwidth signal to 10MHz bandwidth signal (figure 4.4(b) to 4.4(d)) makes the curve of the Alamouti 2x1 distance itself from the curve with no PA effect compared to the case of Class B PA (figure 4.4(a) for 4.4(c)).

Finally, figure 4.4(e) and 4.4(f) show the impact that the signal bandwidth has on the BER curve for Class B PA and Doherty PA, respectively. Here we see that the impact of the bandwidth change is greater in the case of Doherty PA as had already occurred in the SISO configuration simulation.

4.1.3 Polynomial Approximation Configuration Simulation

4.1.3.1 Memoryless Simulation

In order to generate the polynomial that approximates the behavior of the PA, it is necessary to initially collect the input signal and the output signal of the PA, as shown in figure 3.25.

After collecting the signals, considering in this case a memoryless polynomial approximation, it is necessary to choose the value of the order of the polynomial that minimizes the NMSE. In this way, for Class B PA a P equal to 5 and for Doherty PA a P equal to 7 is used. Then, using the scheme of figure 4.5, the NMSE values for the two PA types (considering 1MHz and 10MHz bandwidth signal) and for the three modulation types referenced here are collected, obtaining the results of table 4.1.

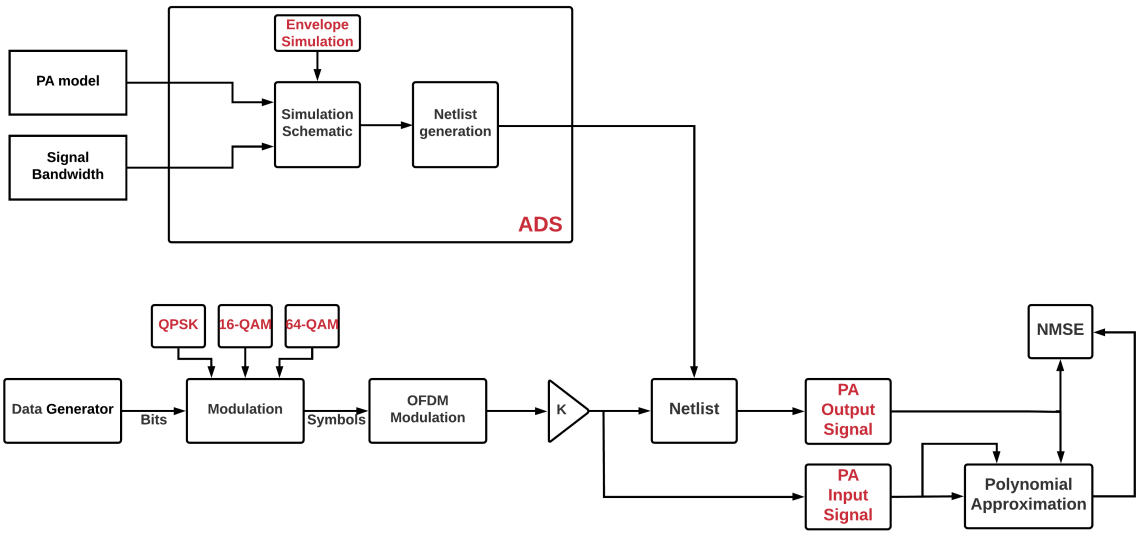

Figure 4.5: NMSE scheme.

PA	Modulation	Bandwidth	NMSE
Class B	QPSK	1MHz	-40.82
Class B	QPSK	10MHz	-23.49
Class B	16-QAM	1MHz	-40.98
Class B	16-QAM	10MHz	-23.39
Class B	64-QAM	1MHz	-40.74
Class B	64-QAM	10MHz	-23.55
Doherty	QPSK	1MHz	-30.29
Doherty	QPSK	10MHz	-14.79
Doherty	16-QAM	1MHz	-30.14
Doherty	16-QAM	10MHz	-14.85
Doherty	64-QAM	1MHz	-30.32
Doherty	64-QAM	10MHz	-14.85

Table 4.1: NMSE results for memoryless polynomial approximation.

From table 4.1 we can conclude that the values are identical by comparing the three modulations with the same bandwidth and analyzing the two PAs separately. In addition, the increase in NMSE is noticeable with the change from Class B PA to Doherty PA. On the other hand, an increase of the NMSE with the increase of the signal bandwidth is observed, as would be expected since the increase of the bandwidth causes a widening of the curves of the characteristics of the PA as verified previously and taking into account that it was considered a memoryless polynomial approximation.

In order to have a better perception of what was mentioned previously, the AM-AM and AM-PM curves collected are compared. Thus, considering the QPSK modulation (since the results are identical) figure 4.6 contains the Class B PA curves and figure 4.7 contains the Doherty PA curves taking into account the two bandwidths.

Figure 4.6 shows that by increasing the signal bandwidth the polynomial approximation curve gets further and further away from the original curve, thus increasing the NMSE. The same is true in figure 4.7. Considering that it is expected because although the increase in bandwidth cause an increase in the NMSE, the error in the demodulation of the signal in the receiver is smaller due to the fact that the polynomial approximation curve approaches the 1MHz bandwidth original curve. Thus, it is expected that the BER curve of the memoryless polynomial approximation for the 10MHz bandwidth signal case will be lower than the curve obtained with the SISO simulation for the same bandwidth.

Finally, after the memoryless polynomial approximation be created, the simulation is performed according to the scheme of figure 3.26 and the memoryless polynomial coefficients present in table 4.2. The obtained results are present in figure 4.8 and in figure 4.9.

As shown in figure 4.6 and figure 4.7, when the approximation is made for the 1MHz bandwidth signal the NMSE is smaller (table 4.1). Thus, the curves of the memoryless polynomial approximation coincide with the SISO simulation curves for both PAs and for all modulations as shown in figure 4.8(a), 4.8(c) and 4.8(e) for the case of Class B PA and figure 4.9(a), 4.9(c) and 4.9(e) for the case of Doherty PA.

On the other hand, the increase of the signal bandwidth to 10MHz causes an increase of the NMSE that, in turn, causes a departure from the AM-AM and AM-PM curves: the curves of the memoryless polynomial approximation to 10MHz bandwidth signal are very similar to the curves of the memoryless polynomial approximation to 1MHz bandwidth signal. Because

of this, it is expected that the BER of the memoryless polynomial approximation to 10MHz bandwidth signal will be similar to the case of the 1MHz bandwidth signal, being thus inferior to that verified in the SISO simulation for this bandwidth. This phenomenon is visible in figure 4.8(b), 4.8(d) and 4.8(f) for the case of Class B PA and figure 4.9(b), 4.9(d) and 4.9(f) for the case of Doherty PA. Here it is obvious that the curves have a distance, which is more visible in 16-QAM and 64-QAM modulations.

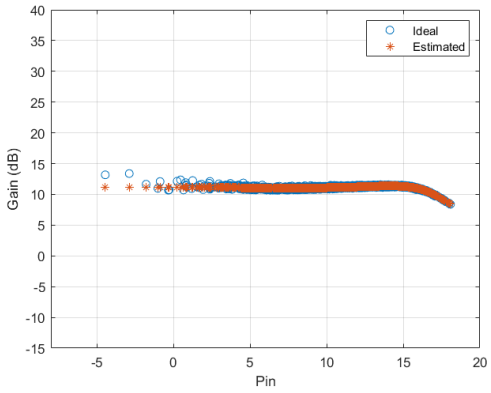

(a) AM-AM curves considering 1MHz bandwidth signal.

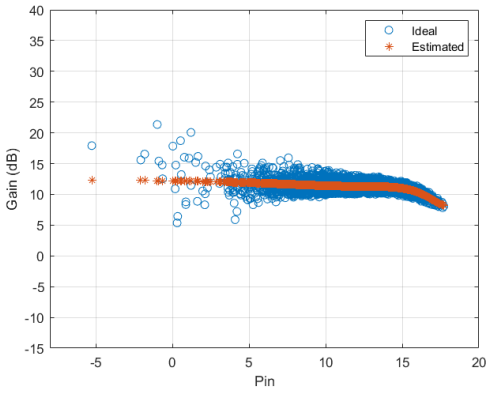

(b) AM-AM curves considering 10MHz bandwidth signal.

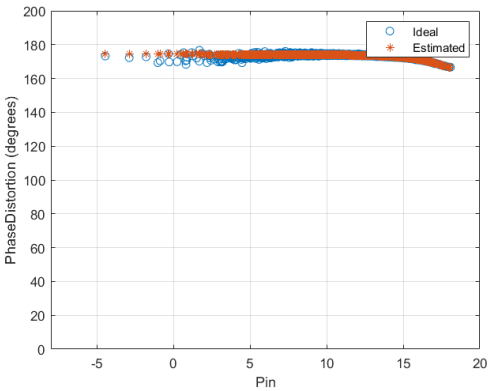

(c) AM-PM curves considering 1MHz bandwidth signal.

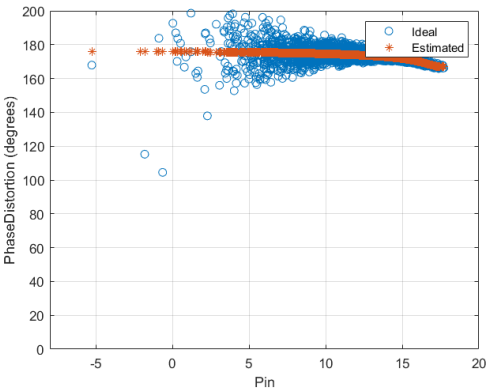

(d) AM-PM curves considering 10MHz bandwidth signal.

Figure 4.6: Class B PA - AM-AM and AM-PM curves compare.

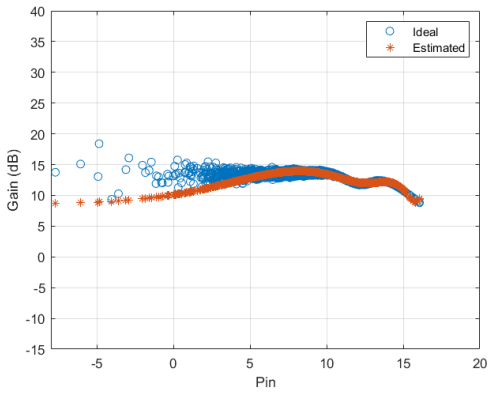

(a) AM-AM curves considering 1MHz bandwidth signal.

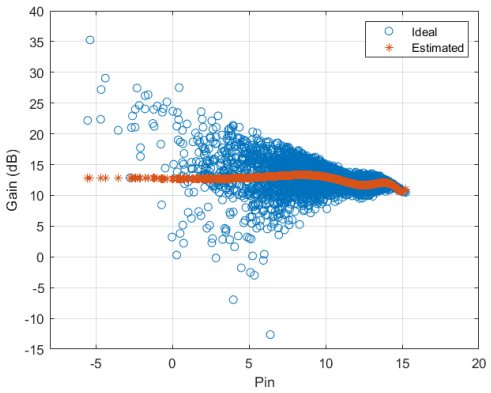

(b) AM-AM curves considering 10MHz bandwidth signal.

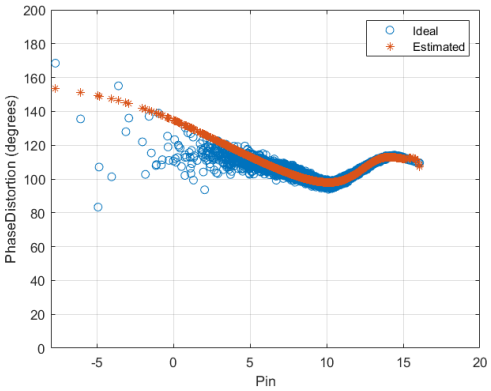

(c) AM-PM curves considering 1MHz bandwidth signal.

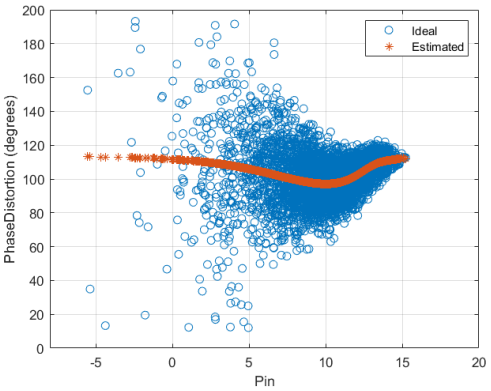

(d) AM-PM curves considering 10MHz bandwidth signal.

Figure 4.7: Doherty PA - AM-AM and AM-PM curves compare.

PA	Signal Bandwidth	Coefficient	Real Part	Imaginary Part
Class B	1MHz	1	$-8.9 * 10^{-1}$	$8.6 * 10^{-2}$
Class B	1MHz	2	$4.9 * 10^{-3}$	$5.0 * 10^{-4}$
Class B	1MHz	3	$-5.6 * 10^{-4}$	$1.6 * 10^{-5}$
Class B	1MHz	4	$1.6 * 10^{-5}$	$2.7 * 10^{-7}$
Class B	1MHz	5	$-1.2 * 10^{-7}$	$-6.1 * 10^{-9}$
Class B	10MHz	1	$-1.0 * 10^{0}$	$9.3 * 10^{-2}$
Class B	10MHz	2	$1.6 * 10^{-2}$	$-2.6 * 10^{-3}$
Class B	10MHz	3	$-1.0 * 10^{-3}$	$2.3 * 10^{-4}$
Class B	10MHz	4	$2.7 * 10^{-5}$	$-4.6 * 10^{-6}$
Class B	10MHz	5	$-2.2 * 10^{-7}$	$2.9 * 10^{-8}$
Doherty	1MHz	1	$1.2 * 10^{0}$	$-5.4 * 10^{-1}$
Doherty	1MHz	2	$-6.7 * 10^{-2}$	$-7.1 * 10^{-1}$
Doherty	1MHz	3	$-1.9 * 10^{-2}$	$9.2 * 10^{-2}$
Doherty	1MHz	4	$2.9 * 10^{-3}$	$-5.0 * 10^{-3}$
Doherty	1MHz	5	$-1.4 * 10^{-4}$	$1.2 * 10^{-4}$
Doherty	1MHz	6	$2.9 * 10^{-6}$	$-1.2 * 10^{-6}$
Doherty	1MHz	7	$-2.3 * 10^{-8}$	$8.1 * 10^{-10}$
Doherty	10MHz	1	$1.2 * 10^{0}$	$-7.1 * 10^{-1}$
Doherty	10MHz	2	$-1.1 * 10^{-1}$	$-6.4 * 10^{-1}$
Doherty	10MHz	3	$-8.6 * 10^{-3}$	$9.1 * 10^{-2}$
Doherty	10MHz	4	$1.8 * 10^{-3}$	$-5.7 * 10^{-3}$
Doherty	10MHz	5	$-9.1 * 10^{-5}$	$1.8 * 10^{-4}$
Doherty	10MHz	6	$1.9 * 10^{-6}$	$-2.7 * 10^{-6}$
Doherty	10MHz	7	$-1.4 * 10^{-8}$	$1.5 * 10^{-8}$

Table 4.2: Memoryless polynomial approximation coefficients.

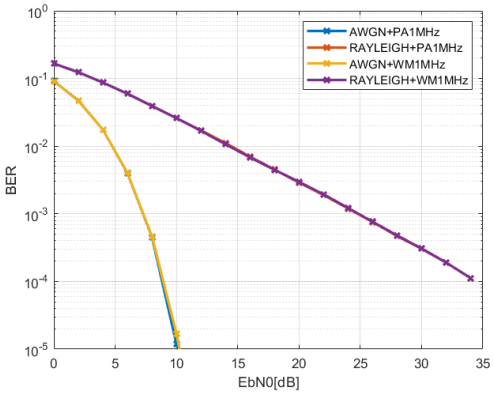

(a) BER for QPSK modulation and signal with 1MHz of bandwidth.

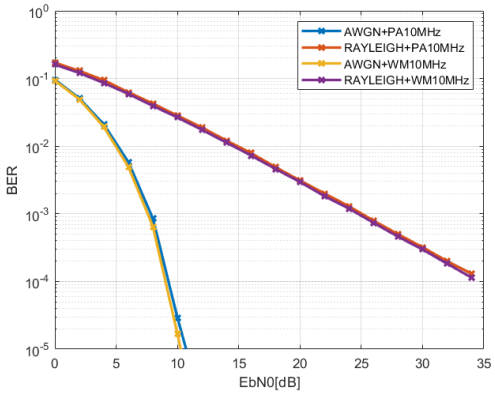

(b) BER for QPSK modulation and signal with 10MHz of bandwidth.

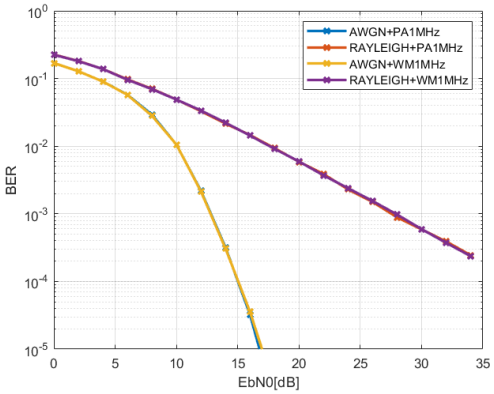

(c) BER for 16-QAM modulation and signal with 1MHz of bandwidth.

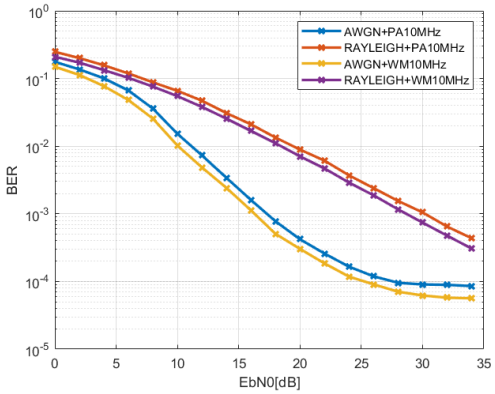

(d) BER for 16-QAM modulation and signal with 10MHz of bandwidth.

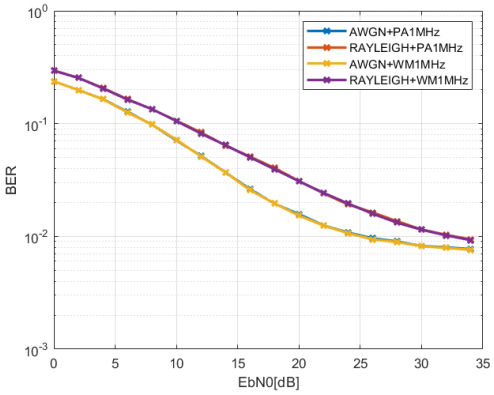

(e) BER for 64-QAM modulation and signal with 1MHz of bandwidth.

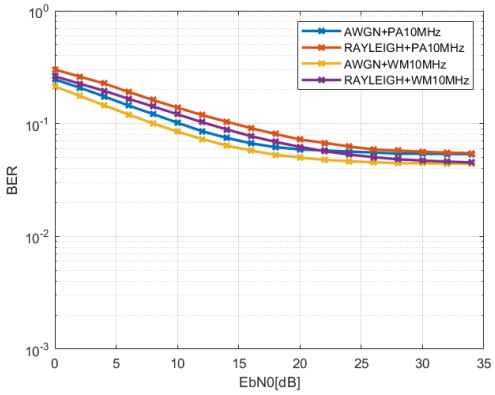

(f) BER for 64-QAM modulation and signal with 10MHz of bandwidth.

Figure 4.8: Memoryless polynomial approximation simulation - Class B PA effect on the BER.

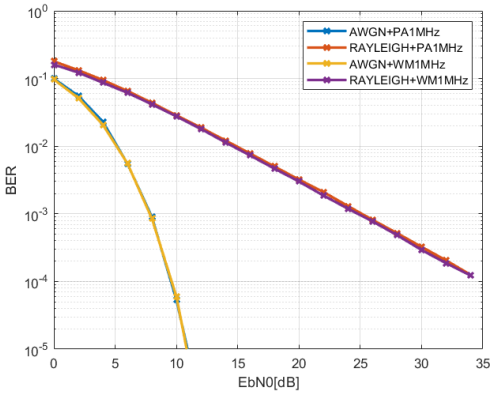

(a) BER for QPSK modulation and signal with 1MHz of bandwidth.

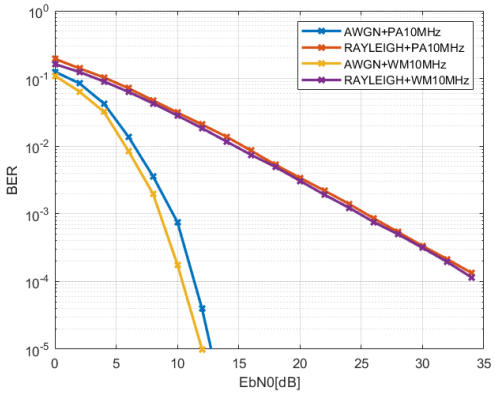

(b) BER for QPSK modulation and signal with 10MHz of bandwidth.

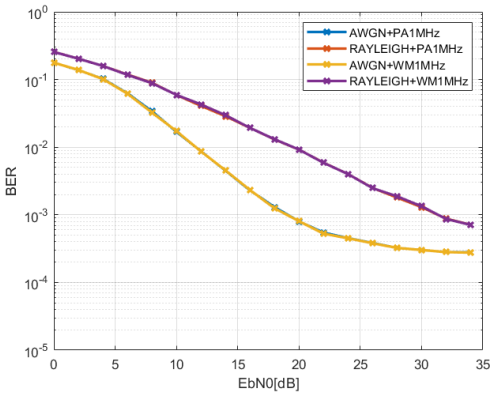

(c) BER for 16-QAM modulation and signal with 1MHz of bandwidth.

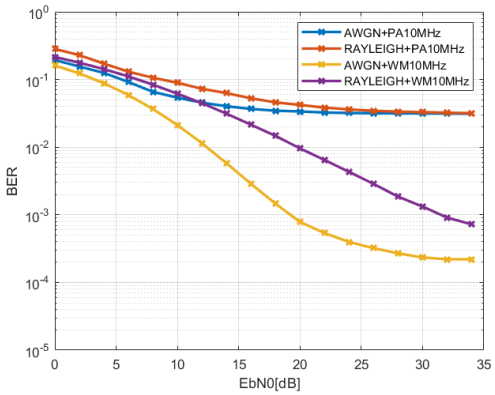

(d) BER for 16-QAM modulation and signal with 10MHz of bandwidth.

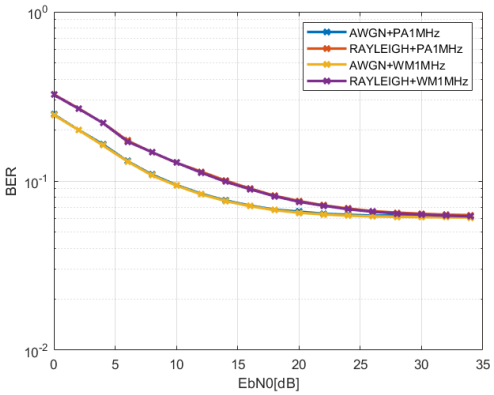

(e) BER for 64-QAM modulation and signal with 1MHz of bandwidth.

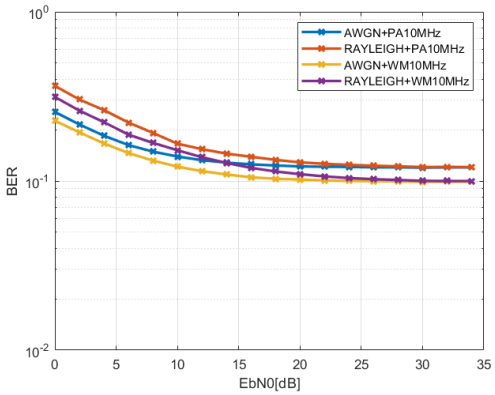

(f) BER for 64-QAM modulation and signal with 10MHz of bandwidth.

Figure 4.9: Memoryless polynomial approximation simulation - Doherty PA effect on the BER.

4.1.3.2 Memory Simulation

After studying the memoryless polynomial approximation, at this point the objective is to study the quality that the memory polynomial approximation has compared to the previous one. For this, the order of the polynomial previously used and the M_1 in order to minimize the NMSE are selected. In this way, an equal M_1 for the two PAs with a value of 3 is chosen.

Then, using the scheme of figure 3.25, the input and output signals are collected and the NMSE values for the PAs, the various modulations and the two bandwidths are calculated, obtaining the results of table 4.3.

Looking at table 4.3 and recalling table 4.1 it is verified that the introduction of memory in the polynomial approximation causes the NMSE to decrease, that is, the memory polynomial approximation curves are expected to approximate more than those obtained in the SISO simulation than the curves of the memoryless polynomial approximation. This fact is shown in figure 4.10 for the case of Class B PA and figure 4.11 for the case of Doherty PA, where it is clear that the AM-AM and AM-PM curves of the memory polynomial approximation almost coincide with the curves obtained in the SISO simulation. Thus, as a closer approximation occurs in the AM-AM and AM-PM curves, it is expected that the BER curves of the memory polynomial approximation are very close to the BER curves obtained in the SISO simulation.

Thus, after the memory polynomial approximation was created, the simulation is done as in the previous case. The results obtained are shown in figure 4.12 and in figure 4.13.

PA	Modulation	Bandwidth	NMSE
Class B	QPSK	1MHz	-47.98
Class B	QPSK	10MHz	-31.56
Class B	16-QAM	1MHz	-48.07
Class B	16-QAM	10MHz	-31.23
Class B	64-QAM	1MHz	-47.96
Class B	64-QAM	10MHz	-31.68
Doherty	QPSK	1MHz	-34.40
Doherty	QPSK	10MHz	-30.51
Doherty	16-QAM	1MHz	-34.14
Doherty	16-QAM	10MHz	-30.64
Doherty	64-QAM	1MHz	-33.88
Doherty	64-QAM	10MHz	-30.65

Table 4.3: NMSE results for memory polynomial approximation.

Analyzing the results obtained for the case of Class B PA, figure 4.12 allows us to conclude that the BER curves of the memory polynomial approximation are almost superimposed with the curves obtained in the SISO simulation for all the studied cases, coinciding with the expected results since the memory polynomial approximation has a smaller NMSE value. In this way, we can better approximate the performance of the Class B PA with a memory than without a memory approach, as was previously shown.

As for Doherty PA, the same is not true. With the increase in the number of data sent simultaneously, together with the increase of the signal bandwidth, the BER curves begin to tend to a minimum value, which it is proportional with this increase, as can be seen in figure 4.13. Such can be justified with the greatest sensitivity to variations of Doherty PA compared to Class B PA.

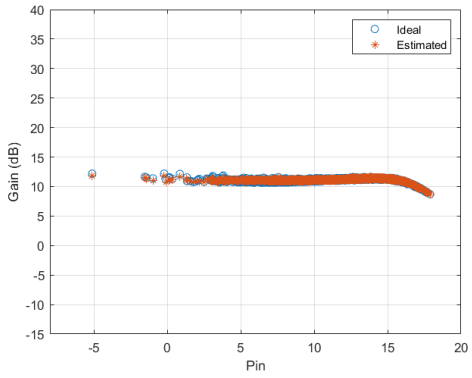

(a) AM-AM curves considering 1MHz bandwidth signal.

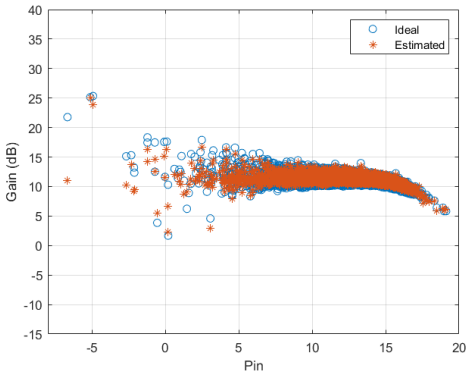

(b) AM-AM curves considering 10MHz bandwidth signal.

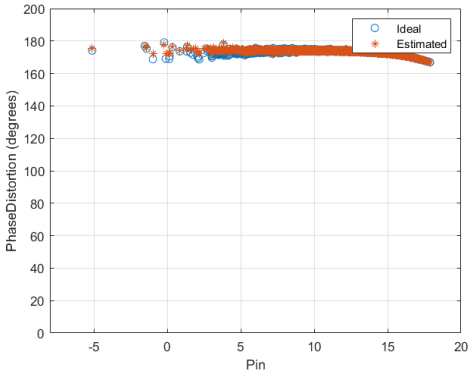

(c) AM-PM curves considering 1MHz bandwidth signal.

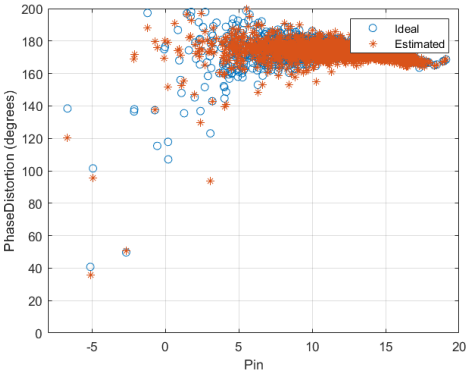

(d) AM-PM curves considering 10MHz bandwidth signal.

Figure 4.10: Class B PA - AM-AM and AM-PM curves compare.

After studying the performance that the polynomial approximation has on the calculation of the BER in relation to the SISO simulation also presented here, we can conclude that if you want a sketch of the BER curves without great quality and in a short time the polynomial approximation is sufficient, either with memory or without memory. On the other hand, if you want a sketched form of the BER curves the SISO simulation is ideal, despite the simulation time. Thus, it is up to the operator to decide, in the context and what he wishes to achieve, which of the options fits best.

In this way a SISO system that allows to simulate any PA with its own characteristics is presented in two different ways: one in which the MATLAB-ADS cosimulation is used and another in which only the MATLAB simulation is used, the ADS being only necessary to create the polynomial approximation.

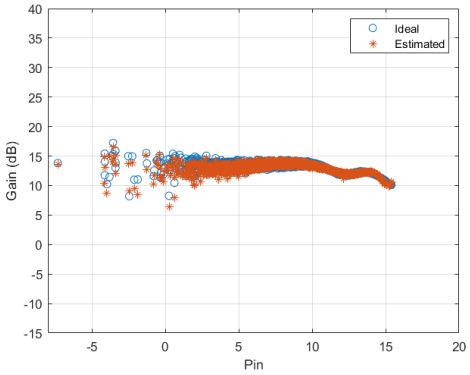

(a) AM-AM curves considering 1MHz bandwidth signal.

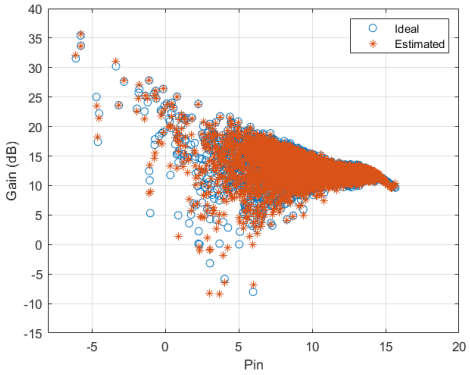

(b) AM-AM curves considering 10MHz bandwidth signal.

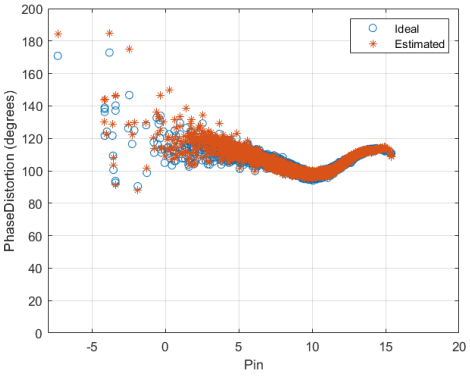

(c) AM-PM curves considering 1MHz bandwidth signal.

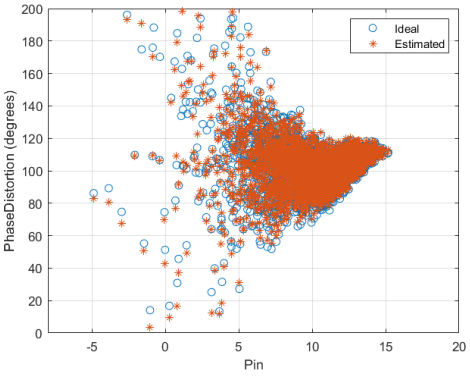

(d) AM-PM curves considering 10MHz bandwidth signal.

Figure 4.11: Doherty PA - AM-AM and AM-PM curves compare.

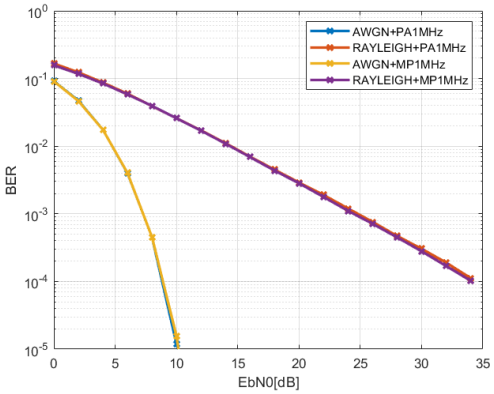

(a) BER for QPSK modulation and signal with 1MHz of bandwidth.

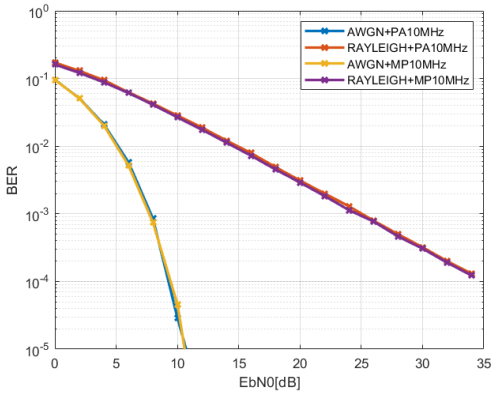

(b) BER for QPSK modulation and signal with 10MHz of bandwidth.

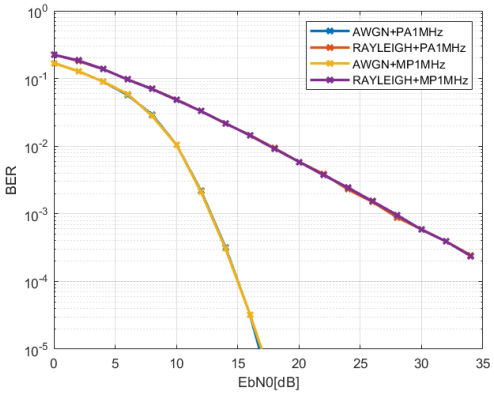

(c) BER for 16-QAM modulation and signal with 1MHz of bandwidth.

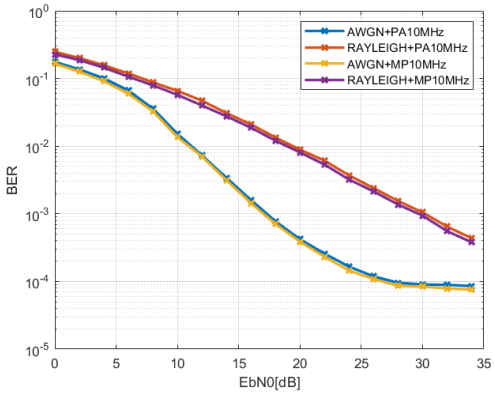

(d) BER for 16-QAM modulation and signal with 10MHz of bandwidth.

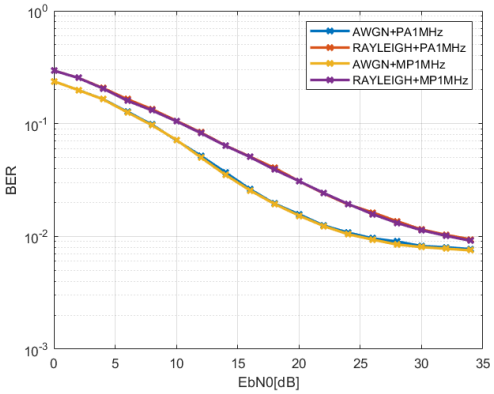

(e) BER for 64-QAM modulation and signal with 1MHz of bandwidth.

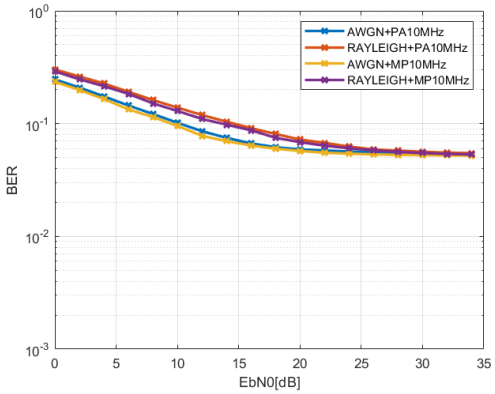

(f) BER for 64-QAM modulation and signal with 10MHz of bandwidth.

Figure 4.12: Memory polynomial approximation simulation - Class B PA effect on the BER.

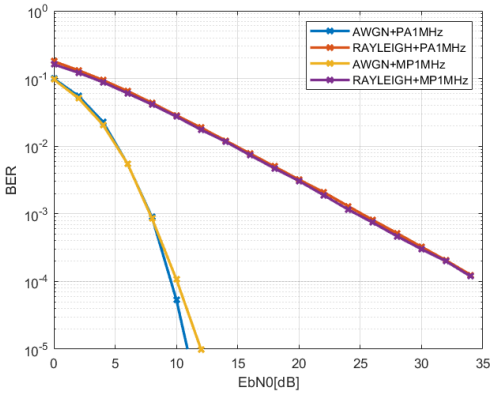

(a) BER for QPSK modulation and signal with 1MHz of bandwidth.

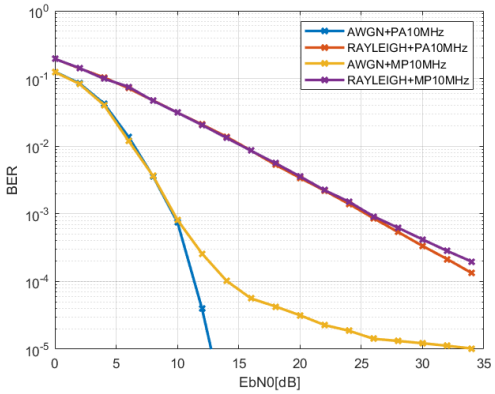

(b) BER for QPSK modulation and signal with 10MHz of bandwidth.

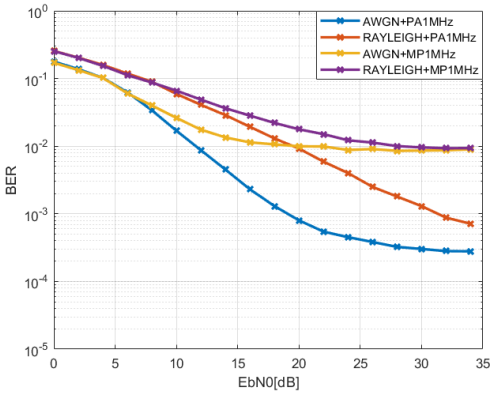

(c) BER for 16-QAM modulation and signal with 1MHz of bandwidth.

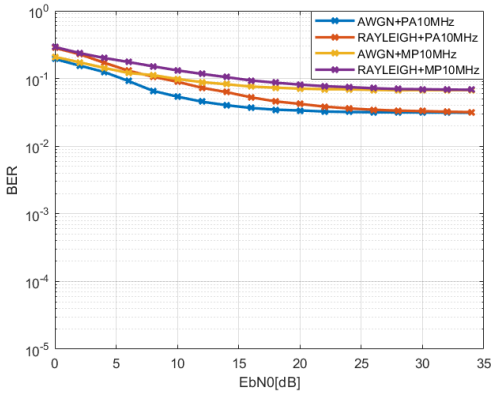

(d) BER for 16-QAM modulation and signal with 10MHz of bandwidth.

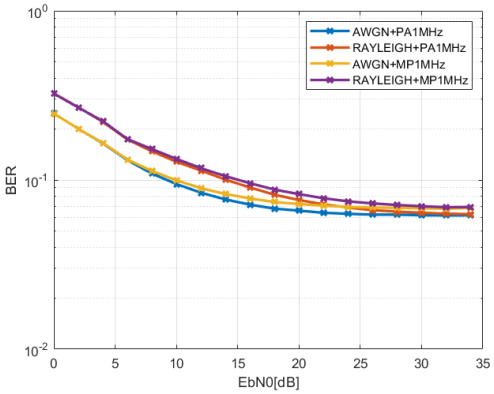

(e) BER for 64-QAM modulation and signal with 1MHz of bandwidth.

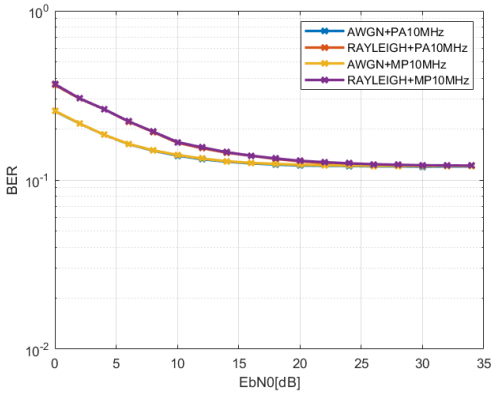

(f) BER for 64-QAM modulation and signal with 10MHz of bandwidth.

Figure 4.13: Memory polynomial approximation simulation - Doherty PA effect on the BER.

Chapter 5

Conclusions

5.1 Summary and Conclusions

Current 4G systems use OFDM modulation which, in spite of guaranteeing great flexibility and robustness to the multipath propagation, causes a high PAPR and, consequently, limitations in the performance of the PAs. Due to this, in order to study the performance of a system, a platform was created that allows its simulation using MATLAB and ADS as support.

In this platform it is possible to choose the type of modulation to use (QPSK, 16-QAM or 64-QAM) as well as the signal bandwidth to be transmitted and the type of PA used in the transmitter. After that, it is possible to simulate the system in two different ways: one in which the MATLAB-ADS cosimulation is used and another in which the behavior of the PA is replaced by a polynomial approximation and the simulation is performed, after the creation of the polynomial, entirely in MATLAB.

In the MATLAB-ADS cosimulation a SISO system and also a particular case of a MISO system, more specifically the Alamouti 2x1 were simulated.

For the case of the SISO system, it has been found that the Doherty PA affects the signals' transmission more than the Class B PA for all modulations analyzed here. In addition, with the increase of the signal bandwidth to be transmitted, the Doherty PA distorts the signal more than the Class B PA, as concluded in the analysis of the characteristics of the PAs in Chapter 3, increasing the BER in the receiver.

Concerning the MISO system, there was also a worsening of the BER in relation to the transmission without PA, and this was more significant in Doherty PA than in Class B PA.

As for the simulation in which a polynomial to approximate the behavior of the PAs in SISO system is used, two cases were tested: initially we considered a polynomial without memory and later one with memory.

For the 1MHz bandwidth signal the results obtained in the memoryless polynomial approximation are identical to those of the SISO simulation. On the other hand, when the signal has a bandwidth of 10MHz, the memoryless polynomial approximation is bad, leading to the distance of the BER curves obtained here compared to those obtained in the SISO simulation, as predicted based on the AM-AM and AM-PM curves.

After that, the polynomial was replaced by a memory polynomial. Here the polynomial approximation is better than the previous one as expected. Although the BER curves are closer to those obtained in the SISO simulation than the memoryless polynomial approxima-

tion there are some deviations.

In this way, we can conclude that the platforms simulation allows us to obtain expected results and that they meet the characteristics of the PAs tested here. In addition, it has been demonstrated here how the OFDM modulation affects the performance of the PAs. Due to this, alternatives are currently being developed that reduce/eliminate the gaps of this modulation, as is the case of 5G systems.

5.2 Future Work

After completing this work, it would be pertinent to construct a practical illustrative set-up of what was done in a simulation environment in order to compare the results obtained in both cases.

In order to understand how the PAs degrade the signal modulated in OFDM, it would be good work to study its nonlinearities as well as to obtain quantitatively its effect in the BER.

As a daring future goal, it would be important to make the simulation scheme more robust by creating a terminal in which the user can choose what they would do according to the options presented here.

The platform has a main advantage, the possibility of being altered and it can analyze any system such as the case of a 5G system.

Bibliography

[1] Diogo Rafael Bento Barros. Amplificador de RF Doherty Assimétrico de 2-Vias. Master's thesis, Universidade de Aveiro, Aveiro, Portugal, 2015.

[2] David Tse and Pramod Viswanath. *Fundamentals of Wireless Communication*. Cambridge University Press, 2005.

[3] Marcus L Roberts, Michael A Temple, Robert F Mills, and Richard A Raines. Evolution of the air interface of cellular communications systems toward 4G realization. *IEEE Communications Surveys & Tutorials*, 8(1):2–23, 2006.

[4] B Anil Kumar and P Trinatha Rao. Overview of advances in communication technologies. In *Electromagnetic Interference and Compatibility (INCEMIC), 2015 13th International Conference on*, pages 102–106. IEEE, 2015.

[5] Mohinder Jankiraman. *Space-Time Codes and MIMO Systems*. Artech House, 2004.

[6] GSM Bands information by country (April 19, 2018). `https://www.worldtimezone.com/gsm.html`. [Online; accessed 07/05/2018].

[7] Stanley Chia, Trevor Gill, Luke Ibbetson, David Lister, Adam Pollard, Ralf Irmer, Daniel Almodovar, Neil Holmes, and Simon Pike. 3G evolution. *IEEE microwave magazine*, 9(4):52–63, 2008.

[8] William Stallings. *Wireless communications & Networks*. Pearson Education India, 2009.

[9] Roger M Whitaker and Steve Hurley. Evolution of planning for wireless communication systems. In *System Sciences, 2003. Proceedings of the 36th Annual Hawaii International Conference on*, pages 10–pp. IEEE, 2003.

[10] Global Mobile Statistics. `http://www.5gamericas.org/en/resources/statistics/statistics-global/`. [Online; accessed 08/02/2018].

[11] Haohong Wang, Lisimachos Kondi, Ajay Luthra, and Song Ci. *4G Wireless Video Communications*, volume 11. John Wiley & Sons, 2009.

[12] The second phase of LTE-Advanced. `www.huawei.com/ilink/en/download/HW_259010`. [Online; accessed 10/07/2018].

[13] By 2020 - 5G will support 7 key performance Indicator's to deliver 50 Gbps. `https://www.linkedin.com/pulse/5g-7-key-performance-indicators-moulay-elmenouar`. [Online; accessed 29/05/2018].

[14] Zizheng Cao, Xuebing Zhang, Longfei Shen, Xiong Deng, Xin Yin, AMJ Koonen, et al. Millimeter Wave Beam Steered Fiber Wireless Systems for 5G Indoor Coverage: Integrated Circuits and SystemsTitle to be Announced. In *Asia Communications and Photonics Conference*, pages S4D–1. Optical Society of America, 2017.

[15] Tadilo Endeshaw Bogale, Xianbin Wang, and Long Bao Le. Machine Intelligence Techniques for Next-Generation Context-Aware Wireless Networks. *arXiv preprint arXiv:1801.04223*, 2018.

[16] The Mobile Economy 2018. `https://www.gsma.com/mobileeconomy/wp-content/uploads/2018/02/The-Mobile-Economy-Global-2018.pdf`. [Online; accessed 08/05/2018].

[17] IB Shirokov and VA Durmanov. Selection of Modulation Type in Digital Data Transmission Systems. In *Microwave and Telecommunication Technology, 2006. CriMiCO'06. 16th International Crimean Conference*, volume 1, pages 375–376. IEEE, 2006.

[18] Junghwan Moon, Juyeon Lee, Junghwan Son, Jungjoon Kim, Seunghoon Jee, Seungchan Kim, and Bumman Kim. Effects of even-order terms on behavior model of envelope tracking transmitters. In *European Microwave Conference (EuMC)*, pages 1193–1196, 2011.

[19] JR Bramwell. Whatever happened to...? A review of previous advanced modulation methods. In *Advanced Modulation and Coding Techniques for Satellite Communications, IEE Colloquium on*, pages 1–1. IET, 1992.

[20] Rong Zeng, Tao Cao, YouJiang Liu, and Jie Zhou. A novel design technique of Doherty power amplifier. In *Microwave Conference Proceedings (CJMW), 2011 China-Japan Joint*, pages 1–3. IEEE, 2011.

[21] Inder Bahl. *Fundamentals of RF and Microwave Transistor Amplifiers*. John Wiley & Sons, 2009.

[22] Nuttapong Srirattana, Arvind Raghavan, Deukhyoun Heo, Phillip E Allen, and Joy Laskar. Analysis and design of a high-efficiency multistage Doherty power amplifier for wireless communications. *IEEE Transactions on Microwave Theory and Techniques*, 53(3):852–860, 2005.

[23] Haesik Kim. *Wireless Communications Systems Design*. John Wiley & Sons, 2015.

[24] John G Proakis. Digital communications. *McGraw-Hill, New York*, 1995.

[25] Sergio Benedetto and Ezio Biglieri. *Principles of Digital Transmission: with wireless applications*. Springer Science & Business Media, 1999.

[26] MNT Castle. All About Modulation-Part-I. *Charan Langton*, pages 1–48, 2005.

[27] L Brunel, A Gueguen, D Mottier, Mathieu Des Noes, F Alves, A Morgado, R Legouable, S Zazo, N Neda, P Martinelli, et al. Physical Layer Simulation Chain Description (Reference chain V0). 2002.

[28] Gustavo Miranda Castilho dos Anjos. MIMO processing techniques for 4G systems. Master's thesis, Universidade de Aveiro, 2013.

[29] Shinsuke Hara and Ramjee Prasad. *Multicarrier Techniques for 4G Mobile Communications*. Artech House, 2003.

[30] Stefania Sesia, Matthew Baker, and Issam Toufik. *LTE-the UMTS Long Term Evolution: from theory to practice*. John Wiley & Sons, 2011.

[31] Yong Soo Cho, Jaekwon Kim, Won Young Yang, and Chung G Kang. *MIMO-OFDM Wireless Communications with MATLAB*. John Wiley & Sons, 2010.

[32] Robert W Chang. Synthesis of band-limited orthogonal signals for multichannel data transmission. *Bell System Technical Journal*, 45(10):1775–1796, 1966.

[33] RR Mosier and RG Clabaugh. Kineplex, a bandwidth-efficient binary transmission system. *Transactions of the American Institute of Electrical Engineers, Part I: Communication and Electronics*, 76(6):723–728, 1958.

[34] Mark Zimmerman and Alan Kirsch. The AN/GSC-10 (KATHRYN) variable rate data modem for HF radio. *IEEE Transactions on Communication Technology*, 15(2):197–204, 1967.

[35] Adão Silva Atilio Gameiro. *Slides Wireless Communications subject*. Aveiro University, Department of Electronic, Telecommunications and Informations, Aveiro, Portugal, 2013.

[36] Robert G Gallager. *Principles of Digital Communication*, volume 1. Cambridge University Press Cambridge, UK:, 2008.

[37] Imtiaz Ahamed and Manoj Vijay. Comparison of different diversity techniques in MIMO antennas. In *Communication and Electronics Systems (ICCES), 2017 2nd International Conference on*, pages 47–50. IEEE, 2017.

[38] Vahid Tarokh, Hamid Jafarkhani, and A Robert Calderbank. Space-time block coding for wireless communications: performance results. *IEEE Journal on selected areas in communications*, 17(3):451–460, 1999.

[39] Siavash M Alamouti. A simple transmit diversity technique for wireless communications. *IEEE Journal on selected areas in communications*, 16(8):1451–1458, 1998.

[40] Steve C Cripps. *Advanced techniques in RF power amplifier design*. Artech House, 2002.

[41] Bumman Kim. *Doherty Power Amplifiers: From Fundamentals to Advanced Design Methods*. Academic Press, 2018.

[42] Guillermo Gonzalez. *Microwave transistor amplifiers: analysis and design*, volume 2. Prentice hall New Jersey, 1997.

[43] Jose Carlos Pedro and Nuno Borges Carvalho. *Intermodulation Distortion in Microwave and Wireless Circuits*. Artech House, 2003.

[44] Shuqi Zhao, Xinning Zhu, Haiyan Wang, and Leijia Wu. Analysis of joint effect of phase noise, IQ imbalance and amplifier nonlinearity in OFDM system. In *Wireless Communications & Signal Processing (WCSP), 2013 International Conference on*, pages 1–6. IEEE, 2013.

[45] Vivek Ashok Bohara and See Ho Ting. Analysis of OFDM signals in nonlinear high power amplifier with memory. In *Communications, 2008. ICC'08. IEEE International Conference on*, pages 3653–3657. IEEE, 2008.

[46] Yan Chen, Chun-hua Zhu, Shou-yi Yang, and Hui Xiao. Spectrum analysis of OFDM-based communication systems with nonlinear high power amplifier. In *Communications and Mobile Computing (CMC), 2010 International Conference on*, volume 2, pages 451–454. IEEE, 2010.

[47] T Deepa and R Kumar. Performance of comparison metrics on M-QAM OFDM systems with high power amplifier. In *Information and Communication Technologies (WICT), 2012 World Congress on*, pages 909–914. IEEE, 2012.

[48] Tushar Kanti Roy and Monir Morshed. High power amplifier effects analysis for OFDM system. *International Journal of Science, Engineering and Technology Research*, 2(5):pp–1119, 2013.

[49] Steve C Cripps. *RF Power Amplifiers for Wireless Communications*. Norwood, MA, USA: Artech House, Inc, 2006.

[50] Wang Huadong, Bao Jingfu, Wu Zhengde, and Huang Jingfu. An Memory polynomial model for power amplifiers. In *Communications, Circuits and Systems, 2008. ICCCAS 2008. International Conference on*, pages 1346–1349. IEEE, 2008.

[51] Andre BJ Kokkeler. Modeling Power Amplifiers using Memory Polynomials. In *12th IEEE Benelux Symposium on Communications and Vehicular Technology in the Benelux, SCVT*, pages 1–6. Citeseer, 2005.

[52] Amandeep Singh Sappal. Simplified Memory Polynomial modelling of Power Amplifier. In *Computing and Communication (IEMCON), 2015 International Conference and Workshop on*, pages 1–7. IEEE, 2015.

[53] Dennis R Morgan, Zhengxiang Ma, Jaehyeong Kim, Michael G Zierdt, and John Pastalan. A generalized memory polynomial model for digital predistortion of RF power amplifiers. *IEEE Transactions on signal processing*, 54(10):3852–3860, 2006.